

**PAGE MISSING FROM AVAILABLE VERSION**

Cover Page and Pgs. I - IV

F.0	Edge Matching	F.0-1
F.1	Continuity Requirements	F.1-1
F.2	Network Abutments	F.2-1
F.3	Automatic Abutment Search	F.3-1
F.4	Doublet Matching Along Abutments	F.4-1
F.5	Abutment Intersections	F.5-1
	F.5.1 Graphical Representation of an Abutment Intersection	F.5-2
	F.5.2 Modifications to the Abutment Assignment Procedure	F.5-6
F.6	Gap-Filling Panels	F.6-1
G.0	Control Point Locations	G.0-1
H.0	Boundary Conditions and Onset Flows	H.0-1
H.1	Reduction of User Specified Boundary Conditions to Standard Formulation	H.1-1
H.2	Program Overrides of User Boundary Condition Specifications	H.2-1
	H.2.1 Superinclined Panel Override	H.2-1
	H.2.2 Nullification of User-Input Boundary Conditions	H.2-2
	H.2.3 Source and Doublet Matching Boundary Conditions	H.2-2
	H.2.4 Closure Boundary Conditions	H.2-3
	H.2.5 The Boundary Condition Hierarchy	H.2-5
H.3	Onset Flows	H.3-1
I.0	Singularity Splines	I.0-1
I.1	Outer Splines	I.1-1
	I.1.1 Source Splines for Analysis Vectors	I.1-2
	I.1.1.1 Source Spline Vectors for Continuous Splines	I.1-2
	I.1.1.2 Neighboring Singularity Parameters	I.1-2
	I.1.1.3 Computation of a Local Coordinate System	I.1-2
	I.1.1.4 The Bilinear Fit at Panel Corner Points	I.1-4
	I.1.1.5 Discontinuous Source Analysis Splines	I.1-5
	I.1.2 Doublet Spline Vectors for Analysis Networks, Doublet Forward Weighted Splines	I.1-7
	I.1.2.1 The Quadratic Least Squares Fit for Panel Corners or Panel Edge Midpoints	I.1-8
	I.1.2.2 Neighboring Points for Least Squares Fit	I.1-10
	I.1.2.3 Construction of a Local Coordinate System	I.1-11
	I.1.2.4 Weights for the Least Squares Fit	I.1-12
	I.1.2.5 Edge Splines for Non-Smooth Abutments	I.1-12
	I.1.2.6 Edge Splines for Smooth Abutments	I.1-17
	I.1.3 Doublet Spline Vectors for Wake Networks	I.1-19
	I.1.4 Source Splines for Design Networks	I.1-19
	I.1.4.1 Source Design 1	I.1-19
	I.1.4.2 Source Design 2, Discontinuous Source Splines	I.1-19
	I.1.4.3 Source Design 2, Continuous Source Splines	I.1-20
	I.1.5 Doublet Splines for Design Networks	I.1-21

I.2	Subpanel Splines	I.2-1
I.2.1	Source Subpanel Splines	I.2-1
	I.2.1.1 Preliminaries	I.2-1
	I.2.1.2 Inversion of the Matrix of Coordinates	I.2-2
	I.2.1.3 The Extension Matrix	I.2-5
I.2.2	Doublet Subpanel Splines	I.2-6
	I.2.2.1 Continuity Requirements	I.2-6
	I.2.2.2 Definition of Kappa Quantities	I.2-7
	I.2.2.3 Computation of Kappa Quantities	I.2-8
	I.2.2.4 The Doublet Extension Matrix	I.2-12
	I.2.2.5 The Matrix of Coordinates $G^D$	I.2-12
	I.2.2.6 Inversion of $G^D$	I.2-14
I.3	Full Panel and Half Panel Splines	I.3-1
I.3.1	Full Panel Spline Matrices	I.3-1
I.3.2	Half Panel Spline Matrices (Background Material)	I.3-3
	I.3.2.1 Requirements for the Source Half Panel Spline Matrix	I.3-3
	I.3.2.2 Computation of $D^S$	I.3-5
	I.3.2.3 The Extension Matrix $XH^S$	I.3-7
	I.3.2.4 Requirements for the Doublet Half Panel Spline Matrix	I.3-8
	I.3.2.5 Computation of $D^D$	I.3-9
	I.3.2.6 The Extension Matrix $XH^D$	I.3-12
I.4	Far Field Moments	I.4-1
I.4.1	The Defining Equations	I.4-1
	I.4.1.1 Source Far Field Moments	I.4-1
	I.4.1.2 Symmetrization	I.4-2
	I.4.1.3 Doublet Far Field Moments	I.4-3
	I.4.1.4 Doublet Velocity Far Field Moments	I.4-4
I.4.2	Construction of the Far Field Moments	I.4-4
	I.4.2.1 Preliminaries	I.4-4
	I.4.2.2 $FFM_{S,1}$	I.4-5
	I.4.2.3 $FFM_{S,2}$	I.4-7
	I.4.2.4 $FFM_{S,3}$	I.4-10
	I.4.2.5 $FFM_{D,0}$	I.4-12
	I.4.2.6 $FFM_{D,1}$	I.4-13
	I.4.2.7 $FFM_{D,2}$ and $FFM_{D,3}$	I.4-13
	I.4.2.8 $FFM_{D,4}$	I.4-14
	I.4.2.9 $FFM_{D,5}$	I.4-16
	I.4.2.10 $FFM_{D,6}$	I.4-18

I.4.3	Basic Far Field Moments	I.4-19
I.4.3.1	Reduction to Line Integrals	I.4-20
I.4.3.2	Computation of the Line Integrals	I.4-22
I.5	Constrained Least Squares	I.5-1
I.5.1	Definition of the Problem	I.5-1
I.5.2	Elimination of the Weights	I.5-1
I.5.3	The Case of No Exact Constraints	I.5-2
I.5.4	Reduction of the General Case	I.5-3
J.0	Panel Influence Coefficient Calculation	J.1-1
J.1	Introduction and Notation	J.1-1
J.1.1	Definitions	J.1-1
J.1.2	Summary	J.1-2
J.1.2.1	Near Field Versus Far Field	J.1-2
J.1.2.2	The Domain of Dependence	J.1-3
J.1.2.3	Near Field and Intermediate Field PIC Calculation	J.1-3
J.1.2.4	Far Field PIC's	J.1-6
J.1.3	Integration Techniques	J.1-7
J.1.4	Notation	J.1-8
J.2	The Distance Algorithm	J.2-1
J.2.1	The Far Field Criterion	J.2-1
J.2.2	The Intermediate Field Criterion	J.2-3
J.3	Supersonic Influence Test	J.3-1
J.3.1	Definition of $D_p$	J.3-1
J.3.2	A Zero Influence Test	J.3-1
J.3.3	Panel Wholly Within the Mach Cone	J.3-4
J.3.4	The Influence Test For a Subpanel	J.3-4
J.3.4.1	The Point of Closest Approach	J.3-5
J.3.4.2	The Winding Number Test	J.3-7
J.3.4.3	Half Panels and Projected Panels	J.3-8
J.4	Cylindrical Coordinates	J.4-1
J.4.1	Fundamental Results	J.4-1
J.4.2	The Mach Disk	J.4-2
J.4.3	The Case of the Mach Disk Lying Within the Panel	J.4-2
J.4.4	Arbitrary Intersection of the Mach Disk With the Panel	J.4-3
J.4.4.1	Corner Points	J.4-4
J.4.4.2	The Phase Function	J.4-4
J.4.4.3	Edges and the Mach Disk	J.4-7
J.4.4.4	Edge Tangents and Normals	J.4-7
J.4.4.5	The Function $P(\phi)$	J.4-10
J.5	Hyperbolic Coordinates	J.5-1
J.5.1	Fundamental Results	J.5-1
J.5.2	Subsonic Edges	J.5-8
J.5.3	Supersonic Edges	J.5-12
J.5.4	Computation of the Integrals	J.5-16
J.6	The Panel Integral Matrices	J.6-1
J.6.1	Preliminaries	J.6-2
J.6.1.1	Transformation Rules	J.6-2
J.6.1.2	Transformation of the Integrals	J.6-3
J.6.1.3	Singularity Strength Coefficients	J.6-5
J.6.1.4	Uniform Formulas for Local Variables	J.6-6
J.6.1.5	Differentiation Formulas	J.6-9

J.6.2	Source Potential and Velocity	J.6-10
	J.6.2.1 Source Potential	J.6-10
	J.6.2.2 Tangential Source Velocity	J.6-12
	J.6.2.3 Normal Source Velocity	J.6-13
J.6.3	Doublet Potential and Velocity	J.6-15
	J.6.3.1 Doublet Potential	J.6-15
	J.6.3.2 Tangential Doublet Velocity	J.6-16
	J.6.3.3 Normal Doublet Velocity	J.6-18
J.6.4	Reduction to Fundamental Integrals	J.6-19
	J.6.4.1 Definition of the Integrals	J.6-20
	J.6.4.2 Source Potential and Velocity	J.6-20
	J.6.4.3 Doublet Potential and Velocity	J.6-23
J.6.5	The Fundamental Integral in Terms of Panel and Edge Functions	J.6-25
	J.6.5.1 Computation of $a$	J.6-25
	J.6.5.2 Computation of $b$	J.6-27
	J.6.5.3 Computation of $\bar{a}$	J.6-28
	J.6.5.4 Computation of $\bar{b}$	J.6-28
	J.6.5.5 Computation of $B$	J.6-30
	J.6.5.6 Computation of $F$	J.6-33
	J.6.5.7 Computation of $H$	J.6-33
J.6.6	The Origin Shift	J.6-35
J.6.7	Finite Parts of Singular Integrals	J.6-41
	J.6.7.1 Definition of a Finite Part	J.6-41
	J.6.7.2 Properties of a Finite Part	J.6-41
	J.6.7.3 Finite Parts and the Integral Equation	J.6-42
	J.6.7.4 Finite Parts and PIC Computation	J.6-42
	J.6.7.5 Summary of Finite Part Integrals	J.6-43
J.7	Edge and Panel Functions	J.7-1
J.7.1	Expressions For Edge and Panel Functions	J.7-1
	J.7.1.1 Subsonic Flow	J.7-1
	J.7.1.2 Subsonic Edges of Subinclined Panels in Supersonic Flow	J.7-2
	J.7.1.3 Supersonic Edges of Subinclined Panels	J.7-3
	J.7.1.4 Superinclined Panels	J.7-3
	J.7.1.5 Uniform Formulas	J.7-4
J.7.2	Computation of Edge and Panel Function Arguments in Reference Coordinates	J.7-4
	J.7.2.1 Computation of $h$	J.7-5
	J.7.2.2 Computation of $v$	J.7-5
	J.7.2.3 Computation of $a$	J.7-7
	J.7.2.4 Computation of $g$	J.7-8
J.8	Rationalization Formulas	J.8-1
J.8.1	Edge Functions	J.8-1
	J.8.1.1 Non-Sonic Edges	J.8-2
	J.8.1.2 Nearly Sonic Edges	J.8-6
	J.8.1.3 Essentially Sonic Edges	J.8-10
J.8.2	Panel Function Computation	J.8-12
	J.8.2.1 The Standard Rationalization	J.8-12
	J.8.2.2 A Special Rationalization	J.8-18

J.9	Far Field PIC's	J.9-1
J.9.1	The Basic Principle	J.9-1
J.9.2	Computation of the Gradient	J.9-4
J.9.3	Source Velocity	J.9-5
J.9.4	Doublet Potential	J.9-6
J.9.5	Doublet Velocity	J.9-7
J.9.6	Symmetrization	J.9-8
J.9.6.1	Source Potential	J.9-9
J.9.6.2	Source Velocity	J.9-9
J.9.6.3	Doublet Potential	J.9-10
J.9.6.4	Doublet Velocity	J.9-10
J.10	Line Vortex PIC's	J.10-1
J.10.1	Computation of $\vec{v}_D^*$	J.10-1
J.11	Singular Behavior of Integrals	J.11-1
J.11.1	Discontinuous Source Strength	J.11-1
J.11.2	Discontinuous Doublet Strength	J.11-5
J.11.2.1	Doublet Potential	J.11-5
J.11.2.2	Doublet Velocity	J.11-5
J.11.3	Discontinuities in Doublet Gradient	J.11-6
J.11.4	Singularities of the Panel Function	J.11-8
J.11.4.1	The Plane $h = 0$	J.11-8
J.11.4.2	Discontinuities Due to $C_0$	J.11-10
J.11.4.3	Discontinuities in $J_k(\psi)$	J.11-12
J.11.4.4	Summary of Panel Function Behavior	J.11-14
J.11.5	Singularities of the Edge Function	J.11-15
J.11.5.1	Supersonic Edges	J.11-15
J.11.5.2	Subsonic Edges	J.11-16
J.11.5.3	Subsonic Nearly Sonic Edges	J.11-17
J.11.5.4	Supersonic Nearly Sonic Edges	J.11-19
J.11.5.5	Essentially Sonic Edges	J.11-19
J.11.6	Singularities in Subsonic Flow	J.11-19
J.11.6.1	Discontinuous Source Strength	J.11-19
J.11.6.2	Discontinuous Doublet Strength	J.11-20
J.11.6.3	Discontinuous Doublet Gradient	J.11-22
J.11.7	Discontinuous Source Strength in Supersonic Flow	J.11-22
J.11.7.1	Source Potential	J.11-22
J.11.7.2	Source Velocity	J.11-23
J.11.8	Discontinuous Doublet Strength in Supersonic Flow	J.11-23
J.11.9	Discontinuous Doublet Gradient in Supersonic Flow	J.11-24
K.0	Matrix Assembly	K.0-1
K.1	Symmetry Planes	K.1-1
K.1.1	One Plane of Geometric Symmetry	K.1-1
K.1.2	Two Planes of Symmetry	K.1-4
K.1.3	Application	K.1-6
K.1.4	Networks Lying on a Plane of Symmetry	K.1-8
K.2	Known Singularity Parameters	K.2-1

K.3	Aerodynamic Boundary Conditions	K.3-1
K.3.1	Combining for Symmetry	K.3-1
K.3.2	Computing Influence on Image Panels	K.3-1
K.3.3	Partial Rows	K.3-3
K.3.4	Data Manipulation Problem	K.3-3
K.3.5	Imposition of the Boundary Conditions	K.3-4
K.4	Closure	K.4-1
K.5	Matching	K.5-1
K.6	The Update Capability	K.6-1
L.0	The Constraint Matrix	L.0-1
M.0	Computation of the Minimal Data Set	M.0-1
M.1	Recovery of the Singularity Parameters	M.1-1
M.2	Singularity Strength Calculation	M.2-1
M.3	Computation of Potential and Normal Mass Flux	M.3-1
N.0	Surface and Wake Flow Properties	N.0-1
N.1	Velocity Computation	N.1-1
N.2	Pressure Formulas	N.2-1
N.2.1	Preliminary Results	N.2-1
N.2.2	Constant Density Flow	N.2-2
N.2.3	Compressible Flow	N.2-3
N.2.4	Limitation of the Formula	N.2-4
N.2.4.1	The Vacuum Pressure Coefficient	N.2-5
N.2.4.2	The Critical Speed	N.2-5
N.2.4.3	The Pressure Coefficient at the Critical Speed	N.2-7
N.2.5	The Isentropic Formula Under Simplifying Assumptions	N.2-7
N.2.5.1	Second Order Theory	N.2-8
N.2.5.2	The Second Order Theory Under Additional Assumptions	N.2-10
N.3	Velocity Corrections	N.3-1
N.3.1	The First Velocity Correction	N.3-1
N.3.2	The Second Velocity Correction	N.3-2
N.4	Onset Flow Calculations	N.4-1
N.4.1	Bernoulli's Equation	N.4-1
N.4.2	Pressure Formulas	N.4-2
N.4.3	Simplifying Assumptions	N.4-4
N.5	Associated Data	N.5-1
0.0	Forces and Moments	0.0-1
0.1	Basic Formulas	0.1-1
0.2	Integration Procedure	0.2-1
0.3	Leading and Side Edge Force	0.3-1
0.3.1	Linearized Three-Dimensional Theory	0.3-1
0.3.2	Application in PAN AIR	0.3-1
0.3.3	Edge Force Verification	0.3-3
0.4	Coordinate Transformations	0.4-1
0.5	Added Mass Coefficients	0.5-1
0.5.1	Formulation of Added Mass Coefficients	0.5-1
0.5.2	Integration Procedures	0.5-2
0.5.3	Orthogonal Transformation	0.5-3
0.5.4	Translation	0.5-4
0.5.5	Symmetric Configuration	0.5-4

## List of Figures

Figures are placed at the end of each numbered section or appendix.

Page

### Section 3

3.1	Region V of space with boundary S	3.4-1
3.2	A surface S dividing regions $V_1$ and $V_2$	3.4-1
3.3	A surface S which does not divide space into 2 separate regions	3.4-2
3.4	Basis function for constant strength panels	3.4-2

### Section 4

4.1	Historical overview of panel methods	4.3-1
4.2	Division of panel into subpanels	4.3-2
4.3	Panel and far field control point	4.3-2

### Section 5

5.1	Network geometry	5.10-1
5.2	Decomposition of panel into 5 planar regions	5.10-1
5.3	Definition of compressibility directions in terms of angles of attack and sideslip	5.10-2
5.4	Superinclined surface, $r = 1$	5.10-2
5.5	Subinclined and Mach-inclined surfaces	5.10-3
5.6	Gap between leading edge of wing and body	5.10-3
5.7	Example of abutment intersection	5.10-4
5.8	Control point locations	5.10-4
5.9	Thin wing boundary conditions	5.10-5
5.10	Two solutions for potential in enclosed volume	5.10-5
5.11	Thick wing boundary conditions	5.10-6
5.12	Boundary conditions on superinclined surfaces	5.10-6
5.13	Singularity parameter locations	5.10-7
5.14	Singularity parameters in the neighborhood of the panel	5.10-8
5.15	Neighboring source parameters for a panel corner point	5.10-9
5.16	Neighboring doublet parameters for a panel corner point	5.10-9
5.17	Neighboring doublet parameters for a panel edge midpoint	5.10-10
5.18	Panel points and midpoints	5.10-10
5.19	Opposite orientations of adjacent networks	5.10-11
5.20	Configuration and image	5.10-11
5.21	Pressure coefficient rules	5.10-12
5.22	Surfaces of integration for leading edge force	5.10-12

### Appendix A

A.1	Thin wing at small angle of attack	A.2-1
A.2	Blunt object at small Mach number	A.2-1
A.3	Small perturbation "engine-on" case	A.2-2

### Appendix B

B.1	An exterior boundary value problem	B.5-1
B.2	A region of finite volume	B.5-1



B.3	Specification of normal flow on both sides of a surface	B.5-2
B.4	A superinclined surface	B.5-2
B.5	A boundary value problem with no unique solution	B.5-3
B.6	The domain of dependence	B.5-3
B.7	A permeable surface inclined to the freestream	B.5-4
B.8	A region which fails to be simply connected	B.5-4
B.9	Airplane and wake	B.5-5
B.10	Leading edge vortices from a highly swept wing	B.5-6
B.11	Panel edge on a network edge	B.5-7
B.12	Two adjacent panel edges	B.5-7
B.13	Three adjacent panels	B.5-8
B.14	Intersection of 3 surfaces (cross-section)	B.5-8
B.15	Region of integration in neighborhood of P	B.5-9

#### Appendix C

C.1	Design boundary conditions on a thin configuration	C.5-1
C.2	Indexing of network points	C.5-1
C.3	A panel	C.5-2
C.4	Design boundary conditions for a thick wing	C.5-2
C.5	A constant doublet strength spline	C.5-3
C.6	Stability for constant doublet spline	C.5-3
C.7	Quadratically varying doublet spline	C.5-4
C.8	A single interval	C.5-4
C.9	Stability for a quadratic doublet spline	C.5-5
C.10	Instability of analysis spline with boundary conditions	C.5-6
C.11	A doublet spline for design problems	C.5-7
C.12	Stability for design boundary conditions	C.5-7

#### Appendix D

D.1	Locations of source singularity parameters	D.3-1
D.2	Doublet analysis and design singularity parameter locations	D.3-2
D.3	Doublet wake singularity parameter locations	D.3-3
D.4	Network and panel indexing	D.3-4
D.5	Network with an edge to be collapsed by the program	D.3-4
D.6	Network with revised geometry	D.3-5
D.7	Panelling of data wing	D.3-5
D.8	A panel	D.3-6
D.9	A subpanel	D.3-7
D.10	Definition of skewness parameters	D.3-8
D.11	Impermissible network (two adjacent collapsed edges)	D.3-9

#### Appendix E

E.1	Surface S in compressibility and scaled coordinates	E.4-1
E.2	Illustration of the transformation law for $\hat{n} dS$	E.4-2
E.3	Definition of the compressibility vector $\hat{c}_0$ in terms of $\alpha_c$ and $\beta_c$	E.4-2

## Appendix F

F.1	Impermissible network intersection (in cross-section)	F.7-1
F.2	Leading edge vortex (in cross-section)	F.7-1
F.3	Simulation of a vortex core by a line vortex	F.7-2
F.4	Multiple pairwise abutments involving the same edges	F.7-2
F.5	Each network edge is a refinement of the other	F.7-3
F.6	Edge 1 is a refinement of edge 2	F.7-3
F.7	Control points on a supersonic leading edge are used for doublet matching	F.7-4
F.8a	Six network wing with wakes	F.7-5
F.8b	Doublet distribution arising from specification of $\mu$ at trailing edge	F.7-5
F.9	One edge is not precisely a refinement of the other	F.7-6
F.10	An abutment intersection with 4 abutments	F.7-6
F.11	An abutment intersection with 6 abutments	F.7-7
F.12	Another abutment intersection with 4 abutments	F.7-8
F.13	Directed graphs corresponding to three abutment intersections	F.7-9
F.14	Defoliation and matching condition assignment for the graph of fig. F13b	F.7-10
F.15	A corner point for which $A_1 = A_2$ , giving rise to a self-loop	F.7-11
F.16	An extra control point at the end of a smooth abutment	F.7-11
F.17	An abutment intersection in which both the initial and terminal ends of an abutment participate in an abutment intersection	F.7-12
F.18	Gap-filling panel	F.7-13
F.19	Gap-filling panels on an abutment with 3 network edges	F.7-13

## Appendix G

G.1	Control point locations	G.1-1
G.2	Division of network edge into two abutments	G.1-1
G.3	Control point recession vectors	G.1-2
G.4	Recession of corner control points when subpanel is triangular	G.1-2
G.5	Abutment with 3 network edges (cross-section)	G.1-3
G.6	Hypothetical locations of a control point	G.1-3

## Appendix H

H.1	Boundary condition locations for source networks	H.4-1
H.2	Boundary condition locations for doublet networks	H.4-2
H.3	Columns of panels illustrated by cross-hatching	H.4-4
H.4	Design of upper surface of thick wing	H.4-4
H.5	Pattern of streamlines on imposition of a closure boundary condition	H.4-5
H.6	Boundary condition categories	H.4-5
H.7	Total internal stagnation	H.4-6
H.8	Onset flow, not parallel to compressibility direction	H.4-6
H.9	Propeller slipstream	H.4-7
H.10	Airplane undergoing small rolling motion	H.4-7

## Appendix I

I.1a	Panel source parameter locations	I.6-1
I.1b	Panel doublet parameter locations	I.6-1
I.1c	Panel singularity parameter locations for a nine-panel network	I.6-2
I.2	Neighboring source parameters for analysis network	I.6-3
I.3	Thin wing with curved planform	I.6-3

I.4a	Neighboring singularity parameters ( $P_0$ away from network edge)	I.6-4
I.4b	Neighboring points for least squares fit ( $P_0$ near network edge)	I.6-4
I.4c	Neighboring points for least squares fit ( $P_0$ near a smooth abutment)	I.6-5
I.5	Basis vectors for local coordinate system for spline vector construction	I.6-6
I.6	Projections to tangent plane of points on curved surface	I.6-6
I.7a	Unequal spacing in a non-smooth abutment (second edge is a refinement of the first)	I.6-7
I.7b	Identification of points on a network edge	I.6-7
I.8	Differentiable 2-D quadratic spline	I.6-8
I.9a	Neighboring singularity parameters for points $P_0$ on a smooth abutment	I.6-9
I.9b	Parameterization of an abutment	I.6-10
I.9c	Panel edge on coarse network	I.6-10
I.10a	Neighboring point for least square fit ( $P_0$ on a doublet design network)	I.6-11
I.10b	Edge of a doublet design network	I.6-11
I.11	Adjacent panels	I.6-12
I.12	Panel defining points and subpanel local coordinate systems	I.6-12
I.13	Subpanel local coordinates	I.6-13
I.14	Triangular coordinates	I.6-13
I.15	Values of differentiable doublet distribution on a square panel	I.6-14
I.16	Values of doublet distribution on square panel with PAN AIR spline	I.6-14
I.17	An interval with midpoint	I.6-15
I.18	Quadratic doublet distribution on a subpanel	I.6-15
I.19	Division on panel into half panels	I.6-16
I.20	Diagram of half panel $i$	I.6-16
I.21	Standard half panel	I.6-17
I.22	Computation of basic far field moments	I.6-17
I.23	Location of global source parameters used in the construction of the discontinuous source analysis spline	I.6-18
I.24	Location of source parameter points for the special case construction of discontinuous source analysis splines	I.6-19
I.25	Computation of panel edge midpoint source strengths for discontinuous SD2 source splines	I.6-20
I.26	Computation of panel corner spline vectors for continuous SD2 source splines	I.6-21

## Appendix J

J.1	Domain of dependence	J.12-1
J.2	Superinclined panel partially within $D_p$ without corners in $D_p$	J.12-1
J.3	Notation used frequently in Appendix J	J.12-2
J.4	Two region approximations to panel	J.12-3
J.5	Region in which intermediate field PIC is not performed	J.12-4
J.6	Splitting a panel into half panels	J.12-4
J.7	$(\tilde{X}, \tilde{Y})$ coordinate system	J.12-5
J.8	Subsonic and supersonic edges	J.12-5
J.9	Point of closest approach	J.12-6
J.10	Subinclined and superinclined panel	J.12-6
J.11	$P_*$ lies in the interior of the subpanel	J.12-7
J.12	Region of integration, $\Sigma' \cap C_h$ for a typical subpanel	J.12-7
J.13	$P_k^\pm, Q_k^\pm$ when $C_h \subset \Sigma'$	J.12-8
J.14	Edge numbering for various panel configurations	J.12-8
J.15	Phase angle $\phi'$ exceeds $\pi$	J.12-9
J.16	Coordinate systems in the $(\xi', \eta')$ plane	J.12-9

J.17	Determining if an edge of $\Sigma'$ is an edge of $\Sigma' \cap C_h$	J.12-10
J.18	Definition of $\rho(\phi)$ , the upper limit of integration for $\rho$	J.12-11
J.19	Region of integration for superinclined panel	J.12-12
J.20	Transformation to (s,t) variables and region of integration	J.12-13
J.21	Numbering of edges of $\Sigma' \cap H_h$	J.12-13
J.22	A region $\Sigma'$ with edge E, oriented tangent $\vec{t}$ and outward edge normal $\vec{n}$	J.12-14
J.23	An edge E and its image E' in the s - t coordinate system (subsonic edge)	J.12-14
J.24	An edge E and its image E' in the s - t coordinate system (supersonic edge)	J.12-15
J.25a	Region of integration for subinclined panel	J.12-16
J.25b	Region of integration for subinclined panel	J.12-17
J.26	Polygon $\Sigma'_\epsilon$ approximating $\Sigma' \cap D_p$	J.12-18
J.27	Illustration of supersonic, nearly sonic edges on which v changes sign	J.12-19
J.28	An example of a superinclined panel with $g^2 = h^2 - a^2 \approx 0$	J.12-19
J.29	Evaluating v on the boundary of $D_p$ : the various special cases	J.12-20
J.30	The value of J' for some special configurations	J.12-21
J.31	Region with nearly sonic edge	J.12-22
J.32	Potential lines of discontinuity in J+	J.12-22
J.33	Panel corners on Mach lines	J.12-23
J.34	A point lies on the extension of an edge (subsonic flow)	J.12-24
J.35	A point lies on the extension of an edge (supersonic flow)	J.12-24
J.36	Edge barely intersects $D_p$	J.12-25
J.37a	The Mach wedge in cross-section	J.12-25
J.37b	Mach wedge behind supersonic panel edge	J.12-26
J.38	Subsonic nearly sonic edge	J.12-27
J.39	The distances h, v, a, g, and R in subsonic flow	J.12-28

#### Appendix K

K.1	Reflection of point or velocity vector in plane of symmetry	K.7-1
K.2	Reflection of point in 2 planes of symmetry	K.7-1
K.3	Vertical tail on a plane of symmetry	K.7-2
K.4	Reflections of abutments at and away from a plane of symmetry	K.7-2
K.5	Abutment on two planes of symmetry	K.7-3
K.6	Extra singularity parameter and control point dependent on existence of updateable network	K.7-3

#### Appendix M

M.1	Neighboring control points for potential spline computation	M.4-1
-----	-------------------------------------------------------------	-------

#### Appendix O

0.1	Effect of leading edge force	0.6-1
0.2	Leading edge force on a three-dimensional thin wing	0.6-1
0.3	Definition of $x_{n,1}$ and $x_{n,2}$	0.6-2
0.4	Edge force correction factors	0.6-3
0.5	Comparison of leading edge suction predicted by PAN AIR with theoretical results	0.6-4
0.6	Comparison of drag predicted by PAN AIR with theory for a delta wing in supersonic flow	0.6-5

## Preface to Release 1.1 of the PAN AIR Theory Document

The major changes that take place in this release of the PAN AIR Theory Document will be found in the technical appendices. These modifications reflect the following technology changes and enhancements that have been implemented since the initial publication of this document:

- o Two new design splines, "source design 2" and "doublet forward weighted" have been implemented (cf. appendices D and I).
- o A discontinuous source spline has been implemented for source analysis networks with the effect that total source strength on a network is more accurately conserved. Accurate conservation of total source strength causes the program to solve more reliably problems having fairly coarsely panelled curved surfaces (cf. appendix I).
- o The control point recession vectors have been modified. The most important modification has been to ensure that network corner control points are recessed along the bisectrix of the two adjacent network edges (cf. appendix G).
- o The algorithm that performs the abutment search has been substantially redesigned to improve its efficiency (appendix F).
- o The assignment of doublet matching conditions at abutment intersections has been completely reworked. The new procedure implements a graph theoretic interpretation of an abutment intersection and is substantially more reliable than the old procedure (cf. appendix F).
- o The computation of leading edge forces has been substantially improved by the implementation of correction factors that correct some discrepancies arising from the nonuniform convergence of the numerical solution as panel density is increased.
- o Added mass coefficients have been implemented.

The authors would like to acknowledge the efforts of the following individuals who provided significant contributions to the revisions of release 1.1:

D. T. Chiang, for his discussions of the automatic abutment search and the two new design splines,

R. T. Medan, for his discussion of edge forces, and

D. J. Purdon, for his discussions of control point locations and added mass coefficients.

In addition, we would like to thank Kathleen Crites and Bonnie Smith for their efforts on the typing and figure preparation of the revisions.

**Preceding Page Blank**

## 4.0 An Overview of PAN AIR

### 4.1 Historical Development of Panel Methods

In this section, we will discuss the features which distinguish PAN AIR from earlier, less complex, panel methods. These features are (a) "continuous geometry," (b) linear source and quadratic doublet variation, and (c) continuity of doublet strength. We will explain how these features make PAN AIR more accurate and reliable than previous methods, and discuss briefly the manner in which these items are implemented in PAN AIR.

Virtually every panel method approximates the configuration geometry with panels whose planform is a quadrilateral. Thus, if the panels themselves are planar, only a small class of configurations (such as cylinders and flat wings) can be described without gaps being left between panels. These gaps tend to be very small, except for highly twisted surfaces. In subsonic flow, the gaps cause little if any numerical error, but in supersonic flow the cumulative effect of the gaps is serious, not because of "leakage" of flow through the gaps, but because the doublet strength jumps abruptly from a non-zero value to zero at a panel edge which does not exactly meet the adjacent edge. In PAN AIR, gaps are closed by means of "piecewise flat" panels, that is, panels which are comprised of several planar regions.

Some panel methods use "curved" panels, generally paraboloidal in shape. These approximate the configuration surface far more accurately in regions of high curvature such as the leading edge of a wing, but necessarily have gaps, even though small ones. Thus they are excellent for the analysis of subsonic flow, but not for supersonic flow.

As we stated earlier, PAN AIR employs a linear source variation and a quadratic doublet variation. That is, the basis function  $b_j$  corresponding to a source parameter is locally linear, while the basis function corresponding to a doublet parameter is locally quadratic. This contrasts with earlier, simpler programs in which the doublet and source variations were locally constant.

The reasons behind the "higher order" singularity distributions in PAN AIR are discussed in detail in Appendix B.4. Briefly, they are as follows. Consider a control point on a panel, and assume the source and doublet distributions in the immediate neighborhood of the control point are polynomials. Then we show in Appendix B.4 that a source distribution locally of the form

$$\sigma(\xi, \eta) = \sum_{N=1}^{\infty} \sum_{i=0}^{2N} a_{i N}^S \xi^i \eta^{2N-i} \quad (4.1.1)$$

or a doublet distribution

$$\mu(\xi, \eta) = \sum_{N=1}^{\infty} \sum_{i=0}^{2N+1} a_{i N}^D \xi^i \eta^{2N+1-i} \quad (4.1.2)$$

does not induce any perturbation velocity locally. That is, even terms in the polynomial source distribution and odd terms in the doublet distribution do not generate a local perturbation velocity. So, since we have concluded that constant source and doublet strengths are insufficient, the next reasonable higher order approximation to use is linear source strength and quadratic doublet strength.

ORIGINATOR AND METHOD NAME (IF ANY)	YEAR	REF #	PANEL GEOMETRY	SOURCE TYPE	DOUBLET TYPE	BOUNDARY CONDITIONS	RESTRICTIONS	COMMENTS
HESS AND SMITH (DOUGLAS)	1962	4.1	FLAT	CONSTANT	NONE	SPECIFICATION OF NORMAL FLOW	NON-LIFTING WINGS AND BODIES ONLY	
RUBBERT (VORTEX LATTICE)	1964	4.2	FLAT	NONE	CONSTANT	NORMAL FLOW	PLANAR WINGS ONLY	
RUBBERT AND SAARIS (A-230)	1968	1.1	FLAT	CONSTANT	CONSTANT	NORMAL FLOW	NEARLY CONSTANT PANEL DENSITY	
WOODWARD	1968	1.2	FLAT	CONSTANT	LINEAR	NORMAL FLOW	WINGS MUST BE PLANAR	
HESS	1972	4.3	FLAT	CONSTANT	LINEAR	NORMAL FLOW	WINGS AND BODIES ONLY	
ROBERTS AND RUNDLE	1973	4.4	PARABOLOIDAL	QUADRATIC	QUADRATIC	NORMAL FLOW		NUMERICAL INTEGRATION - VERY EXPENSIVE
MERCER, WEBER AND LESFORD	1973	4.5	FLAT	NONE	SMOOTH, CUBIC/QUADRATIC	NORMAL FLOW IN LEAST SQUARES SENSE	PLANAR WINGS	SUBSONIC AND SUPERSONIC CUBIC SPANWISE, QUADRATIC CHORDWISE
MARINO AND KUO	1974	4.6	CONTINUOUS, HYPERBOLOIDAL	CONSTANT	CONSTANT	POTENTIAL	NO THIN CONFIGURATIONS	
JOHNSON AND RUBBERT	1975	4.7	PARABOLOIDAL	LINEAR	QUADRATIC	NORMAL FLOW		
EHLERS AND RUBBERT (MACH LINE PANELING)	1976	4.8	FLAT	LINEAR	CONTINUOUS QUADRATIC	NORMAL FLOW	PLANAR WINGS, SPECIAL PANELING	SUPERSONIC FLOW
EHLERS ET AL ("PILOT CODE")	1977	4.9	CONTINUOUS, PIECEWISE FLAT	LINEAR	CONTINUOUS QUADRATIC	ARBITRARY IN $\phi, \nabla\phi$		SUBSONIC AND SUPERSONIC
PAN AIR	1980		CONTINUOUS, PIECEWISE FLAT	LINEAR	CONTINUOUS, QUADRATIC	ARBITRARY IN $\phi, \nabla\phi$		SUBSONIC AND SUPERSONIC

Figure 4.1 - Historical Overview of Panel Methods



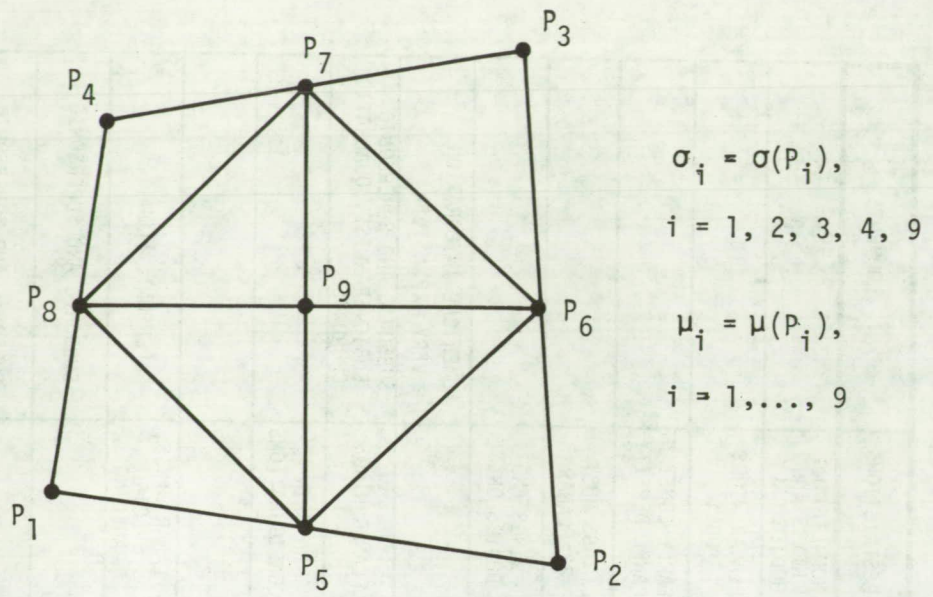


Figure 4.2 - Division of panel into subpanels.

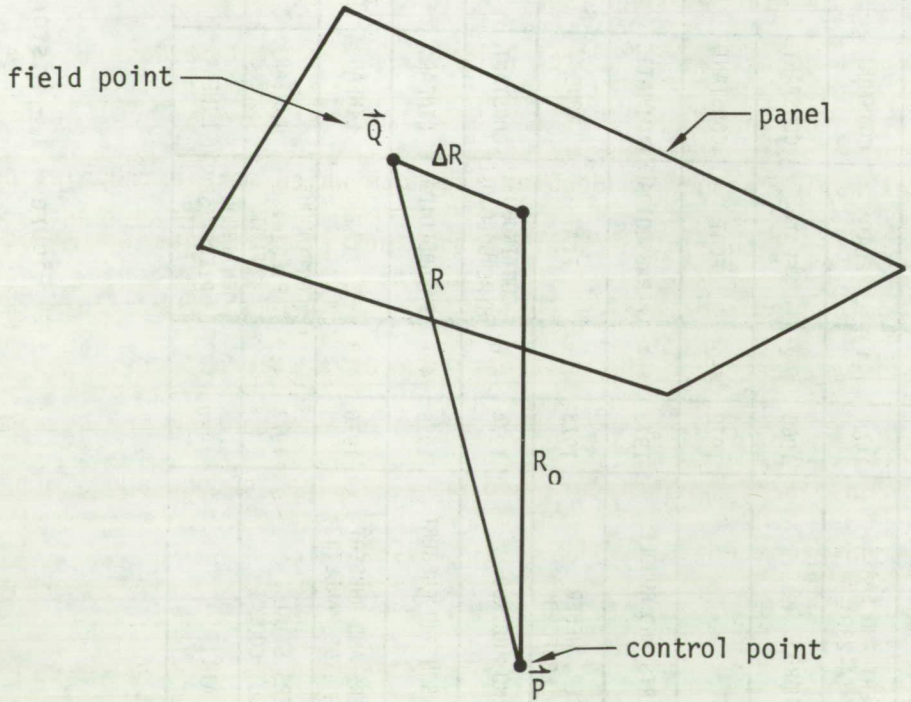


Figure 4.3 - Panel and far field control point

## 5.5 Singularity Splines

In this section we will discuss without details the construction of spline matrices for analysis and wake networks. The technical details of the spline construction, and all discussion of splines for design networks, will be reserved for Appendix I. In figure 5.13, we illustrate the locations of source parameters on a source analysis network, and the locations of doublet parameters on a doublet analysis or wake network.

Source parameters on analysis networks are located at panel centers only. Doublet parameters on analysis networks are located at panel centers and in addition along network edges as illustrated. The value of a source parameter is always the value of source strength at the parameter location, and similarly for a doublet parameter. The "extra" doublet parameters occur at those points at which an "extra" corner control point was stationed because of edge matching considerations (see figure 5.7). Doublet parameters are required on network edges (while source parameters are not) because of the quadratic variation of the approximation to the doublet strength. A quadratic variation causes rapid changes in doublet strength which make extrapolation of the doublet values from the interior of the network to the edges ill-advised. The source strength approximation is only linear, however. Finally, doublet parameters are only located on the upstream edge of a wake network. The doublet strength on a wake network is defined to be constant in the streamwise direction, and thus doublet parameters are only required on one edge in order to define the doublet strength on the entire network.

### 5.5.1 The Matrices $B^S$ and $B^D$

The outer spline matrices define the source strength and doublet strength at certain points on the panel as linear combinations of source and doublet parameters in the neighborhood of the panel. While a single doublet outer spline matrix has been found satisfactory for all purposes, it has been found that two source outer splines matrices are generally required. One of the source outer spline matrices helps define a continuous source distribution used in post processing applications, where it is essential for processing considerations that source strength be a uniquely defined function on a network. The other source outer spline matrix helps define a discontinuous source distribution used in AIC matrix construction, where it is important that the total source strength be accurately measured by the corresponding integral of the splined source distribution.

To be precise, consider the panel and network in figure 5.14. A source outer spline matrix  $B^S$  is a  $5 \times 9$  matrix which gives the value of source strength at  $P_1, P_2, P_3, P_4,$  and  $P_9$  in terms of the source parameters

$\{\lambda_i^S, i = 1, \dots, 9\}$  located at the nine panel centers marked by a circle. The matrix  $B^D$  is a  $9 \times 21$  matrix giving the values of doublet strength at  $P_1, \dots, P_9$  in terms of the doublet parameters  $\{\lambda_i^D, i=1, \dots, 21\}$  located at the 21 panel centers marked by an x. Because  $\mu$  is a continuous locally quadratic function whereas  $\sigma$  is only a locally linear function,  $\mu$  must be defined at 9 points on a panel by  $B^D$  while  $\sigma$  is only defined by 5 points by  $B^S$ . The values of  $\sigma$  at the 5 points are called "panel source parameters," while the values of  $\mu$  at the 9 points are called "panel doublet parameters."

### 5.5.2 Definition of SPSPL

The subpanel spline matrices (one source matrix SPSPL<sup>S</sup> and one doublet matrix SPSPL<sup>D</sup> for each of the eight triangular regions composing the panel) each define the coefficients of the polynomial distribution of singularity strength on the triangular region as a linear combination of the singularity strengths at the panel points P<sub>i</sub> mentioned above. Thus, on each triangular region, source and doublet strengths  $\sigma(\xi', \eta')$  and  $\mu(\xi', \eta')$  are defined in terms of local coordinates  $(\xi', \eta')$

$$\begin{aligned} \sigma(\xi', \eta') &= \sigma_0 + \sigma_\xi \xi' + \sigma_\eta \eta' \\ \mu(\xi', \eta') &= \mu_0 + \mu_\xi \xi' + \mu_\eta \eta' \\ &\quad + \frac{1}{2} \mu_{\xi\xi} \xi'^2 + \mu_{\xi\eta} \xi' \eta' + \frac{1}{2} \mu_{\eta\eta} \eta'^2 \end{aligned} \quad (5.5.1)$$

where the constants  $\sigma_0, \sigma_\xi, \sigma_\eta, \mu_0, \dots, \mu_{\eta\eta}$  are defined by the subpanel spline matrices:

$$\begin{Bmatrix} \sigma_0 \\ \sigma_\xi \\ \sigma_\eta \end{Bmatrix} = [\text{SPSPL}^S] \begin{Bmatrix} \sigma(P_1) \\ \sigma(P_2) \\ \sigma(P_3) \\ \sigma(P_4) \\ \sigma(P_9) \end{Bmatrix} \quad (5.5.2)$$

and

$$\begin{Bmatrix} \mu_0 \\ \mu_\xi \\ \vdots \\ \mu_{\eta\eta} \end{Bmatrix} = [\text{SPSPL}^D] \begin{Bmatrix} \mu(P_1) \\ \vdots \\ \mu(P_9) \end{Bmatrix} \quad (5.5.3)$$

### 5.5.3 Construction of B Matrices for Continuous Singularity Distributions

A B matrix associated with a continuous singularity distribution is constructed one row at a time. Each row defines the singularity strength at a panel corner, edge midpoint, or panel center in terms of surrounding singularity parameters. This identical row vector then becomes part of the B matrix of each panel which shares the particular grid point. This insures that the value of the singularity strength is identical as one approaches the grid point from the interior of any of the panels sharing it.

The source strength at a panel corner is obtained from the source singularity parameters located at the centers of the four panels sharing that corner, as illustrated in figure 5.15. The dependence of  $\sigma$  on  $\lambda_1, \dots, \lambda_4$  is determined by a bilinear fit procedure described in Appendix I.1. Essentially, this procedure determines what "bilinear" function (a bilinear function in two variables ( $\xi, \eta$ ) is a quadratic function which reduces to a linear function for constant  $\xi$  and  $\eta$ )

$$f(\xi, \eta) = a + b\xi + c\eta + d\xi\eta \quad (5.5.4)$$

is determined by the four values  $\lambda_i$ , and then sets  $\sigma_1$  to be the "value" the function takes at that point. By "value", we mean a row vector  $(a_1, a_2, a_3, a_4)$ , so that

$$\sigma_1 = [a_1 \ a_2 \ a_3 \ a_4] \begin{Bmatrix} \lambda_1 \\ \lambda_2 \\ \lambda_3 \\ \lambda_4 \end{Bmatrix} \quad (5.5.5)$$

regardless of the values of the  $\lambda_i$ 's.

Now, finding the row vector that describes the source strength at a panel center is very simple, since a source parameter is located there. To obtain a matrix  $B^S$  for a panel, we assemble the row vectors corresponding to the 5 grid points. Each row vector has length 4, but by adding zeros each row vector expands to length 9. Thus each row vector has one entry from each of the 9 source parameters in the neighborhood of the panel. While only four parameters lie in the neighborhood of a particular corner point, (cf. figure 5.14) nine parameters lie in the neighborhood of at least one of the panel corners. Collecting the five row vectors, we have the 5 x 9 matrix  $B^S$ , which was first introduced by equation (4.2.8).

Thus, for the panel in figure 5.14,

$$B^S = \begin{bmatrix} 0 & * & * & 0 & * & * & 0 & 0 & 0 \\ * & * & 0 & * & * & 0 & 0 & 0 & 0 \\ 0 & 0 & 0 & * & * & 0 & * & * & 0 \\ 0 & 0 & 0 & 0 & * & * & 0 & * & * \\ 0 & 0 & 0 & 0 & * & 0 & 0 & 0 & 0 \end{bmatrix} \quad (5.5.6)$$

where the columns of  $B^S$  are arranged according to the integer labels given to the source parameters in figure 5.14. Here, an asterisk denotes some generally non-zero entry.

The outer doublet spline matrix  $B^D$ , introduced in equation (4.2.9), is similarly constructed row by row. To obtain the row vector describing  $\mu$  at a panel corner, a least squares fit is used. As shown in figure 5.16,  $\mu(P)$  is obtained by finding the quadratic function  $\mu(\xi, \eta)$  which best goes through the 12 values  $\lambda_i^D$  at the 12 doublet parameter locations in the neighborhood of  $P$  in a weighted least squares sense (a quadratic function in two variables certainly can not go through 12 values exactly). The computation of the weights is discussed in Appendix I.1.2.4. The quadratic function thus obtained (its 6 coefficients are each row vectors of length 12, since they depend on the  $\lambda_i^D$ ) is evaluated at  $P$  to obtain  $\mu(P)$ . This weighted least squares procedure will be described in detail in Appendix I.5.

To obtain a row vector defining  $\mu$  at a panel edge midpoint, we again use a weighted least squares fit, though this time we only fit to 8 neighboring singularity parameters, as illustrated in figure 5.17. If the grid point lies near the network edge, a special treatment (which is described in Appendix I.1) is used.

#### 5.5.4 Construction of the Discontinuous Source Outer Spline Matrix

The discontinuous source outer spline matrix is constructed by means of a two stage process. First, a linear source distribution over the whole panel is determined in terms of the panel's neighboring source parameters  $\lambda_i^S$ ,  $i = 1, \dots, 9$  by means of a weighted least squares procedure. Second, this distribution is evaluated at the five points  $P_1, P_2, P_3, P_4, P_9$  to give the dependency of the five "panel source parameters" upon the neighboring source parameters  $\lambda_i^S$ .

This page has been left blank intentionally



It is the first step of this process that ensures that total source strength is accurately measured. This accuracy is achieved by the combination of the linear fit and the fact that the panel's own source parameter is heavily weighted in the least squares fitting procedure.

It is appropriate to observe here that although the discontinuous source outer spline is not explicitly constrained to be continuous, it is in fact very nearly continuous wherever the configuration is sufficiently finely panelled that the angle between adjacent panel normals is less than, say,  $10^\circ$ .

#### 5.5.5 Construction of SPSP

Next, let us consider the method by which the subpanel spline matrices define singularity distributions within a panel. In referring to the panel illustrated in figure 5.18, we will write  $\sigma_i$  for  $\sigma(P_i)$  and  $\mu_i$  for  $\mu(P_i)$ .

Recall that  $\sigma_1, \sigma_2, \sigma_3, \sigma_4$  and  $\sigma_9$  are defined in terms of neighboring source singularity parameters by the matrix  $B^S$ . We then define

$$\sigma_5 = \frac{1}{2} (\sigma_1 + \sigma_2) \quad , \quad \sigma_6 = \frac{1}{2} (\sigma_2 + \sigma_3) \quad , \quad \sigma_7 = \frac{1}{2} (\sigma_3 + \sigma_4) \quad , \quad \text{and} \quad \sigma_8 = \frac{1}{2} (\sigma_4 + \sigma_1) \quad .$$

We have now defined  $\sigma_i$  at all vertices of all 8 triangular regions, and we now define a linear distribution  $\sigma(\xi', \eta')_i$ ,  $i = 1, \dots, 8$  on each triangular region by specifying it to be the unique linear distribution to attain the appropriate values at the 3 vertices of the triangle.

in (5.9.9) over the combined surface  $S_1 \cup S_2$ , while in fact we only integrate the expression over  $S_1$ . The evaluation of the integral over  $S_2$ , the edge force, requires the use of some special extrapolation and correction techniques. The basic idea is to evaluate the limit in the expression for edge force, (cf. ref. 5.2);

$$\text{edge force per unit length} = (\pi/8)\beta_n \left[ \lim_{x_n \rightarrow 0} (\mu/\sqrt{x_n}) \right]^2$$

(here,  $\beta_n$  is an edge normal compressibility factor and  $x_n$  is the distance from the edge) by evaluating the expression  $(\mu/\sqrt{x_n})$  at panel centers near the edge. A correction factor is then applied to the result to account for some nonuniform convergence effects arising from the fact that PAN AIR does not allow  $\mu$  to behave like  $c\sqrt{x_n}$  in the neighborhood of the leading edge. For more details of the edge force computation, see appendix 0.

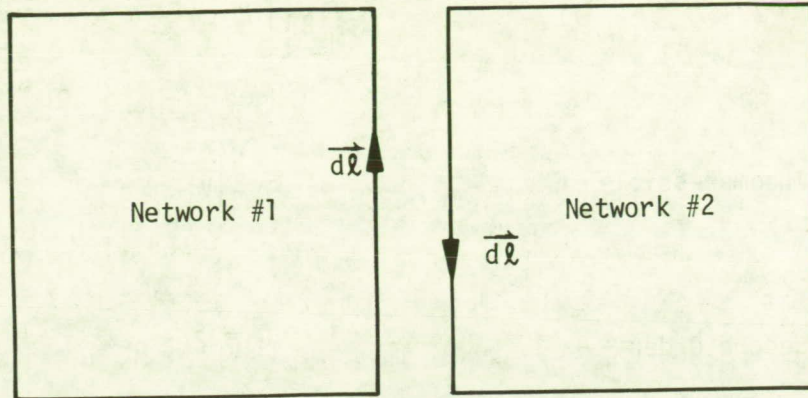


Figure 5.19 - Opposite orientations of adjacent networks

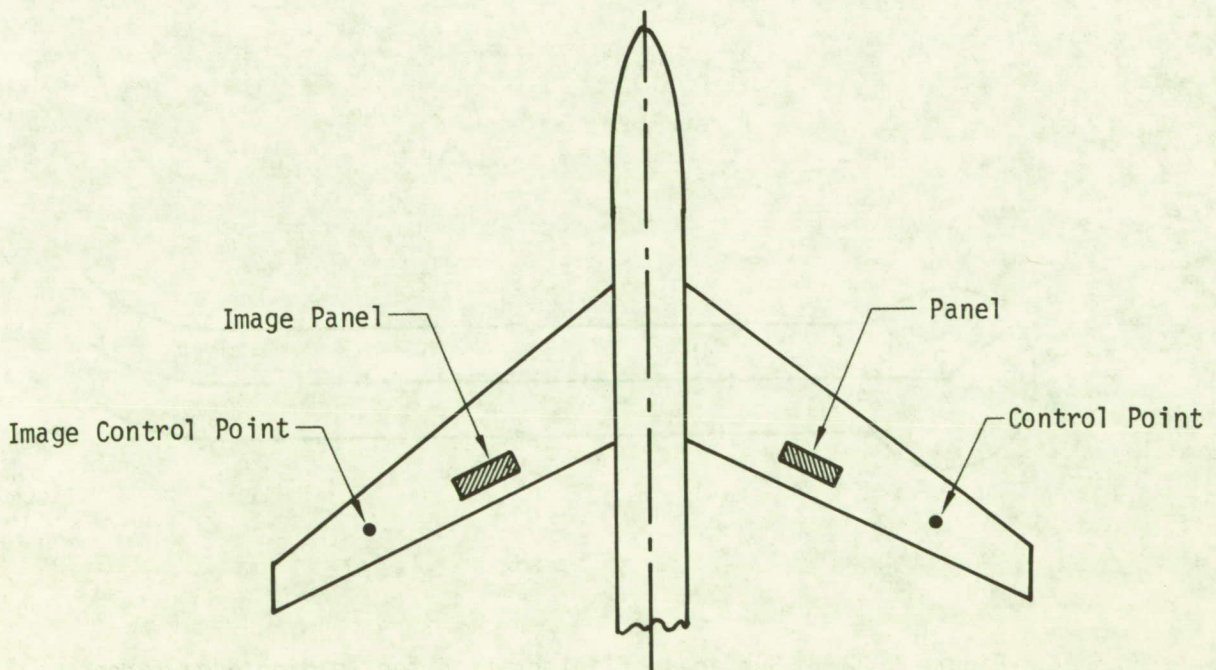


Figure 5.20 Configuration and image

<u>RULE</u>	$C_p$
Isentropic	$\frac{2}{\gamma M_\infty^2} \left\{ \left[ 1 + \frac{\gamma-1}{2} M_\infty^2 (1 -  \vec{V} ^2) \right]^{\frac{\gamma}{\gamma-1}} - 1 \right\}$ <p style="text-align: center;">used if <math>M_\infty &gt; .01</math></p>
Incompressible	$1 -  \vec{V} ^2$ <p style="text-align: center;">used if <math>M_\infty \leq .01</math></p>
Second Order	$1 -  \vec{V} ^2 + M_\infty^2 u$
Slender Body	$-(2u + v^2 + w^2)$
Linear	$-2u$
Reduced Second Order	$1 -  \vec{V} ^2$

Figure 5.21 Pressure coefficient rules

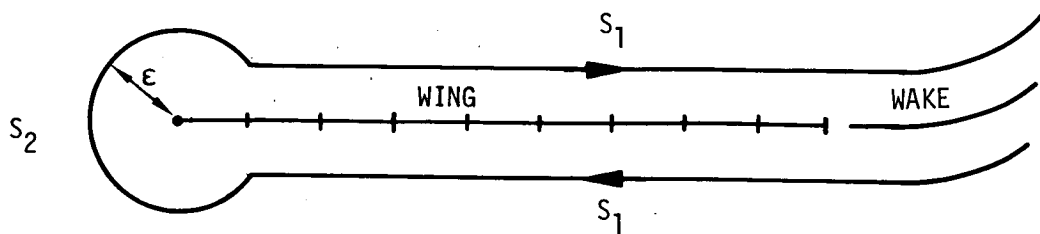


Figure 5.22 - Surfaces of integration for leading edge force

## 7.0 References

### PAN AIR Documents

PAN AIR - A Computer Program for Predicting Subsonic or Supersonic Linear Potential Flows about Arbitrary Configurations Using a Higher Order Panel Method.

Volume II, User's Manual (Version 1.0), by K. Sidwell, J. E. Bussoletti, and P. K. Baruah, NASA CR-3252, 1980.

Volume IV, Maintenance Document (Version 1.0), by P. K. Baruah, et. al., NASA CR-3254, 1980.

### Other References

- 1.1 Rubbert, P. E., and Saaris, G. R.: "Review and Evaluation of Three Dimensional Lifting Potential Flow Analysis Method for Arbitrary Configurations," AIAA paper 72-188, January 1972.
- 1.2a Woodward, F. A.: "Analysis and Design of Wing-Body Combinations at Subsonic and Supersonic Speeds," *Journal of Aircraft*, Vol. 5, No. 6, Nov.-Dec. 1968, pp. 528-534.
- 1.2b Woodward, F. A.: "An Improved Method for the Aerodynamic Analysis of Wing-Body-Tail Configurations in Subsonic and Supersonic Flow, Part I - Theory and Application," NASA CR-2228, Part I (1973).
- 1.3 Kellogg, O. D.: Foundations of Potential Theory, New York, Dover Publishing Company, 1953.
- 1.4 Liepmann, H. W., and Roshko, A.: Elements of Gasdynamics, New York, John Wiley and Sons, 1957.
- 1.5 Ward, G. N.: Linearized Theory of Steady High-Speed Flow, Cambridge University Press, 1955.
- 2.1 Landahl, M. T.: Unsteady Transonic Flow, Pergamon Press, 1961.
- 4.1 Hess, J. L., and Smith, A. M. O.: Calculation of Nonlifting Potential Flow About Arbitrary Three-Dimensional Bodies, ES40622, Douglas Aircraft Company, 1962.
- 4.2 Rubbert, P. E.: Theoretical Characteristics of Arbitrary Wings by a Nonplanar Vortex Lattice Method, D6-9244, The Boeing Company, 1964.
- 4.3 Hess, J. L.: Calculation of Potential Flow About Arbitrary 3-D Lifting Bodies, Douglas Report MDC-J5679-01, October 1972.
- 4.4 Roberts, A., and Rundle, K.: Computation of First Order Compressible Flow About Wing-Body Configurations, AERO MA No. 20, British Aircraft Corporation, February 1973.
- 4.5 Mercer, J. E., Weber, J. A., and Lesferd, E. P.: Aerodynamic Influence Coefficient Method Using Singularity Splines, NASA CR-2423, May 1974.

- 4.6 Morino, L. and Kuo, Ching-Chiang: "Subsonic Potential Aerodynamics for Complex Configurations: A General Theory," AIAA Journal, Vol, 12, No. 2, pp. 191-197, February 1974.
- 4.7 Johnson, F.T., and Rubbert, P. E.: "Advanced Panel-Type Influence Coefficient Methods Applied to Subsonic Flow," AIAA Paper 75-50, January 1975.
- 4.8 Ehlers, F. E., and Rubbert, P. E.: A Mach Line Panel Method for Computing the Linearized Supersonic Flow Over Planar Wings, NASA CR-152126, 1979.
- 4.9 Ehlers, F. E., Epton, M. A., Johnson, F. T., Magnus, A. E., and Rubbert, P. E.: A Higher Order Panel Method for Linearized Supersonic Flow, NASA CR-3062, 1979.
- 5.1 Lieblein, S. and Stockman, N. O.: "Compressibility Corrections for Internal Flow Calculations," Journal of Aircraft, Vol. 9, No. 4, pp. 312-313, April 1972.
- 5.2 Hancock, G. J., and Garner, H. C.: On the Application of Subsonic Linearized Wing Theory to Second-Order Forces and Moments, British Aeronautical Research Council Reports and Memoranda, No. 3758, 1975.
- B.1 Butter, D. J., Compressibility Corrections Used in Panel Methods, HSA-MAE-R-FDM-0039, British Aircraft Corporation, November, 1978.
- B.2 Johnson, F. T., Lu, P., Tinoco, E. N., and Epton, M. A.: An Improved Panel Method for the Solution of Three-Dimensional Leading Edge Vortex Flows, NASA CR-159173, 1979.
- B.3 Lass, H.: Vector and Tensor Analysis, New York, McGraw-Gill, 1950.
- F.1 Jones, R. T., and Cohen, D.: High Speed Wing Theory, No. 6, Princeton Aeronautical Paperbacks, Princeton, N. J., Princeton U. Press, 1960.
- F.2 Deo, N.: Graph Theory with Applications to Engineering and Computer Science, Prentice-Hall, 1974.
- J.1 Johnson, F. T.: A General Panel Method for the Analysis and Design of Arbitrary Configurations in Subsonic Flows, NASA CR-3079, 1979.
- J.2 Handbook of Mathematical Functions, M. Abramowitz and I. A. Stegun, editors, National Bureau of Standards, 1964.
- J.3 Robinson, A. "On Source and Vortex Distributions in the Linearized Theory of Steady Supersonic Flow," Quart. J. Mech. Appl. Math., I, pp. 408-432, 1948.
- I.1 Faddeeva, V. N.: Computational Methods in Linear Algebra, New York, Dover Publications.
- O.1 Ashley H. and Landahl, M.: Aerodynamics of Wings and Bodies, Addison - Wesley, 1965.

- 0.2 Medan, R. T.: Aerodynamic Loads Near Cranks, Apexes, and Tips of Thin, Lifting Wings in Incompressible Flow, AGARD-CP-204, 1976, No. 18.
- 0.3 Sidwell, K.: Added Mass Coefficients from the PAN AIR System, NCSC Document D180-24636-1, April 1978.

## D.1 Networks

A network is an array (with, say, M rows and N columns) of points in space which define a portion of the configuration geometry. In addition, source and doublet distributions are defined on the network (that is, the network is a "composite" network), with singularity parameter locations and spline methods determined by the network's "source type" and "doublet type".

### D.1.1 Network Types

The possible source types are "analysis", "source design 1," "source design 2," and "null", while the doublet types are "analysis", "doublet forward weighted," "design", "wake 1", "wake 2", and "null". Source and doublet analysis networks are used in conjunction with boundary conditions defining impermeability. Design networks are used in conjunction with "design" boundary conditions, that is, those which specify tangential velocity. Note that a "doublet forward weighted" network is really a doublet design network. A network of type "null" is used to denote that the source or doublet strength is zero; one could equally well use an analysis network in conjunction with the uniform boundary condition

$$\sigma = 0$$

or

$$\mu = 0$$

To model a wake, as described in section B.2, one would generally use a doublet wake network in conjunction with a source null network. The boundary conditions, which are only imposed at the wake leading edge, specify the matching of doublet strength on that edge to the doublet strength at the trailing edge of the adjacent wing network(s). In figures D.1 through D.3, we illustrate the singularity parameter locations corresponding to each of these network types.

### D.1.2 Wake Networks and the Kutta Condition

Two types of wake networks are available. In wake 1 networks, the doublet strength is variable along the leading edge, and constant in the indicially perpendicular direction. In wake 2 networks, the doublet strength is constant over the entire network. In the example of figure B.9, the wake extending behind the wing would generally be modeled with a wake 1 network, while the portion of the wake extending back from the body would be modeled with a wake 2 network.

The two types of wake networks have distinct purposes. The wake 1 network is PAN AIR's approach to satisfying the Kutta condition (see below), while the purpose of the wake 2 network is to carry over the doublet strength from the wing to the plane of symmetry.

The Kutta condition, which should hold at the trailing edge, is

$$\Delta C_p = 0 \quad (D.1.1)$$

where  $C_p$  is the pressure coefficient. If the freestream direction is the x direction, and the freestream has unit magnitude, then (cf. (C.1.5)) for a



thin wing, the linear expression for  $\Delta C_p$  is

$$\Delta C_p = -2 \frac{\partial \mu}{\partial x} \quad (D.1.2)$$

Now, the boundary conditions on the wake insure doublet continuity from the thin wing to the wake. In addition, it follows from section J.11 that the zero normal mass flux boundary conditions along the trailing edge of the wing insure the continuity of the x-component of the doublet gradient.

Now, the wake spline is such that the doublet strength is constant in the streamwise direction, that is,

$$\left. \frac{\partial \mu}{\partial x} \right|_{\text{wake}} = 0 \quad (D.1.3)$$

Since the normal mass flux boundary conditions insure matching of the doublet x-derivative, we have, in light of (D.1.2),

$$\left. \Delta C_p \right|_{\text{trailing edge of wing}} = 0 \quad (D.1.4)$$

Thus for a thin wing, the use of a wake 1 network results in the satisfaction of the Kutta condition, using the linear pressure coefficient formula. It is therefore natural to use the wake 1 network to satisfy the Kutta condition for a thick wing. This is done in PAN AIR, even in the absence of a theoretical justification of its validity.

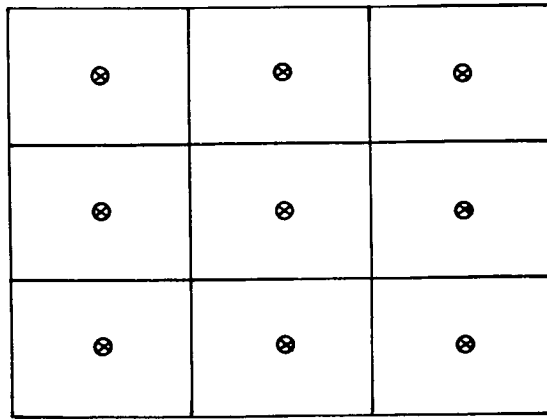
Wake 2 networks have a purpose which is not related to the Kutta condition. In figure B.9, we show a wake 1 network emanating from the wing trailing edge. Now, the body is not a lifting surface, and therefore one would not in general expect a panel method to require a wake emanating from the body. The wake 2 network is required in PAN AIR, however, because in its absence the doublet matching boundary conditions on the wake 1 network would drive the doublet strength to zero along its inboard edge.

Because the doublet strength on the wake is constant, the doublet gradient is zero, and thus the surface vorticity,  $\hat{n} \times \nabla \mu$ , is zero. This corresponds to the physics of the configuration; that is, the body "sheds" no vorticity.

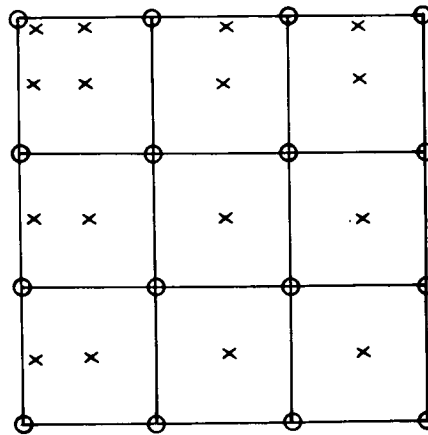
### D.1.3 Indexing

We now discuss the indexing system used internally in PAN AIR. The user specifies an array  $[CP(I,J)]$  of panel corner points, where  $I$ ,  $1 \leq I \leq M$ , is called the row index, and  $J$ ,  $1 \leq J \leq N$ , is called the column index. The upper surface is defined by an upward pointing unit normal  $\hat{n}$  whose direction is the vector cross product (direction of increasing column index)  $\times$  (direction of increasing row index). In figure D.4, we illustrate a network with  $\hat{n}$  pointing up from the paper. The network edges are labeled in counterclockwise fashion as shown, and each panel's corner points are similarly labelled in counterclockwise fashion. The point  $CP(1,1)$  is called the origin of the

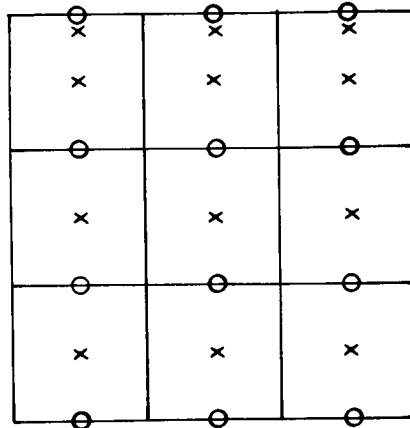
a. Source analysis network



b. Source design 1 network



c. Source design 2 network

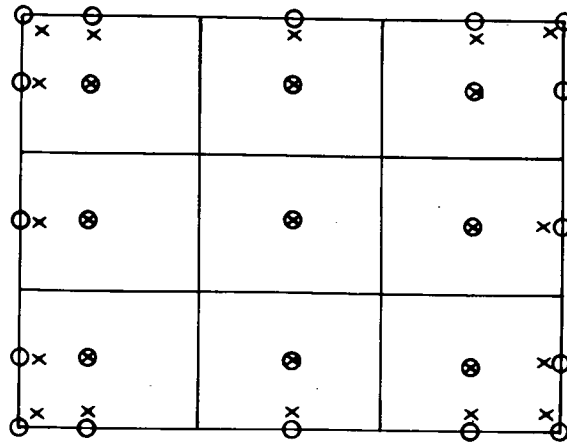


○ source parameter locations

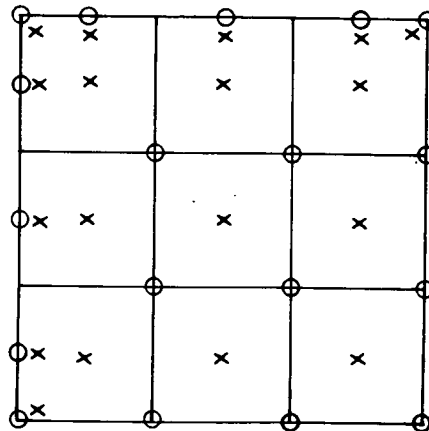
× locations of corresponding non-trivial boundary conditions

Figure D.1 - Locations of source singularity parameters

a. Doublet analysis, doublet forward weighted



b. Doublet design



○ doublet parameter locations  
 × boundary condition locations

Figure D.2 - Doublet analysis and design singularity parameter locations

### F.3 Automatic Abutment Search

In this section we describe the procedure used to identify "pairwise abutments." An edge segment  $S$  (the line connecting two adjacent boundary mesh points) is said to form a pairwise abutment with a network edge  $E$  provided the end points  $\vec{s}_-$  and  $\vec{s}_+$  of  $S$  satisfy  $d(\vec{s}_\pm, E) < \epsilon$  where  $\epsilon$  is some user specified tolerance distance. Here, distance from a point  $\vec{s}$  to an edge  $E$  is defined in the usual way,  $d(\vec{s}, E) = \min_{\vec{e} \in E} d(\vec{s}, \vec{e})$ .

The practical implementation of this definition requires that one know how to compute the distance from a point  $\vec{s} = \vec{s}_-$  or  $\vec{s}_+$  to an edge  $E$ . Let edge  $E$  consist of edge segments  $T_i$  connecting points  $\vec{t}_{i-1}$  and  $\vec{t}_i$ ,  $i = 1, 2, \dots, n$ . Then  $d(\vec{s}, E)$  is given by the formula

$$d(\vec{s}, E) = \min_{1 \leq i \leq n} d(\vec{s}, T_i) \quad (\text{F.3.1})$$

where the distance from a point to a line segment is given by

$$d(\vec{s}, T_i) = \begin{cases} |\vec{s} - \vec{t}_{i-1}| & (\vec{s} - \vec{t}_{i-1}, \vec{t}_i - \vec{t}_{i-1}) < 0 \\ |\vec{s} - \vec{t}_i| & (\vec{s} - \vec{t}_i, \vec{t}_i - \vec{t}_{i-1}) > 0 \\ \frac{|(\vec{s} - \vec{t}_{i-1}) \times (\vec{t}_i - \vec{t}_{i-1})|}{|\vec{t}_i - \vec{t}_{i-1}|} & \text{otherwise} \end{cases} \quad (\text{F.3.2})$$

Having clearly defined the concept of a pairwise abutment of an edge segment with an edge, we now describe what is meant by a pairwise abutment of an "edge portion" with an edge. First, by "edge portion" we mean a subset  $P$  of some network edge consisting of contiguous edge segments,  $S_k, \dots, S_1, \dots, S_m$ . The edge portion  $P$  then, forms a pairwise abutment with  $E$  provided each of the edge segments  $S_1$  does. If the situation illustrated in figure F.4 occurs, several pairwise abutments of edge portions  $P, Q, R$  with edge  $E$  will be defined. There are, however, limitations on the permissibility of configurations of the form of figure F.4. These limitations are noted in the User's Manual, sec. B.3.5.

Clearly the process of determining all pairwise abutments requires a large amount of computation for a configuration with many networks. (The amount of work is proportional to  $N_{ES}^2$  where  $N_{ES}$  is the number of edge segments in the configuration.) In PAN AIR this computational effort is reduced by avoiding the computation of the distances  $d(\vec{s}_\pm, E)$  whenever the edge of which  $S$  is a segment is sufficiently far away from  $E$  that a pairwise abutment is impossible.

This page has been left blank intentionally.

#### F.4 Doublet Matching Along Abutments

The purpose of doublet matching boundary conditions is to ensure that equation (F.1.1) holds at every point along an abutment, even though a boundary condition of this form is imposed at only a finite number of points. In this section we discuss the enforcement of the doublet matching condition at control points along the interior of the abutment while the enforcement of doublet matching at the ends of an abutment is treated in section F.5.

The ability of a finite number of boundary conditions to cause doublet matching along the full abutment depends directly on the splining techniques used to define the doublet strength along network edges. We discuss this subject in section I.1.2.5, but we will summarize here the results we derive there.

Given any pair of network edges belonging to an abutment, we call the first edge a refinement of the other if, at every point where a panel corner is located on the second edge, a panel corner is also located on the first edge. According to this definition, each network edge in figure F.5 is a refinement of the other, while in figure F.6, edge 1 is a refinement of edge 2.

We show in section I.1.2.5 that if an abutment contains edges  $E_1, \dots, E_n$ , and some edge  $E_k$  is a refinement of each of the other  $(n-1)$  edges of the abutment, then doublet matching can be forced to take place along the entire abutment provided it occurs at the endpoints of the abutments, and at the panel edge midpoints on edge  $E_k$ . In practice, precise doublet matching will not occur because PAN AIR uses a "least squares" rather than a differentiable edge spline (see section I.1.2.5). The extent to which doublet matching fails to occur is very small, and has been found experimentally to be negligible.

The program takes into consideration the above results when assigning one edge of an abutment to be the "matching edge", that is, the edge at whose panel edge midpoints doublet matching boundary conditions are imposed. Thus, when no special considerations intervene, the edge with the densest paneling is assigned to be the matching edge. Assuming that the program user has in fact provided one edge in the abutment which is a refinement of all the other edges, then that edge is clearly the most densely paneled edge, and so doublet matching will occur.

Under certain circumstances, the program does not assign the most densely paneled edge in the abutment as the matching edge. The first such case arises from a matching edge of a doublet design or doublet wake network taking part in the abutment.

Unlike doublet analysis networks, design and wake networks are asymmetric; boundary conditions are only imposed along certain edges of these networks, called matching edges, as illustrated in figures D.2 and D.3. When a matching edge of a design or wake network belongs to an abutment, the program assigns it to be the matching edge for the abutment, even if it is not the most densely paneled edge. This is done mostly for convenience; the user is not likely to know what boundary condition to impose at the control points along the matching edge and so the program evades this dilemma by assigning doublet matching boundary conditions there.

The other circumstances under which the most densely paneled edge is not chosen as the matching edge is illustrated in figure F.7. To be specific, whenever the curve defined by an abutment is "supersonic" (that is, no point on the edge is in the domain of dependence of any other point), then that network edge which is a leading edge (that is, upstream of the remainder of the network) is assigned as a matching edge.

The basis for this assignment is largely empirical. Experience with the PAN AIR "pilot code" with the configuration shown in figure F.8a, illustrates the need for imposing doublet matching on the leading supersonic edges of networks in supersonic flow. When doublet matching was imposed along the trailing edges of networks 1, 2, and 3, the solution was completely erratic, while shifting the matching boundary conditions to the leading edges of networks 4, 5, and 6 resulted in a solution which was physically reasonable.

The reasons for the numerical problems resulting from the assignment of matching edges as shown in figure F.8a are not precisely known. It is known, however, that specification of normal mass flux in a two-dimensional, linearized, planar, supersonic flow problem is equivalent to specification of the doublet gradient. We may see this by combining equation (C.1.5), which states that  $\Delta C_p$  is proportional to  $\partial \mu / \partial x$ , with equations (11-1) and (11-3) of reference F.1, which states that  $\Delta C_p$  is proportional to normal mass flux.

Thus for a two-dimensional configuration, the specification of zero normal mass flux at panel center points, in combination with doublet matching at the trailing edge, is equivalent to the situation in figure C.10, with the trailing edge boundary condition becoming specification of  $\mu$ . But this set of boundary conditions, in conjunction with the doublet analysis spline, does not have a unique solution. We see this by noting that the doublet distribution  $\mu_0(x)$  shown in figure F.8b satisfies  $\mu = 0$  at the leading and trailing edges, and  $\partial \mu / \partial x = 0$  at panel centers. Thus, if some solution  $\mu(x)$  exists which satisfies the boundary conditions above, so does  $\mu(x) + \alpha \mu_0(x)$  for all real numbers  $\alpha$ . Thus it is not permissible to specify  $\mu$  at the trailing edge of a two-dimensional network on which normal mass flux is specified at panel centers.

Of course, the configuration in figure F.8a is not a two-dimensional one. Nevertheless, it seems to have enough resemblance to a two-dimensional configuration that the imposition of doublet strength specification on the trailing edge of networks 1, 2, and 3 is an unstable boundary condition specification for the doublet analysis network spline in use on those networks.

Summarizing, PAN AIR selects the network edge to be used for doublet matching along an abutment according to the following criteria:

- (i) Matching edge of a doublet design network
- (ii) Matching edge of a doublet wake network
- (iii) If neither (i) nor (ii) occur, and the abutment is supersonic, the leading edge of the most "downstream pointing" network is used.
- (iv) If none of the above occur, the most densely panelled network edge is selected for matching.

Thus, to insure precise doublet matching, a program user must be sure, for every abutment containing a matching edge of a doublet design or wake network, that this edge is a refinement of all the other network edges. Similarly, if the abutment contains a supersonic edge, the leading edge of the most downstream pointing network must be a refinement of the others. Finally, in all other cases, some edge must be a refinement of all the others (recall that, if two edges have identical paneling, each is a refinement of the other).

If these rules are followed, the edge chosen by the program as the matching edge will in fact always be the most densely paneled one, so precise doublet matching will occur. This does not necessarily mean that minor violations of the rules will be serious. For instance, in figure F.9 (ignoring the gap - filling panels for the moment), the edge of the network A is not quite a refinement of the edge of network B. There is no reason to believe, however, that the doublet discontinuities which result from the small discrepancies in figure F.9 are significant.

Next we must discuss the complications introduced into the above procedure by considerations of symmetry. Fortunately, these are few and simple. First, we must recognize that either all of an abutment lies on a plane of symmetry or else no portion of it lies on a plane of symmetry - an abutment cannot partially abut a plane of symmetry. If a network edge lies on a plane of symmetry along part of its length and then breaks away, PAN AIR will recognize two abutments and place an extra control point at the network course grid point at which the breakaway takes place.

Now when an abutment lies on a plane of symmetry, doublet matching along that abutment takes place automatically whenever the potential is symmetric with respect to that plane of symmetry. Consequently we find in PAN AIR that abutment doublet matching conditions are imposed only on selected symmetry conditions when the abutment lies on a plane of symmetry. These are given:

- o If an abutment lies on the 1st plane of symmetry, impose edge matching on  $\hat{\phi}^{AS}$ ,  $\hat{\phi}^{AA}$  only.
- o If an abutment lies on the 2nd plane of symmetry, impose edge matching on  $\hat{\phi}^{SA}$ ,  $\hat{\phi}^{AA}$  only.
- o If an abutment lies on both planes of symmetry impose edge matching on  $\hat{\phi}^{AA}$  only.

(Remark: The various symmetrized potentials,  $\hat{\phi}^{SS}$ ,  $\hat{\phi}^{AS}$ , etc., are defined as follows. The superscripts S or A indicate whether the given function is symmetric or antisymmetric in a particular plane of symmetry. The first (second) superscript indicates the function's symmetry property with respect to the first (second) plane of symmetry.)



This page has been left blank intentionally.

## F.5 Abutment Intersections

Within the interior of an abutment, the equation

$$\sum s_j \mu_j = 0 \quad (\text{F.5.1})$$

can easily be imposed by assigning a particular edge as the matching edge, and imposing (F.5.1) at the panel edge midpoints on this edge.

At abutment intersections, points where two or more abutments meet, (see figure F.10), the choice of points at which to impose (F.5.1) becomes more difficult. Only one matching boundary condition may be imposed at a network corner point (since only one control point is located there), yet the corner point lies at the end of two distinct abutments. We will say that a corner point C is "assigned" to an abutment A if the boundary condition imposed at C is doublet matching across A.

A second complication is the danger of overspecification. Consider the abutment intersection, formed by four networks, illustrated in figure F.10. Let us define  $\mu_j$  to be the doublet strength at the corner of network  $N_j$  at this intersection. In order to obtain doublet matching, we require

$$\mu_1 = \mu_2 = \mu_3 = \mu_4 \quad (\text{F.5.2})$$

But these are only three equations. Thus, if we assign corner point  $C_1$  to abutment  $A_1$ ,  $C_2$  to  $A_2$ , and  $C_3$  to  $A_3$ , that is, impose the boundary conditions

$$\begin{aligned} \mu_1 &= \mu_2 \text{ at } C_1 \\ \mu_2 &= \mu_3 \text{ at } C_2 \\ \text{and } \mu_3 &= \mu_4 \text{ at } C_3 \end{aligned} \quad (\text{F.5.3})$$

we have satisfied (F.5.2). If we were to assign corner point  $C_4$  to abutment  $A_4$  in addition, the resulting boundary condition

$$\mu_4 = \mu_1 \text{ at } C_4 \quad (\text{F.5.4})$$

would be redundant, since it follows from (F.5.3). If a row of the AIC matrix corresponding to (F.5.4) were generated, the resulting matrix would therefore be singular, since this row would be a linear combination of three rows corresponding to (F.5.3).

Thus overspecification must be avoided if the program is to provide a numerical solution to the potential flow problem. This is straightforward for any reasonable example, but clearly the program must follow a well-defined method which assigns corner points to abutments in such a manner that doublet matching occurs at all abutments while no overspecification occurs. As an example, the abutment intersection in figure F.11 may arise from a realistic airplane configuration, yet an automatic procedure assigning corner points to abutments is not obvious. In this section, then, we will describe a graph theoretic interpretation of this abutment intersection problem together with the corresponding solution of this problem. This will be accomplished in two phases. In section F.5.1 we will describe the graphical representation of an

abutment intersection in the "usual case" together with the corresponding abutment assignment procedure. Following this, in section F.5.2 we will outline those special features supported by PAN AIR that affect abutment assignment together with the modifications to the basic assignment procedure that enable PAN AIR to correctly implement those special features.

### F.5.1 Graphical Representation of an Abutment Intersection

In figures F.10, F.11 and F.12 we present diagrams for three examples of abutment intersections. We will denote by  $P_{AI}$  (the abutment intersection point), the point at which the various abutments meet. The directed graph  $G$  associated with the abutment intersection is constructed as follows.

Let a small sphere  $S$  be constructed with  $P_{AI}$  as its center. The nodes of  $G$  are to be identified with the points at which the various abutments pierce  $S$ . The branches of  $G$  are to be identified with the lines on  $S$  along which the various networks involved in the abutment intersection cut the surface of  $S$ . An orientation (direction) for a branch/line is induced in a natural way by the orientation of the network that generates it. To see how this is done, let  $N$  be a network that is involved in the abutment intersection and let  $L_N (= N \cap S)$  be the line along which  $N$  cuts  $S$ . Denote by  $N'$  the subsurface of  $N$  that lies outside of  $S$ . Notice that the line  $L_N$  is part of the boundary of  $N'$ . Now since  $N'$  is a subsurface of  $N$ , the orientation of  $N$  provides an orientation for  $N'$ . An orientation for  $N'$  in turn provides an orientation (that is, a direction of traversal) for the boundary of  $N'$ . This traversal direction is, of course, the usual counterclockwise traversal of the boundary when the network is viewed from above. If then, one traces the boundary of  $N'$  in the traversal direction provided by its orientation, part of the trace will move along the line  $L_N$  in a unique direction. This direction is the orientation of  $L_N$ . If we denote the abutment at the beginning of the line  $L_N$  by  $A_N^-$  and the abutment at the end by  $A_N^+$ , then we say that the branch induced by network  $N$  points from node/abutment  $A_N^-$  to node/abutment  $A_N^+$ .

The procedure given above generates a directed graph  $G$  lying on the sphere  $S$ . Such a graph can be spread out on a plane simply by puncturing  $S$  at some point that does not lie on the graph and then stretching the surface  $S$ , with the graph  $G$  imbedded in it, out onto a plane.

The graphs generated by the abutment intersections of figures F.10, F.11 and F.12 are drawn in figure F.13.

An alternative (and consistent) interpretation of branch orientation is possible if, as is usually the case, the abutment intersection point  $P_{AI}$  coincides with a corner point of network  $N$  lying at the last point of edge  $k_N^-$  and at the first point of edge  $k_N^+$  (\*). When this happens, we denote by

\* Remark: Usually it will happen that  $k_N^+ = k^*$  where  $k^* = \text{mod}(k_N^-, 4) + 1$ . However if edge  $k^*$  is a collapsed edge of network  $N$ , we will have  $k_N^+ = \text{mod}(k_N^- + 1, 4) + 1$ .

$A_N^-$  the abutment in which edge  $k_N^-$  participates and by  $A_N^+$  the abutment in which  $k_N^+$  participates. Having done this, we say that branch/network N proceeds from node/abutment  $A_N^-$  to node/abutment  $A_N^+$ .

Once the directed graph representing an abutment intersection has been constructed, it is quite an easy matter to write down all of the doublet matching conditions of the form (F.5.1) associated with the abutments in the abutment intersection. Given a node/abutment A, we compute the values  $s_i$  associated with the doublet matching condition according to the following rules:

$$s_i = \begin{cases} +1 & \text{if branch/network } N_i \text{ is directed away from A} \\ -1 & \text{if branch/network } N_i \text{ is directed toward A} \\ 0 & \text{if branch/network } N_i \text{ is not connected to A} \end{cases} \quad (\text{F.5.5})$$

Using these rules, together with the graphs provided by figure F.13, we obtain the following sets of matching conditions

Figure F.10

$$\begin{array}{l} A_1: \quad + \mu_1 \quad - \mu_2 \quad = 0 \\ A_2: \quad \quad + \mu_2 \quad - \mu_3 \quad = 0 \\ A_3: \quad \quad \quad + \mu_3 \quad - \mu_4 \quad = 0 \\ A_4: \quad - \mu_1 \quad \quad \quad + \mu_4 \quad = 0 \end{array} \quad (\text{F.5.6})$$

Figure F.11

$$\begin{array}{l} A_1: + \mu_1 \quad - \mu_2 \quad - \mu_3 \quad = 0 \\ A_2: \quad \quad \quad + \mu_3 \quad - \mu_4 \quad - \mu_6 \quad = 0 \\ A_3: \quad \quad \quad \quad \quad \mu_4 \quad + \mu_5 \quad = 0 \\ A_4: \quad \quad \quad \quad \quad \quad \quad + \mu_6 \quad - \mu_7 \quad = 0 \\ A_5: \quad \quad + \mu_2 \quad \quad \quad - \mu_5 \quad \quad \quad = 0 \\ A_6: - \mu_1 \quad \quad \quad \quad \quad \quad \quad + \mu_7 \quad = 0 \end{array} \quad (\text{F.5.7})$$

Figure F.12

$$\begin{array}{l} A_1: \quad \mu_1 \quad - \mu_2 \quad + \mu_3 \quad = 0 \\ A_2: \quad \quad \quad \mu_2 \quad \quad \quad = 0 \\ A_3: \quad \quad \quad - \mu_3 \quad + \mu_4 \quad = 0 \\ A_4: \quad - \mu_1 \quad \quad \quad - \mu_4 \quad = 0 \end{array} \quad (\text{F.5.8})$$

(The reader is urged to verify the correctness of these matching conditions by carefully re-examining the original figures).

The matching conditions given above have been written down in a format such that they can be readily re-expressed in the shorthand form

$$A(G) \mu = 0 \quad (F.5.9)$$

where  $\mu$  is the vector of doublet values associated with the branches/networks of the graph and  $A(G)$  is called the incidence matrix associated with a directed graph  $G$ . For the three graphs given in figure F.13, the incidence matrices are

Fig. F.13a

$$A(G) = \begin{bmatrix} 1 & -1 & 0 & 0 \\ 0 & 1 & -1 & 0 \\ 0 & 0 & 1 & -1 \\ -1 & 0 & 0 & 1 \end{bmatrix} \quad (F.5.10)$$

Fig. F.13b

$$A(G) = \begin{bmatrix} 1 & -1 & -1 & 0 & 0 & 0 & 0 \\ 0 & 0 & 1 & -1 & 0 & -1 & 0 \\ 0 & 0 & 0 & 1 & 1 & 0 & 0 \\ 0 & 0 & 0 & 0 & 0 & 1 & -1 \\ 0 & 1 & 0 & 0 & -1 & 0 & 0 \\ -1 & 0 & 0 & 0 & 0 & 0 & 1 \end{bmatrix} \quad (F.5.11)$$

Fig. F.13c

$$A(G) = \begin{bmatrix} 1 & -1 & 1 & 0 \\ 0 & 1 & 0 & 0 \\ 0 & 0 & -1 & 1 \\ -1 & 0 & 0 & 1 \end{bmatrix} \quad (F.5.12)$$

Having expressed the doublet matching conditions at an abutment intersection in terms of an incidence matrix  $A(G)$  for the directed graph  $G$  describing the abutment intersection, we are now in a position to avail ourselves of the many powerful results from graph theory. In fact, graph theory not only provides theorems that yield much information about the structure of abutment intersections, it also provides a number of powerful algorithms that, when suitably tailored, generate the doublet-matching boundary condition assignments required by PAN AIR. The standard reference for all graph theoretical results quoted in this appendix will be ref. F.2, N. Deo, "Graph Theory with Applications to Engineering and Computer Science." Throughout the remainder of this appendix, it is assumed that the reader has at least a nodding familiarity with the elements of graph theory.

The first result from graph theory that we shall need is given (cf. THEOREMS 7-2 and 9-6, ref. F.2)

Theorem\* Let  $G$  be a connected directed graph containing  $n$  nodes and having incidence matrix  $A(G)$ . Then  $\text{rank}(A(G)) = n-1$ . Furthermore, any set of  $n-1$  rows selected from  $A(G)$  is a linearly independent set.

\* For the reader familiar with electrical circuit theory, this result is equivalent to the result that for a connected circuit with  $n$  nodes, the Kirchoff current law provides  $n$  relations, any  $n-1$  of which are linearly independent.

This result can be extended to directed graphs  $G$  that are not connected by observing that any such graph can be written as the union of connected components. Thus, for a graph  $G$  with  $k$  components, we write

$$G = \bigcup_{i=1}^k G_i \quad (\text{F.5.13})$$

The theorem can now be applied individually to each component  $G_i$ . In fact, whenever  $G$  is not connected, PAN AIR performs doublet-matching assignments by treating separately each component  $G_i$  of  $G$ . Consequently, to simplify the discussion, we shall always assume in what follows that the graph  $G$  associated with an abutment intersection is a connected graph.

We now turn to the problem of assigning doublet matching conditions (nodes) to replace user specified boundary conditions at control points lying on a network (branch) involved in the abutment intersection. At this point we treat just the simple "usual case" characterized by the following conditions:

- (i) the graph  $G$  associated with the abutment intersection is connected,
- (ii) each branch/network in the graph has a doublet distribution,
- (iii) each branch/network in the graph has a control point available for use as a doublet matching control point whose hypothetical location is essentially coincident with the abutment intersection point  $P_{AI}$ .

When these assumptions are made, the following procedure ensures that  $n-1$  abutment matching conditions are selected to replace user specified boundary conditions on  $n-1$  networks

- A.1 Form a spanning tree  $T \subseteq G$ .  $T$  must contain all of  $G$ 's nodes but have no loops. (Remark: By a theorem of graph theory,  $T$  will contain  $(n-1)$  branches.)
- A.2 Select any node of  $G(T)$  and label it as the ground node.
- A.3 Defoliate  $T$  by removing one branch at a time until all  $(n-1)$  branches have been removed. Algebraically, this is accomplished by constructing a sequence of trees  $T = T_n \supseteq T_{n-1} \supseteq \dots \supseteq T_1$  where  $T_j$  is obtained from  $T_{j+1}$  by finding a node of degree 1 in  $T_{j+1}$  (not the ground node), and removing that node and the single branch to which it is attached. As this is done, the doublet matching condition associated with the node is assigned to replace a user boundary condition on the network associated with the branch.

In figure F.14 we illustrate the application of this procedure to the graph given by figure F.13b.

## F.5.2 Modifications to the Abutment Assignment Procedure

The many special features supported by PAN AIR, especially those features associated with symmetry, add considerable complication to the basic algorithm for performing doublet matching at abutment intersections. In addition to symmetry, the most significant complicating features are,

- (i) an edge of a network may be marked "no doublet edge matching" by the user.
- (ii) a network's corner control point may be a "non-matching corner point" in the sense that there is no boundary condition (i.e., AIC row) associated with the corner control point that might be replaced with a doublet matching condition.

This presentation of our response to these complications will consist of three parts. First, we will describe some of the general considerations that must be taken account of. Second, we will outline the numerous ways by which symmetry, "no-doublet edge matching" and "non-matching corner points" affect the properties of networks, corner control points, user boundary conditions, edges, abutments and abutment intersections. Third we will describe the algorithm employed by PAN AIR that produces a consistent set of doublet matching assignments while satisfying the constraints imposed by PAN AIR's special program features.

### General Considerations

In addressing the problem of symmetry, we adopt the fundamental point of view of formulating separately the boundary value problems for the various symmetric and antisymmetric parts of the perturbation potential. Thus, when two planes of geometric symmetry are present, four symmetrized potentials ( $\hat{\phi}^{SS}$ ,  $\hat{\phi}^{AS}$ ,  $\hat{\phi}^{AA}$ ,  $\hat{\phi}^{SA}$ , see appendix K for definitions) will generally be required and a separate boundary value problem will be formulated for each. If an abutment intersection lies away from any plane of symmetry, doublet matching assignments will be the same for all symmetry conditions and indeed will be the same as if no symmetry were present at all. On the other hand, if the abutment intersection point lies on a plane of symmetry, doublet matching assignments will be performed separately for each symmetry condition and it becomes important to know the following facts about the abutment intersection:

- o which plane(s) of symmetry the abutment intersection point lies on,
- o which plane(s) of symmetry the individual abutments lie on,
- o which (if any) plane of symmetry an individual network may lie in. (N.B. A network is said to lie in a plane of symmetry if all its points lie on the plane of symmetry so that the network normal is parallel to the plane of symmetry normal.)

The first of these facts must be known in order to determine which planes of symmetry are active, in the following sense: the first (second) plane of symmetry is said to be active if  $P_{AI}$  lies on the first (second) plane of symmetry and the symmetry condition under consideration is either  $\hat{\phi}^{SS}$  or  $\hat{\phi}^{SA}$  (for the second plane of symmetry:  $\hat{\phi}^{SS}$  or  $\hat{\phi}^{AS}$ ). This information is important for two reasons.

First, for an abutment lying in an active plane of symmetry, doublet matching is automatically satisfied by virtue of the symmetry properties of the symmetrized potentials. Consequently, a doublet matching condition is never explicitly imposed for an abutment lying on an active plane of symmetry. Second, the doublet distribution on a network lying in an active plane of symmetry is identically zero so that such networks do not participate at all in the assignment of doublet matching conditions.

### Other Significant Considerations

Here we outline the ways in which the properties of networks, corner control points, etc. are modified by PAN AIR program features. In addition we will discuss briefly the mechanisms by which modifications take place.

#### Properties of Networks

- o A network may lie in a plane of symmetry. A network will lie in a plane of symmetry if (i) the user explicitly informs PAN AIR of this fact in the program input, or (ii) by examination of the network's mesh points PAN AIR determines that all points on the network are closer than the geometric tolerance distance to a plane of symmetry.
- o The program user will assign to each network one of the following network doublet types:

Doublet Analysis	(DA)
Doublet Design 1	(DD1)
Doublet Forward Weighted	(DFW)
Doublet Wake 1	(DW1)
Doublet Wake 2	(DW2)
No Doublet	(NOD)

Only those networks not marked "no doublet" are of interest when one is analyzing doublet matching at an abutment intersection.

- o If a network's doublet type is not "no doublet", the user may specify the doublet value at all control points. Even if this specification is  $\mu = 0$ , such networks are treated differently from "no doublet" networks in the sense that these networks are always involved in doublet matching along abutments and at abutment intersections. In particular, the abutment intersection processing may replace a specified doublet boundary condition with a doublet matching condition.

#### Properties of Corner Control Points

- o A corner control point may be a "matching corner point" in the sense that no user specified boundary condition is available to generate an AIC row that has been reserved for the control point. Thus, the control point must have a doublet matching condition assigned to it. A "matching corner point" is any corner control point of the following types:
  - (i) any corner control point lying on the matching edge of a DW1 network. This includes corners 1 and 2 as well as any extra control points along the matching edge.



- (ii) the matching corner control point of a DW2 network
  - (iii) any corner control point lying on edges 1 and 4, the "doublet matching" edges, of a DD1 network.
  - (iv) an extra control point on a DA, DD1 or DFW network as long as that edge is not marked "no doublet edge matching."
- o A corner control point may be a "no matching corner point" in the sense that no AIC row has been reserved for any boundary condition associated with that control point. Control points of this type include:
- (i) corner points 3 and 4 of DW1 networks
  - (ii) corner points 2, 3 and 4 of DW2 networks
  - (iii) corner point 3 of DD1 networks
  - (iv) any extra control point on an edge that is marked with either "no doublet edge matching" (a user specification) or "non-matching edge" (edges 2, 3 and 4 of DW1 networks; all edges of DW2 networks and edges 2 and 3 of DD1 networks)
  - (v) a regular corner control point (that is, one that has an AIC row reserved for it) for which both adjacent edges are marked "no doublet edge matching."
- o A corner control point is said to lie on a plane of symmetry if its hypothetical location lies on a plane of symmetry. It is possible for a control point to lie on two planes of symmetry.
- o A corner control point is said to lie in a plane of symmetry if it lies on a plane of symmetry and, in addition, the panel normal at the control point is parallel to the plane of symmetry's normal. (In PAN AIR, the only control points that lie in a plane of symmetry are the control points on networks that themselves lie in a plane of symmetry.)
- o A corner control point always has associated with it two abutment ends. (Note: the initial end of an abutment is denoted by  $\overline{(+1)}$  (Abutment index) while the terminal end of an abutment is denoted by  $(-1)$  (Abutment index).) The orientation of the network provides an ordering for these abutment ends, e.g.  $\langle A_1, A_2 \rangle$ , where  $A_1$  and  $A_2$  are abutment end indices. In figure F.15 we illustrate the anomalous situation in which  $A_1 = A_2$ . In the process of constructing the graph associated with an abutment intersection, such a situation gives rise to a self-loop, which is subsequently ignored.
- o The single corner control point at the end of a smooth abutment has associated with it two non-smooth abutments as illustrated in figure F.16.

## Properties of User Boundary Conditions

- o When a doublet matching condition is assigned to a network lying in an inactive plane of symmetry, the doublet matching condition will replace the user specified antisymmetric boundary condition. An antisymmetric boundary condition has the general form

$$a_A(\vec{w} \cdot \hat{n})_A + c_D \mu + t_D \cdot \vec{\nabla} \mu = b \quad (\text{F.5.14})$$

(Note: A doublet network lying in a plane of symmetry must be assigned an antisymmetric boundary condition of the form given above.)

## Properties of Edges

- o A network edge may be marked "no doublet edge matching" by the program user. When this is done, the network's doublet strength along that edge will not participate in any doublet matching conditions for the abutment(s) in which that edge is involved.
- o A network edge may be marked "closure edge" by the user. If in addition the user has specified that the closure boundary condition override doublet matching, the network's control points will not be used for doublet matching along the interior of the closure edge. It is generally permissible for control points at the ends of a closure edge to be used for doublet matching.
- o Certain network edges are implicitly marked "matching edge" by PAN AIR. These include:
  - (i) Edge 1 of a DW1 network
  - (ii) Edges 1 and 4 of a DD1 network
- o Certain network edges are implicitly marked "non-matching edge" by PAN AIR. These include:
  - (i) Edges 2, 3 and 4 of a DW1 network
  - (ii) All edges of a DW2 network
  - (iii) Edges 2 and 3 of a DD1 network
- o Every portion of a network edge is involved in exactly one abutment.

## Properties of Abutments

- o Abutments involving any interior edge of a network are forbidden
- o The initial end of an abutment may participate in an abutment intersection with the terminal end of an abutment. (Figure F.17 illustrates how this situation can arise for a tube panelled as one network.) Since doublet matching must, in general be imposed at both ends of an abutment it is necessary to distinguish the initial and final ends of an abutment during abutment intersection analysis. As noted above, the scheme used by PAN AIR labels the initial end with (+1) (abutment index) and the terminal end with (-1) (abutment index).

- o An abutment may lie on 0, 1 or 2 planes of symmetry. If any portion of an abutment lies on a plane of symmetry, the whole of the abutment lies on that plane of symmetry. If an abutment lies on an active plane of symmetry, doublet matching along that abutment is automatically satisfied by virtue of the symmetry properties of the symmetrized potentials  $\phi^{ij}$ . Thus, doublet matching conditions are never enforced for an abutment lying on an active plane of symmetry.
- o Smooth abutments do not explicitly enter into the analysis of an abutment intersection.

#### Properties of Abutment Intersections

- o An abutment intersection may lie on 0, 1 or 2 planes of symmetry.

#### Selection of Matching Conditions

We now describe the process by which doublet matching assignments are made while carefully taking into account the considerations outlined above.

The basic procedure for performing doublet matching will remain essentially the same as the tree defoliation procedure outlined at the end of section F.5.1. The complete procedure, however, will be significantly more complex at each stage of processing. A summary of the stages of the complete procedure is given -

- B.1 Construct the graph  $G$  containing just those branches corresponding to networks whose type is not "no doublet" and do not lie in an active plane of symmetry. During this construction process, some relabelling of nodes may be performed to account for the "no doublet edge matching" feature.
- B.2 Form a spanning tree for  $G$ ,  $T \subset G$ . If  $G$  has  $k$  components ( $G = \bigcup_{i=1}^k G_i$ ),  $T$  will have  $k$  components,  $T = \bigcup_{i=1}^k T_i$  (\*). In contrast with the earlier algorithm,  $T$  is not an arbitrary spanning tree of  $G$ , but rather is constructed with careful regard for the properties of the networks/branches of  $G$ .
- B.3 Without first selecting a ground node, each component tree  $T_i$  is defoliated, the removal of each branch providing an association of a node with a branch. At the end of this process, there will be left one node that is not associated with any branch, and this node becomes the ground node for the tree.

\* Note, however, that if some component  $G_i$  of  $G$  contains only one node, all of its branches being self loops, then  $T_i = \emptyset$ . In practice, self loops cause no special difficulty for the doublet matching problem simply because the doublet strength on a network that generates a self loop "matches itself."

- B.4 Finally, the assignments are examined to determine if the requisite doublet matching conditions have in fact been associated with eligible branches. In addition, it is verified that all of those branches that must receive a doublet matching condition have in fact done so.

Several remarks about this algorithm are appropriate before proceeding with its detailed exposition. First, steps B.1 and B.4 are essentially deterministic given the specification of the problem. Steps B.2 and B.3, on the other hand are substantially heuristic, step B.2 being ambiguous with regard to the choice of spanning tree and step B.3 being ambiguous with regard to the defoliation strategy. Although the detailed exposition of the algorithm will resolve most of these ambiguities, the solutions presented should not be regarded as unique. They are, nevertheless, very good.

B.1 The detailed description of an abutment intersection includes the following information

- o Symmetry condition,  $\hat{\phi}_{SS}$ ,  $\hat{\phi}_{AS}$ ,  $\hat{\phi}_{AA}$  or  $\hat{\phi}_{SA}$ .
- o A description of the plane(s) of symmetry that the abutment intersection point lies on.

For each network/control point/branch N involved in the abutment intersection, the following information is given.

- o The abutment ends in which N participates at  $P_{AI}$  are given in positive sequence  $\langle A_1, A_2 \rangle$ . The two edge segments of N that are involved in the abutments  $A_1, A_2$  are denoted  $E_1, E_2$  respectively. Because of the requirement that  $A_1$  and  $A_2$  be given in positive sequence, an oriented traversal of the boundary of N would encounter edge segment  $E_1$  followed immediately by edge segment  $E_2$ .
- o "No doublet edge matching" information is given for each edge segment  $E_i$ .
- o Let  $\hat{t}_i$  denote unit vectors drawn along edge segments  $E_i$ , pointing away from  $P_{AI}$ . Let  $\hat{s} = (\hat{t}_1 + \hat{t}_2) / |\hat{t}_1 + \hat{t}_2|$  and let  $\hat{c}_0$  be the compressibility axis. Then the "compressibility axis downstream parameter"  $\alpha$  is defined by

$$\alpha = \hat{s} \cdot \hat{c}_0 \quad (F.5.15)$$

This parameter is given for each branch.

- o Each branch is classified as follows:
  - 0, no doublet network
  - 2, doublet network, but no corner control point is available to enforce doublet matching

- 3, doublet network with regular corner control point, but at least one of the edges  $E_i$  is marked "no doublet edge matching"
- 4, doublet network with regular corner control point.
- 5, doublet network with "matching" corner control point

o The plane of symmetry in which N lies, if any, is given.

For each abutment-end/node involved in the abutment intersection, the following information is given

- o The global abutment-end index
- o a flag indicating which planes of symmetry the abutment end lies on

Given this information, the graph G is constructed in two stages. First, a graph  $G_0$  is constructed using all those branches in classes 2, 3, 4 and 5 that do not lie in an active plane of symmetry. Next, each branch of  $G_0$  is examined for any "no doublet edge matching" marks on either end. If such a mark is found, the corresponding end of the branch is detached from the node to which it is attached and a new node is created. The resulting graph is the graph G that we seek. Finally all of the newly created nodes together with those nodes (abutment-ends) lying on an active plane of symmetry are marked as "preferred ground nodes." Doublet matching conditions corresponding to "preferred ground nodes" are never enforced.

B.2 Without loss of generality, we may suppose that the graph generated in step B.1 is connected. If in fact G is not connected, we simply perform steps B.2, B.3 and B.4 separately on each of G's components.

Any given connected graph will, in general, possess many spanning trees and the problem of determining all of the spanning trees of a particular graph is very difficult (cf. ref. F.2, p. 280). The problem of determining a spanning tree is fairly simple, however, and the standard algorithm is given in (ref. F.2, pp 277-279). Basically this algorithm proceeds by considering in some order, each branch of the graph as a candidate for membership in the spanning tree. If a branch causes a closed loop, it is rejected, and if it does not cause a closed loop it is accepted.

It is clear that the spanning tree resulting from this procedure depends crucially upon the order in which branches are examined. In PAN AIR, branches are considered in order of decreasing priority in accordance with the following priority scheme:

$$p = \begin{cases} 2 & \text{class 2 branches} \\ 3 + \alpha & \text{class 3 branches} \\ 4 + \alpha & \text{class 4 branches} \\ 5 & \text{class 5 branches} \end{cases} \quad (\text{F.5.16})$$

Thus, branches with the highest values of p are considered first for potential membership in the spanning tree. Here,  $\alpha$  is the "compressibility axis downstream parameter" defined above by equation (F.5.15).

B.3 In this step of the algorithm, we must select a defoliation scheme for the spanning tree  $T$ . If  $T$  has  $n$  nodes, then there are precisely  $n$  distinct defoliation schemes that assign nodes to branches, one corresponding to each choice of ground node in subalgorithm A.3 of section F.5.1. Thus, one possibility that suggests itself is to examine each of the  $n$  possible defoliation schemes and determine which one provides the most suitable set of assignments. It turns out that such a complex procedure is not necessary and that a fairly straightforward modification of subalgorithm A.3 generates a suitable choice of ground node without an exhaustive search(\*).

The modified defoliation algorithm proceeds as follows. As before, we set  $T_n = T$  and define a sequence of trees  $T_n \supset T_{n-1} \supset \dots \supset T_1$  such that  $T_j$  is obtained from  $T_{j+1}$  by identifying in  $T_{j+1}$  a node of degree 1 and removing that node and the single branch to which it is attached. If there is more than one node of degree 1 available, the choice is made by means of the following prioritization scheme based upon node type ("preferred ground node" or not) and branch class (2,3,4 or 5):

Node Type	Branch Class		
	2	3 or 4	5
"preferred ground node"	5	3	1
not a "preferred ground node"	2	4	6

Priority classes for removing a node/branch combination

Given this prioritization scheme, the node/branch combination in the highest priority class is selected for defoliation. In the event that there is more than one node/branch combination, the one with the lowest value of  $p$  (see above) is selected if the node is a "preferred ground node" while the highest value of  $p$  (cf. equation F.5.16) is selected if the node is not a "preferred ground node."

B.4 The algorithm described above will have achieved a successful set of doublet matching assignments provided the following conditions are satisfied

- (i) all "matching corner point" branches (branch class 5) are included in the spanning tree  $T$ .
- (ii) a "preferred ground node" is never assigned to a class 5 branch (i.e., priority class 1 is never selected.)
- (iii) the ground node actually selected for a tree  $T$  is a "preferred ground node," if any appear in  $T$ .

(\*) Note that a completely exhaustive examination of all possible matching assignments possible for a connected graph  $G$  would involve  $(n \cdot s)$  separate cases, where  $n$  is the number of nodes in  $G$  and  $s$  is the number of spanning trees.

This page has been left blank intentionally.

## F.6 Gap-Filling Panels

Whenever a gap whose size is greater than the user-specified tolerance distance occurs between portions of two or more network edges which form an abutment, gap-filling panels are defined. The placement of gap-filling panels is illustrated for an abutment containing two network edges in figure F.9.

We now briefly outline the process by which gap-filling panels are constructed, first considering the case of two network edges. First, each edge in the abutment is "parametrized." That is, each panel corner point on the edge is assigned a real number  $t$  between 0 and 1 inclusive, where  $t$  is the ratio of two distances. The first distance is the sum of the lengths of the panel edges between the starting point of the abutment and the panel corner point in question, while the second distance is the sum of the lengths of all the panel edges on a network edge. Thus  $t$  represents the proportion of the entire edge length which one has traveled in proceeding from the start of the abutment to the panel corner point in question. In figure F.9, each panel corner point is given a value  $t$ .

Now, suppose the distinct values of  $t$  which occur for the two network edges are  $t_0, t_1, \dots, t_n$ , where

$$0 = t_0 < t_1 < \dots < t_n = 1 \quad (\text{F.6.1})$$

In the example of figure F.9,  $n = 9$ , since there are 11 panel corner points other than the initial points, and the values  $t = .80$  and  $t = 1.0$  occur twice.

Now, up to  $n$  gap-filling panels may be constructed to fill the gap in the abutment. For each integer  $i$ ,  $1 < i < n$ , the quadrilateral region with corner points lying on the two network edges, with respective parameter values  $t = t_{i-1}$  and  $t = t_i$  is examined. If  $t_i$  is not the parameter value of a corner point (for instance,  $.30$  is not the parameter value of any cornerpoint on network A in figure F.9), linear interpolation between corner points is used to find the point on the panel edge with that parameter value. If three or more of the four edges of this quadrilateral region have length greater than the user-specified tolerance distance  $\epsilon$ , a gap-filling panel is defined.

Thus, for the abutment in figure F.6, no gap-filling panels would be defined, since the gap size is uniformly smaller than  $\epsilon$ , and so all potential gap-filling panels have two edges of length less than  $\epsilon$ . On the other hand, if, in figure F.9,  $\epsilon$  were approximately  $.05$  times the abutment length, seven gap-filling panels would be defined, while two potential ones would be discarded because two edges of the panels would be too short. The reason that very small gap-filling panels are never defined is that numerical difficulties could occur in measuring the influence of these panels on control points. It is not known at this time under which circumstances the resulting doublet discontinuity might be significant.

Next, we address the question of how to define the doublet strength on the gap-filling panels so that doublet continuity is attained. The edge splines constructed in appendix I assure that, if one edge is a refinement of the other, then the doublet strength matches at points on the two network edges with the same parameter value  $t$ . Thus we want the doublet strength to be constant on the panel along the direction perpendicular to the direction of the abutment.



We illustrate this in figure F.18. The four corner points of the panel are  $P_i$  and  $P_{i+1}$  on edge A and  $P_i$  and  $P_{i+1}$  on edge B. We then define  $M_i$  as the midpoint of the segment  $P_i P_{i+1}$ , and  $M_i'$  similarly. Then, since  $P_i$ ,  $P_{i+1}$ , and  $M_i$  each has the same parameter value as its primed counterpart, it also has the same doublet strength, namely  $\mu$ ,  $\mu_{i+1}$ , or  $\mu_i'$  respectively. Thus, we have defined  $\mu$  at six of the nine panel defining points, and we define  $\mu$  at the remaining three panel defining points in the natural way.

This defines  $\mu$  uniquely on the whole panel (see section 5.5). Further, it insures continuity of  $\mu$  on the whole edge  $P_i P_{i+1}$  and the whole edge  $P_i' P_{i+1}'$ , since these two gap-filling panel edges are subsets of ordinary panel edges. Thus the doublet strength on the network edges is defined by a single quadratic function in one variable, and therefore agrees with the doublet strength on the gap-filling panel edge everywhere, since it agrees at three points.

Finally we must consider the case of three or more network edges meeting in an abutment, as illustrated in cross-section in figure F.19. There, network  $E_0$  is the most densely paneled network edge, and so, if the user has followed the paneling rules, it is a refinement of edges  $E_1$  and  $E_2$ . We construct gap-filling panels as illustrated in order to fill the gap in the abutment.

It still remains to be decided how to define the doublet strength on the gap filling panels. We want the doublet strength to be continuous across edges  $E_1$  and  $E_2$ , while at  $E_0$  we want

$$\mu_0 - \mu(1) - \mu(2) = 0 \quad (\text{F.6.2})$$

where  $\mu(j)$  is the doublet strength on the gap-filling panel spanning the gap from  $E_0$  to  $E_j$ . On the other hand, the doublet edge splines and matching boundary conditions insure

$$\mu_0 - \mu_1 - \mu_2 = 0 \quad (\text{F.6.3})$$

where  $\mu_j$  is the doublet strength on edge  $E_j$ . Thus the specification

$$\begin{aligned} \mu(1) &= \mu_1 \\ \mu(2) &= \mu_2 \end{aligned} \quad (\text{F.6.4})$$

insures doublet continuity (in the form (F.1.1)) everywhere.

Thus the general procedure used by Pan Air for gap-filling panels in abutments with three or more network edges is:

- a. choose the most densely paneled edge (which should be a refinement of all the other network edges),
- b. define gap-filling panels in the gap between the finest edge  $E_0$  and each other edge  $E_j$ , just as if this were an abutment with only two edges, and

- c. define the doublet strength on the gap-filling panels to be equal to the doublet strength on the edge  $E_j$ .

Note that this procedure works even if there are only two edges in the abutment. Further, it insures that the equation

$$\sum s_j \mu_j = 0 \quad (F.6.5)$$

is imposed along all network edges.

This page has been left blank intentionally.

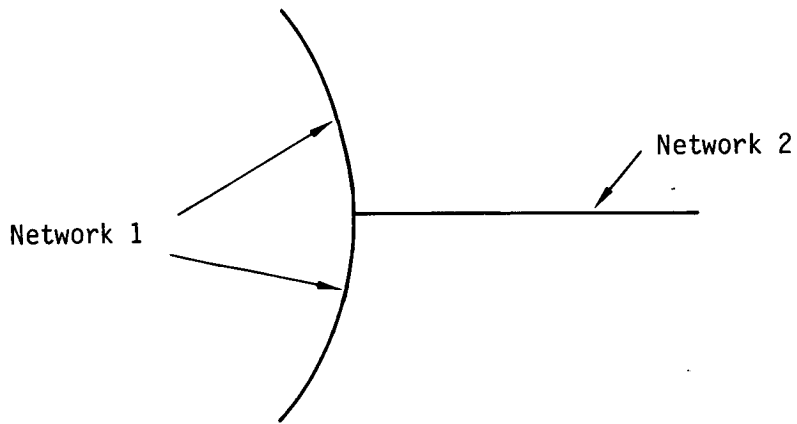
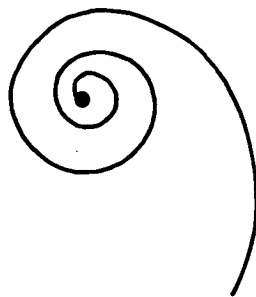


Figure F.1 - Impermissible network intersection  
(in cross-section)



● = region where viscous effects dominate

Figure F.2 - Leading edge vortex (in cross-section)

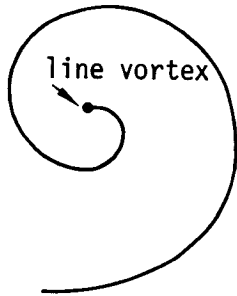


Figure F.3 - Simulation of a vortex core  
by a line vortex

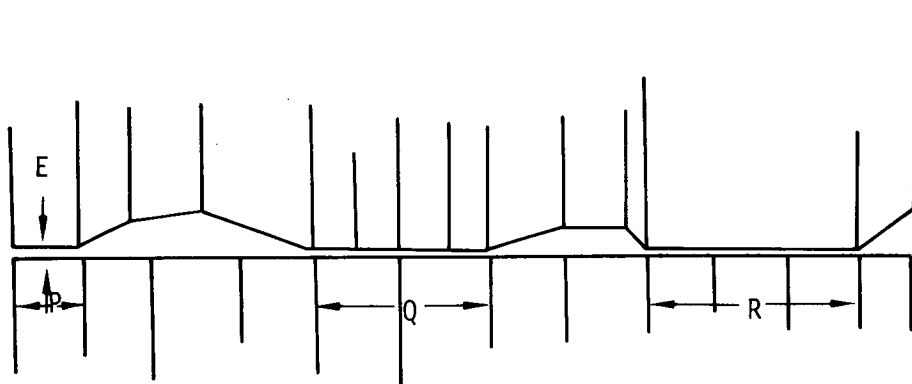


Figure F.4 - Multiple pairwise abutments involving  
the same edges

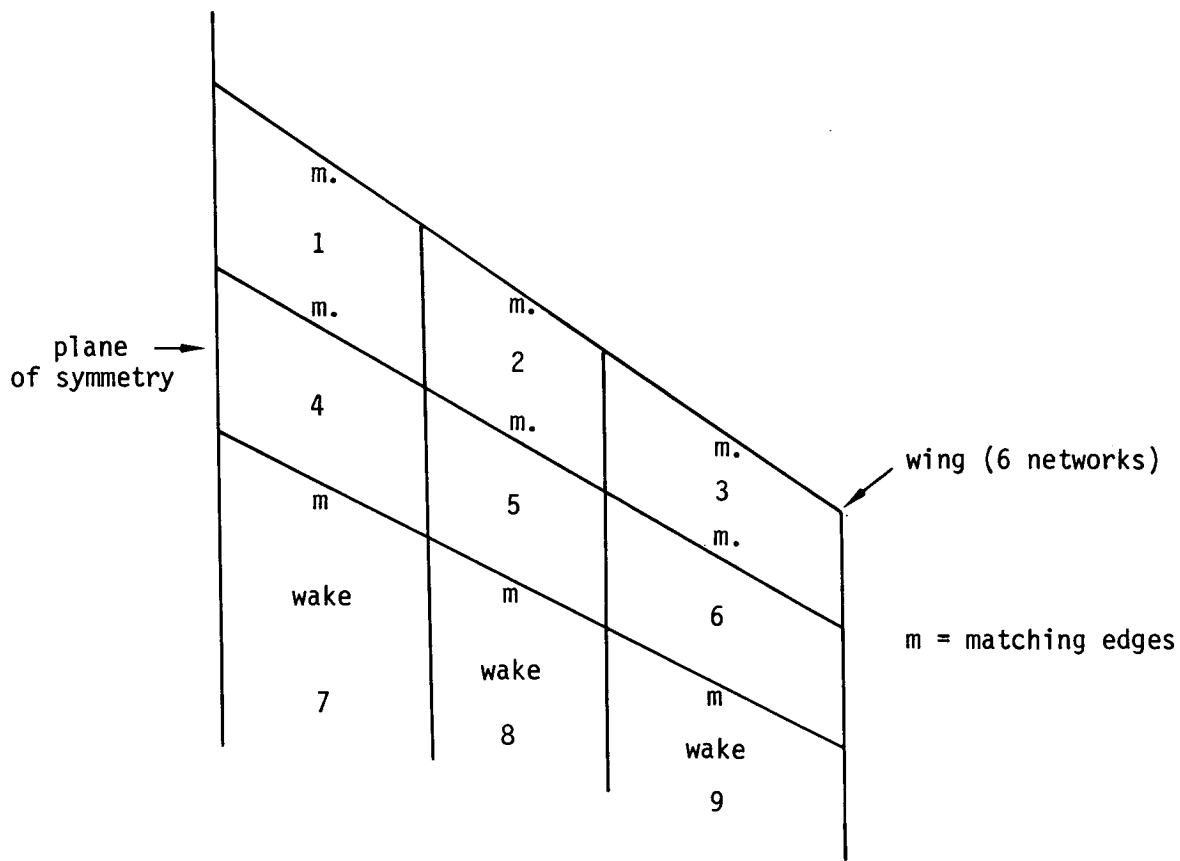


Figure F.8a - Six network wing with wakes

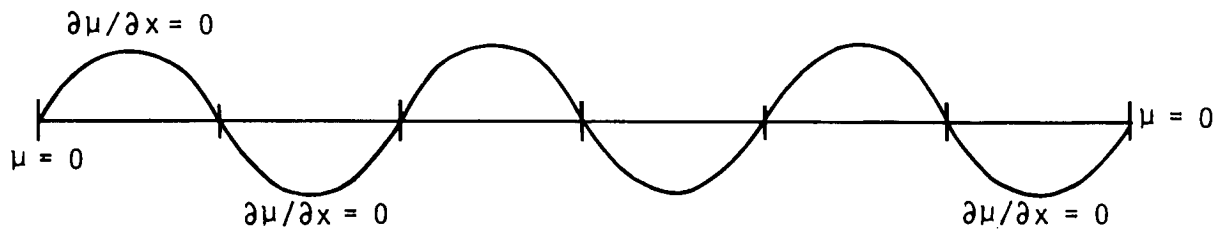


Figure F.8b - Doublet distribution arising from specification of  $\mu$  at trailing edge

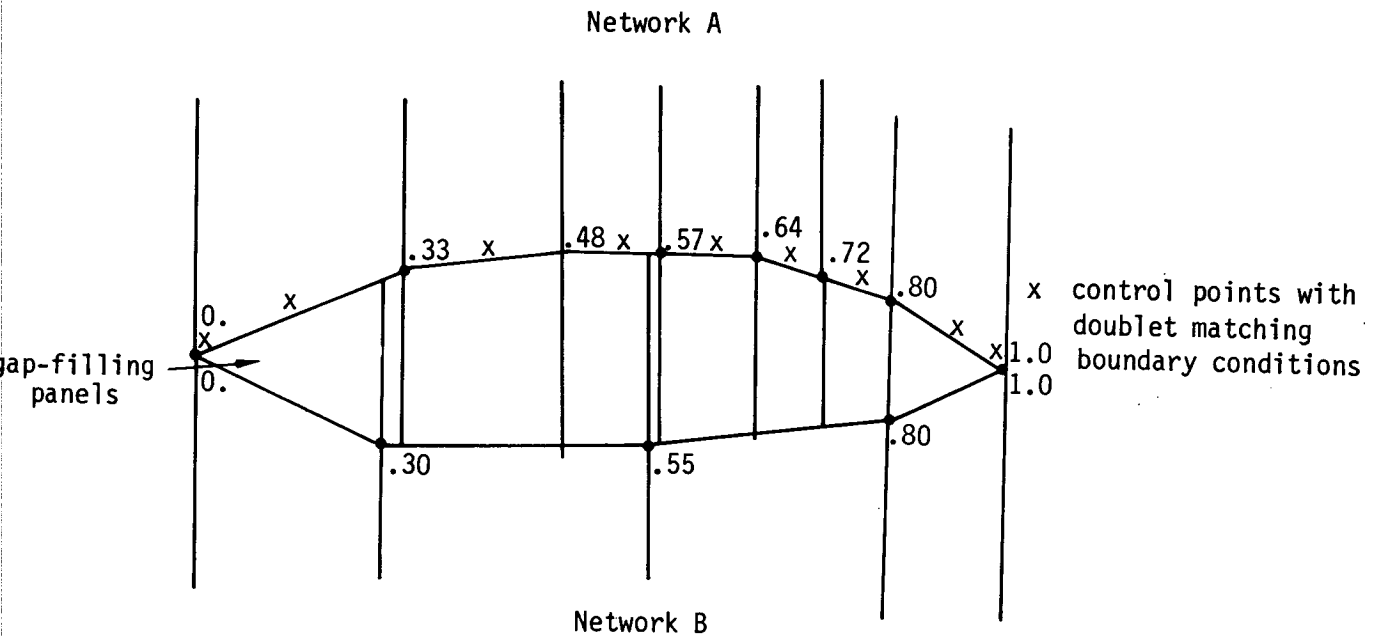


Figure F.9 - One edge is not precisely a refinement of the other

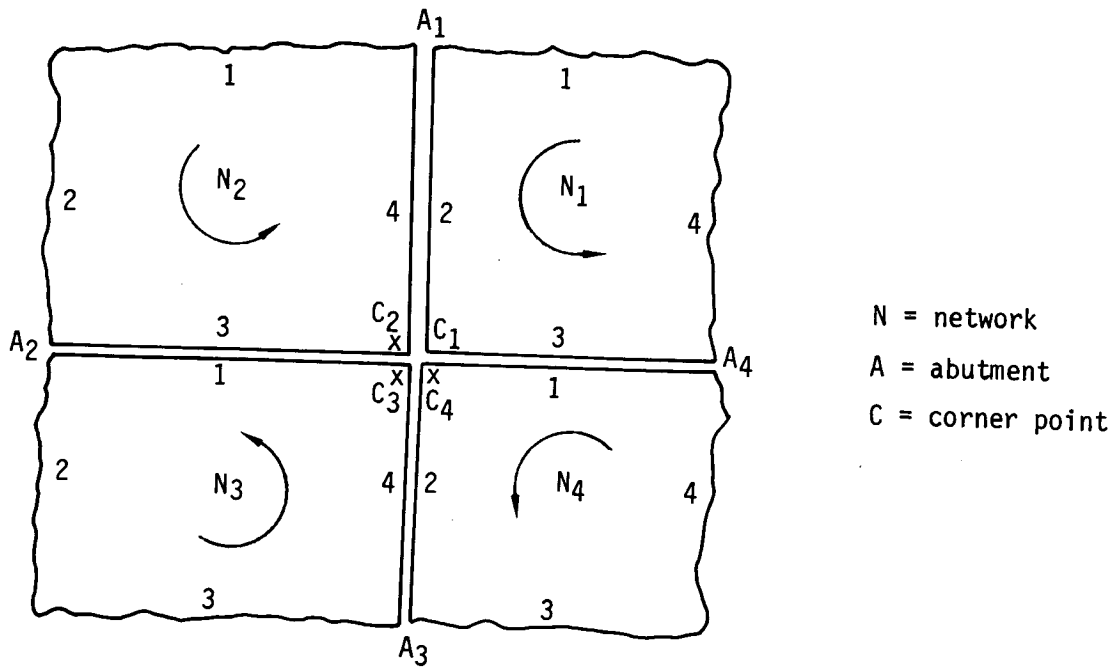


Figure F.10 - An abutment intersection with 4 abutments

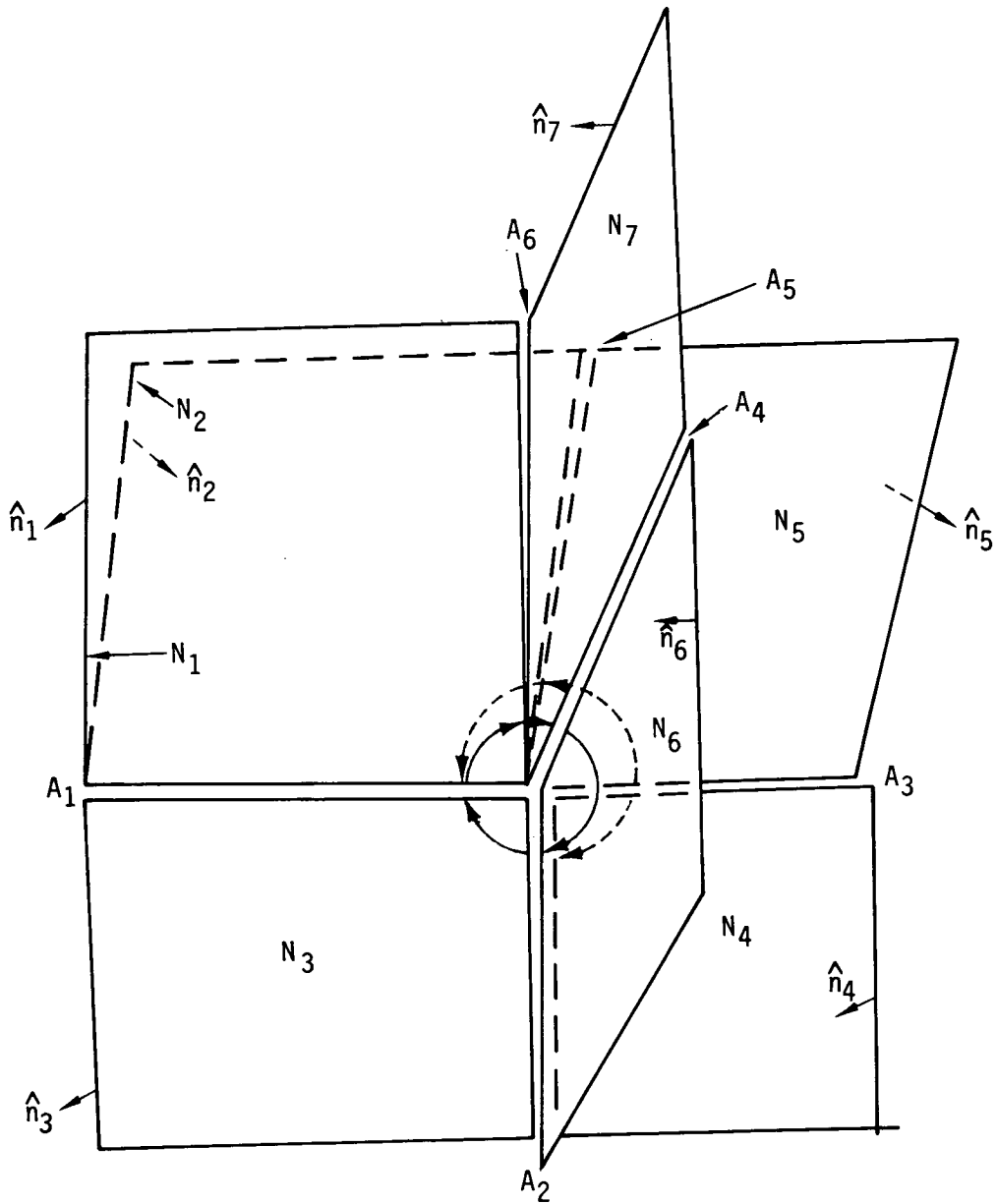


Figure F.11 - An abutment intersection with 6 abutments



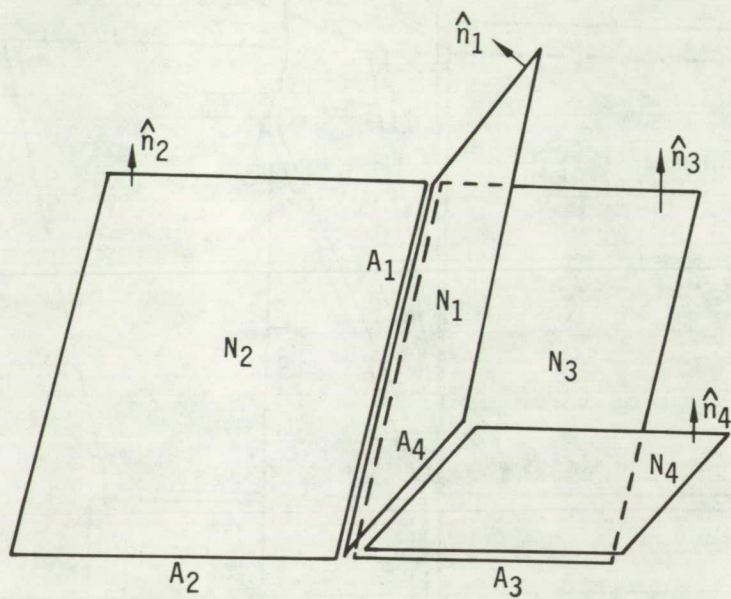


Figure F.12 - Another abutment intersection with 4 abutments

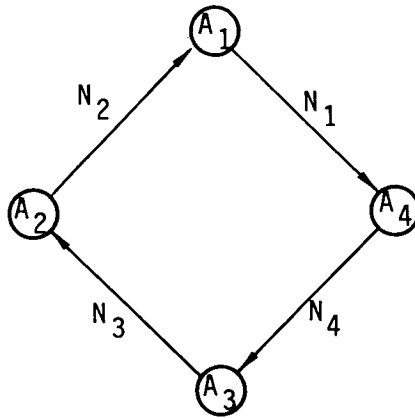


Figure F.13a

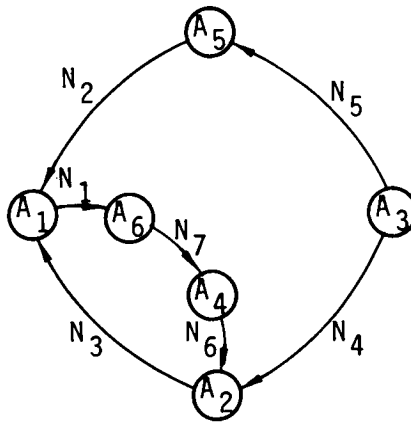


Figure F.13b

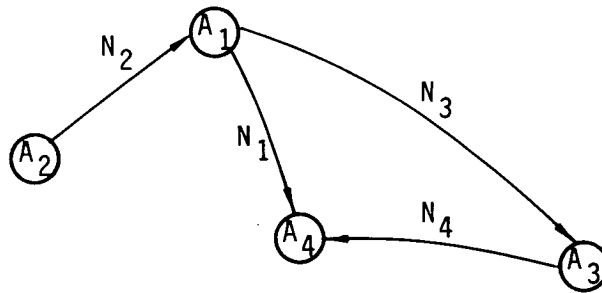
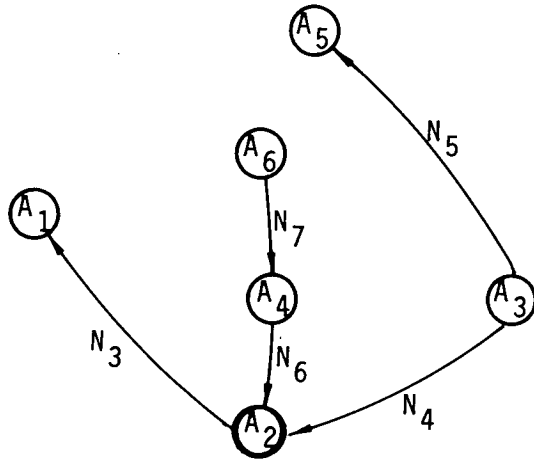
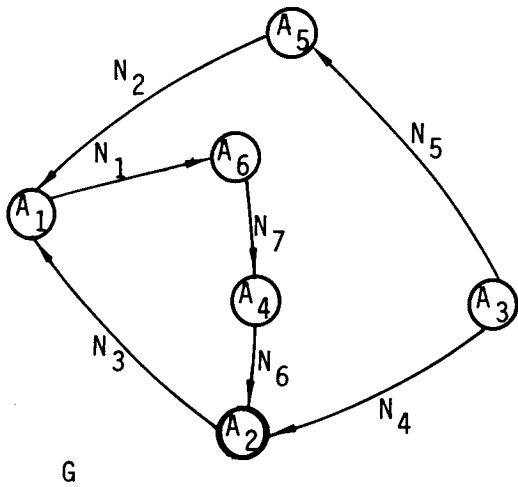
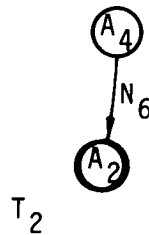
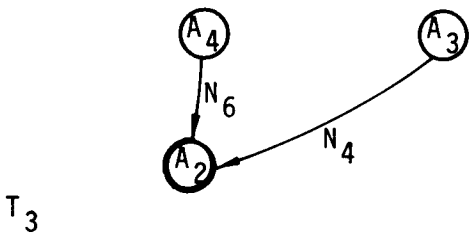
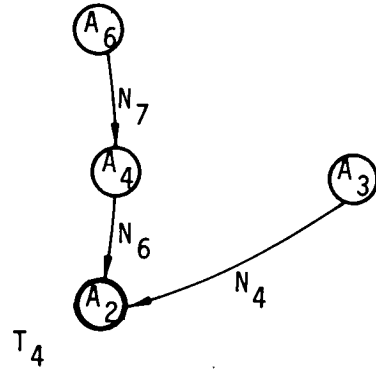
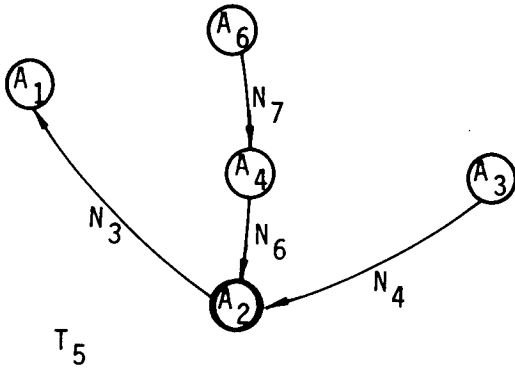


Figure F.13c

Figure F.13 Directed graphs corresponding to three abutment intersections



$T = T_6$  ( $A_2 = \text{ground node}$ )



Matching Assignments:  $A_5 - N_5, A_1 - N_3, A_6 - N_7, A_3 - N_4, A_4 - N_6$

Figure F.14 Defoliation and matching condition assignment for the graph of Figure F.13b

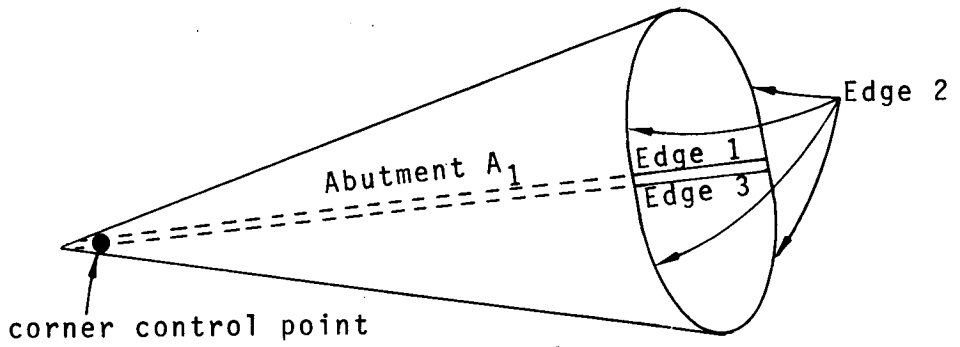


Figure F.15 A corner control point for which  $A_1 = A_2$ , giving rise to a self loop.

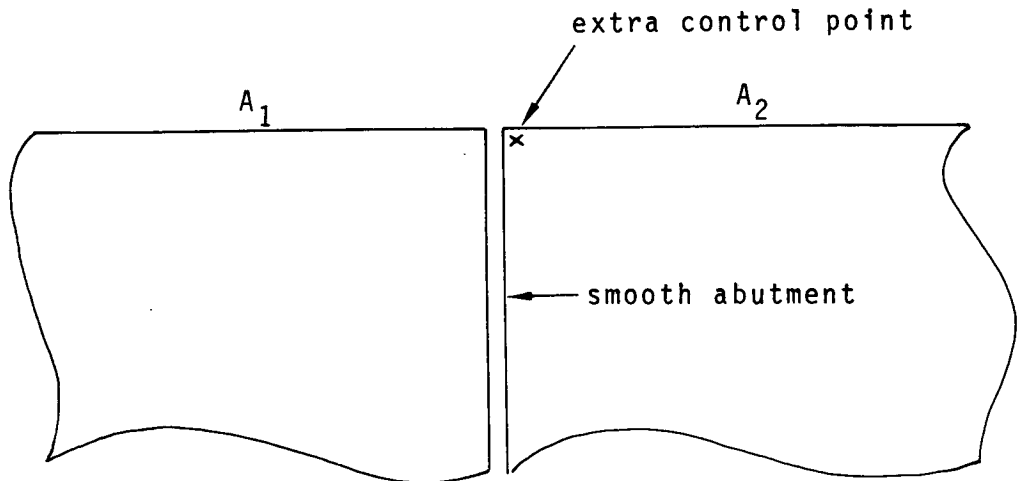


Figure F.16 An extra control point at the end of a smooth abutment.

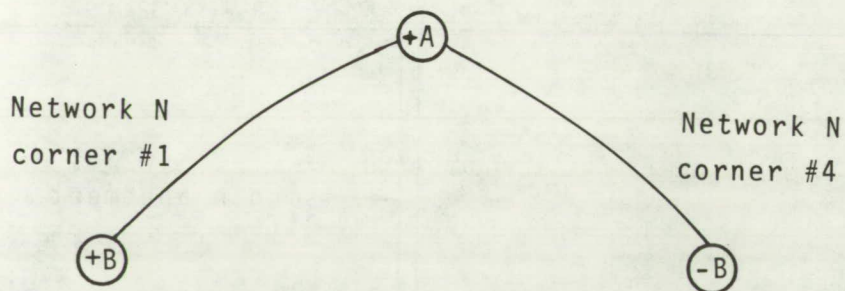
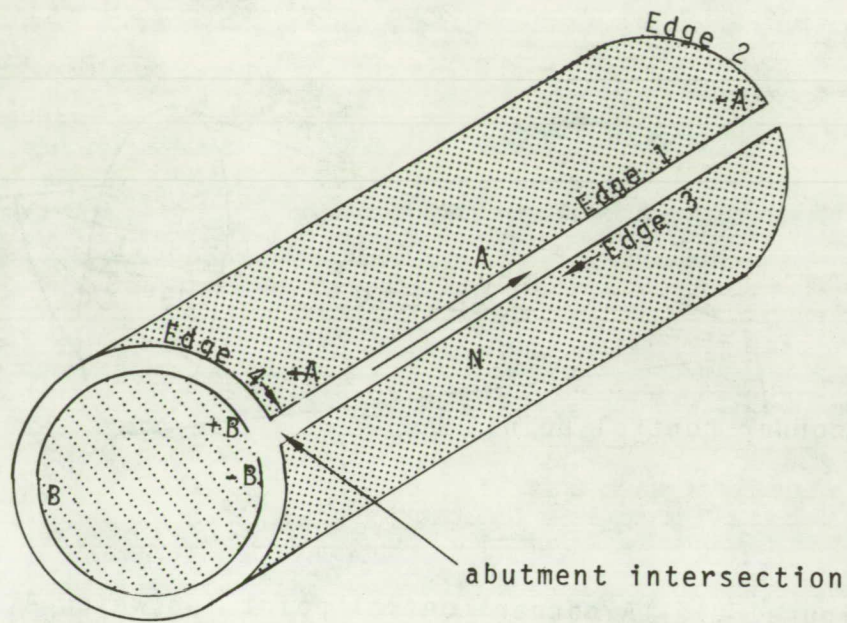


Figure F.17 An abutment intersection in which both the initial and terminal ends of an abutment participate in an abutment intersection



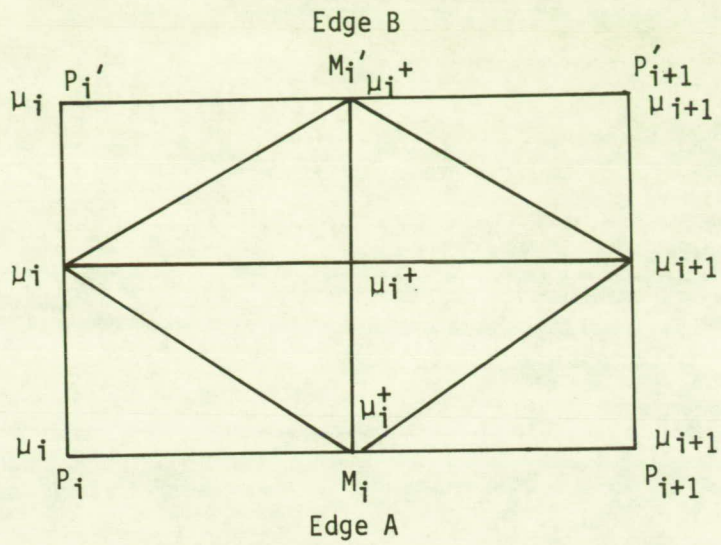


Figure F.18 - Gap-filling panel

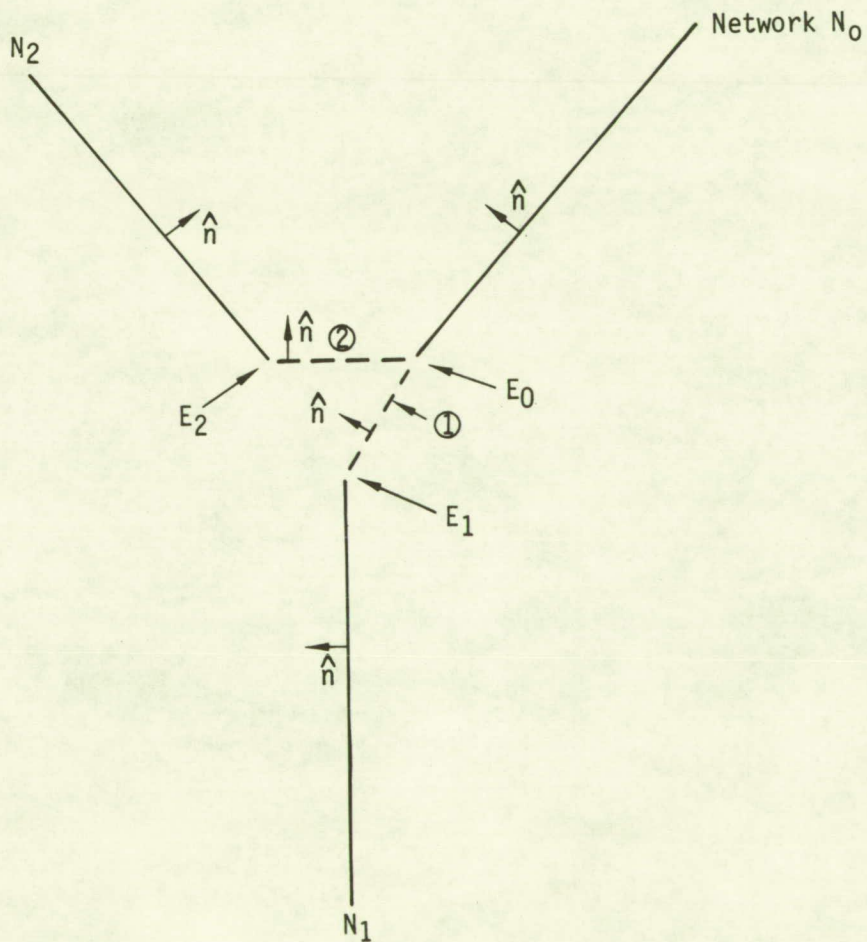


Figure F.19 - Gap-filling panels on an abutment with 3 network edges

## G.0 Control Point Locations

In figure G.1 we illustrate the possible location of points on a network, called control points, at which boundary conditions are defined. These locations are independent of the source type or doublet type of the network; however, we will see in Appendix H that meaningful boundary conditions are not necessarily imposed at all control points (for instance, on wake networks, boundary conditions are only imposed along one edge).

Note that controls points are illustrated as being located near, but not directly on, midpoints of panel edges lying on network edges. This is due to the disastrous results which would occur from attempting to measure the velocity or potential at a control point that lies directly on a panel edge (see section J.11). Later in this section we describe the procedure used to recede control points from the panel edge.

When a network edge is divided into distinct portions belonging to separate abutments, as illustrated in figure G.2, an extra control point, in addition to those in figure G.1, is defined. The same data are computed for these control points as for ordinary control points.

In order to determine its location, a control point is placed in one of three categories: panel center control points, edge midpoint control points, and panel corner control points. The latter two categories are only defined along the network perimeter. The control point is defined by prescribing a "hypothetical location" (the center point, edge midpoint, or corner point at which the control point would ideally be located), and a "recession vector" which describes the extent to which the control point is receded into a subpanel from its hypothetical location.

The size of the "recession vector" has been determined experimentally. Basically, it has been chosen as small as possible without causing severe numerical error. We refer to figure G.3 in defining the recession vectors. There, we show an edge control point as  $P_5$  and a corner point at  $P_1$ ; for control points at other points or edge midpoints the procedure is identical.

Panel center control points are only receded very slightly from the center point  $P_9$  since the doublet distribution is differentiable and the source distribution is continuous at  $P_9$ ; as a result (see section J.11) the potential and velocity induced by the singularity distributions are very well behaved at  $P_9$ . It is still necessary to recede the control point slightly, however, because influence coefficients can not be computed for a point lying directly on a sub-panel edge, because the calculations yield singular results there. So, we choose the recession vector to be

$$\vec{R} = \frac{(\vec{P}_8 - \vec{P}_9) + (\vec{P}_7 - \vec{P}_9)}{200} \quad (G.0.1)$$

Edge control points are receded considerably further because of the discontinuities in doublet derivative, surface slope, and source strength which occur at network edges. Thus, for the control point located at  $P_5$ , we define its recession vector to be

$$\vec{R} = \delta \left\{ \frac{|\vec{P}_8 - \vec{P}_5|}{|\vec{P}_8 - \vec{P}_5| + |\vec{P}_9 - \vec{P}_5|} (\vec{P}_9 - \vec{P}_5) + \frac{|\vec{P}_9 - \vec{P}_5|}{|\vec{P}_8 - \vec{P}_5| + |\vec{P}_9 - \vec{P}_5|} (\vec{P}_8 - \vec{P}_5) \right\} \quad (\text{G.0.2})$$

where

$$\delta = \begin{cases} \frac{\min \{ |\vec{P}_8 - \vec{P}_5|, |\vec{P}_9 - \vec{P}_5|, |\vec{P}_1 - \vec{P}_5| \}}{10 |\vec{P}_9 - \vec{P}_5|} & \text{if } |\vec{P}_1 - \vec{P}_5| > 0 \\ 1/10 & \text{otherwise} \end{cases} \quad (\text{G.0.3})$$

The recession vector  $\vec{R}$  bisects the angle between the vectors  $(\vec{P}_8 - \vec{P}_5)$  and  $(\vec{P}_9 - \vec{P}_5)$ . If  $\delta$  were unity, the head of the recession vector  $\vec{R}$  emanating from point  $P_5$  would lie on the line segment joining points  $P_8$  and  $P_9$ . If edge 1 is collapsed as in figure G.4, then  $\delta$  is taken to be a tenth. The recession vector  $\vec{R}$  would also be used for any control points located at  $P_1$  and  $P_2$  in this case. If edge 1 is not collapsed, then  $\delta$  will be at most a tenth and possibly less, if the panel is skewed. The recession vectors for other edge midpoint control points are defined analogously, control points whose hypothetical locations are  $P_6, P_7, P_8$  being withdrawn, respectively, into triangles 6, 7, and 8.

For the corner control point located at  $P_1$  which does not lie on a collapsed edge the recession vector is

$$\vec{R} = \frac{1}{10} \left\{ \frac{|\vec{P}_5 - \vec{P}_1|}{|\vec{P}_8 - \vec{P}_1| + |\vec{P}_5 - \vec{P}_1|} (\vec{P}_8 - \vec{P}_1) + \frac{|\vec{P}_8 - \vec{P}_1|}{|\vec{P}_8 - \vec{P}_1| + |\vec{P}_5 - \vec{P}_1|} (\vec{P}_5 - \vec{P}_1) \right\} \quad (\text{G.0.4})$$

This particular construction provides the recession vector  $\vec{R}$  with properties similar to the edge control point recession vector in (G.0.2). Note that the recession vector in (G.0.4) lies in subpanel 1. The recession vectors for other corner control points are handled in a similar fashion.

Some geometric quantities in addition to location and hypothetical location are computed by the program for each control point. One of these is the subpanel on which the control point actually lies. This is needed later (see section J.8) to insure that an average potential and velocity are computed correctly in measuring the influence that the sub-panel on which the control point lies exerts on the control point.



Also, for each edge or corner control point at which a matching boundary condition is imposed, a set of "extra hypothetical locations" and their associated sign is computed. These arise from the matching boundary condition (see section F.1)

$$\sum s_j \mu_j = 0 \quad (G.0.5)$$

where the  $\mu_j$  are the values of doublet strength on different networks.

In figure G.5, we illustrate an abutment containing three network edges. Although the control point is receded from the edge, the matching boundary condition involves singularity strengths at the edge; in this example (G.0.5) becomes

$$\sum_{i=0}^2 s_i \mu(H_i) = 0 \quad (G.0.6)$$

where  $H_0$  is the (default) hypothetical location of the control point, while  $H_1$  and  $H_2$  are extra hypothetical locations.

In Appendix F we indicate how the signs  $s_j$  are computed; here we describe the computation of the extra hypothetical locations. Hypothetical locations are computed one abutment at a time by parametrizing the abutment (see section F.4), a process that assigns to each panel corner point or edge midpoint  $P$  on that portion of a network edge belonging to an abutment a real number  $t(P)$  between 0 and 1.

In figure G.6, we illustrate an abutment with two network edges. Given the control point and default hypothetical location  $H_0$ , we compute the extra hypothetical location  $H_1$  as follows. Parametrization of the abutment gives us  $t(H_0)$ , and also assigns a value  $t$  to every panel corner point and edge midpoint on the edge of network 1.

By interpolation between these points, we find  $H_1$  as the point satisfying

$$t(H_1) = t(H_0) \quad (G.0.7)$$

In addition to the coordinates of the extra hypothetical locations, the program determines the panel and subpanel on which each extra hypothetical location lies, so that the doublet strength can be computed there later.

Our discussion of matching boundary conditions has assumed we are dealing with doublet matching. In the case of a source matching boundary condition (which may occur on the edge of a source design network)

$$\sum s_j \sigma_j = 0 \quad (G.0.8)$$

and extra hypothetical locations and signs are computed as before.

There are two final pieces of geometric data, associated with control points, which we have not yet discussed. These are the normal and conormal of the subpanel on which the control point lies. The normal is needed in post-processing to compute velocity from the potential and the normal mass flux (see Appendix N), while the conormal  $\tilde{n}$  is needed to compute the normal mass flux from the velocity influence coefficient matrix by the formula

$$\vec{v} \cdot \tilde{n} = \vec{w} \cdot \hat{n} \quad (G.0.9)$$

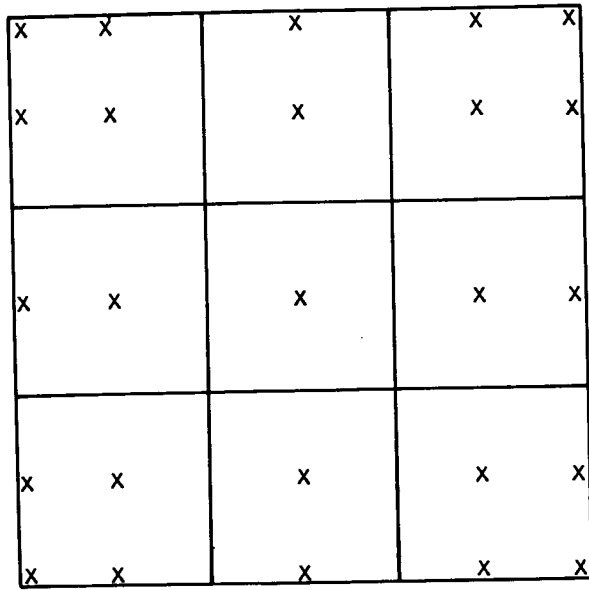
The computation of the normal is described in section D.2, while

$$n = [B_0] \tilde{n} \quad (G.0.10)$$

where

$$[B_0] = I + (s\beta^2 - 1) \hat{c}_0 \hat{c}_0^T \quad (G.0.11)$$

by equation (E.3.9).



x = control point location

Figure G.1 - Control point locations

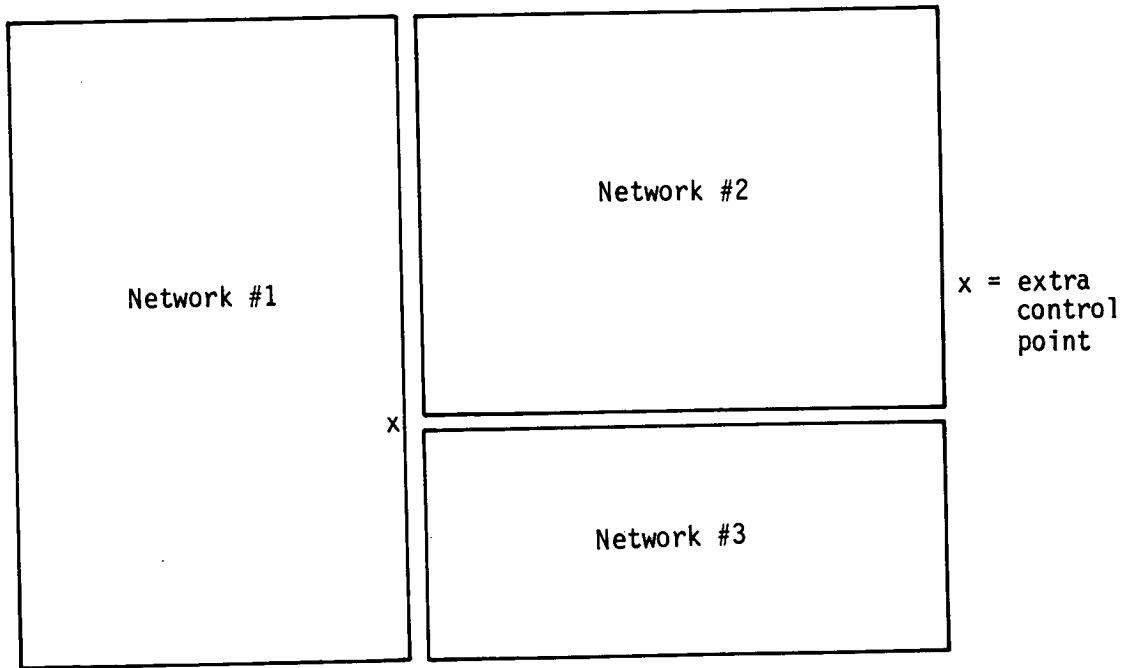


Figure G.2 - Division of network edge into two abutments

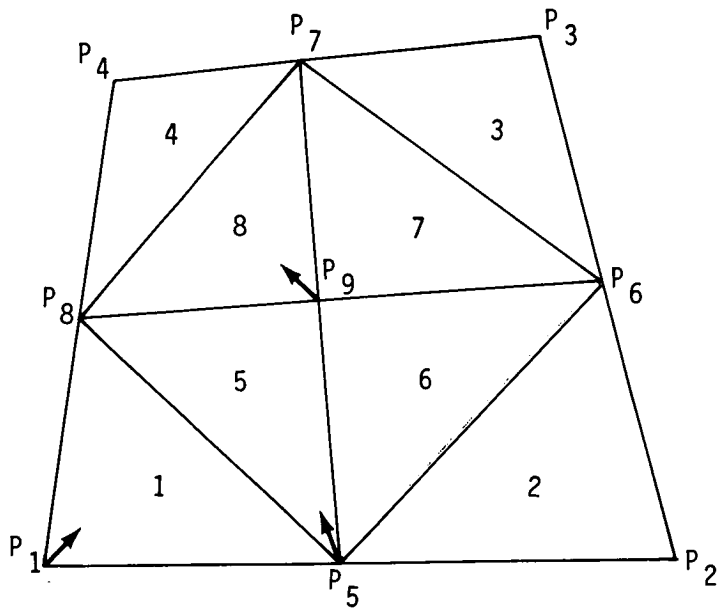


Figure G.3 - Control point recession vectors

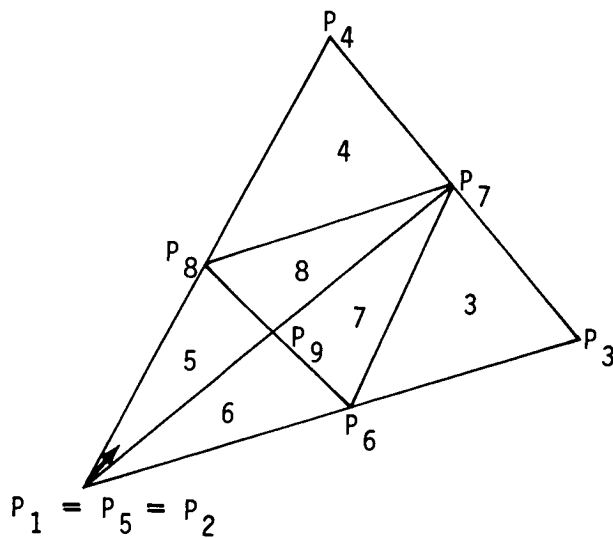


Figure G.4 - Recession of corner control points when subpanel is triangular

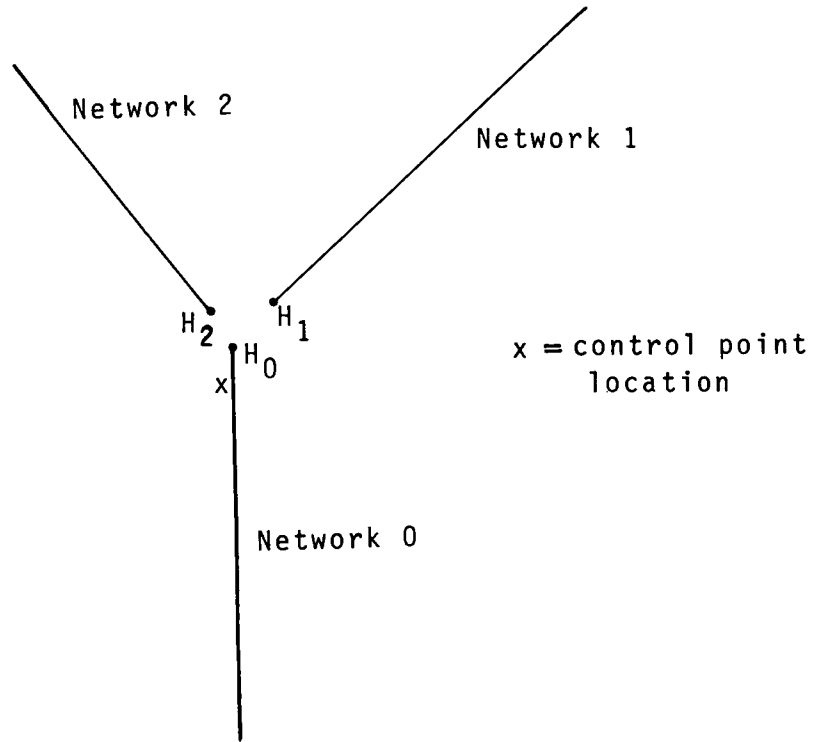


Figure G.5 - Abutment with 3 network edges (cross-section)

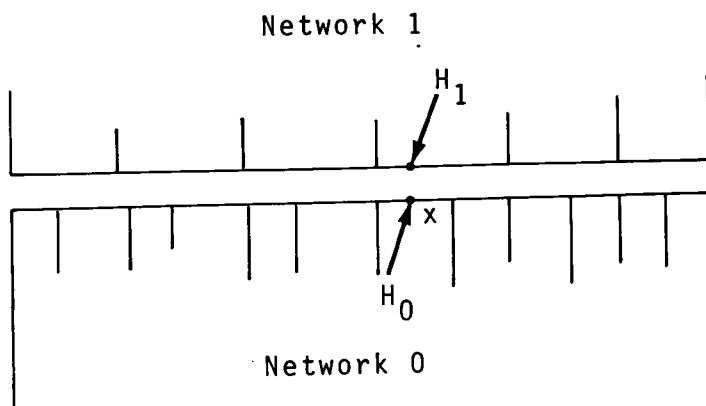


Figure G.6 - Hypothetical locations of a control point

G.1-4 (11/30/81)

## I.0 Singularity Splines

Singularity splines define the source and doublet distributions on the entire configuration in terms of the source and doublet singularity parameters. These distributions are defined by a collection of matrices. First, the source and doublet distributions on a subpanel (recall from section 5.5 that a panel is partitioned into eight subpanels) are each defined by a "subpanel spline matrix" (denoted, respectively,  $SPSPL^S$  and  $SPSPL^D$ ) in terms of five "panel source parameters" and nine "panel doublet parameters." Thus there are eight of each of these matrices associated with each panel.

Next, the panel source and doublet parameters are defined by "outer spline matrices" (denoted, respectively, by  $B^S$  and  $B^D$ ) in terms of singularity parameters located in the neighborhood of the panel. Each panel has associated with it a continuous doublet spline matrix, a continuous source spline matrix and, possibly, a discontinuous source spline matrix.

The subpanel spline matrices are defined by equation (5.5.7). That is,  $[SPSPL^S]^{3 \times 5}$  relates the three coefficients  $\sigma_0, \sigma_\xi, \sigma_\eta$  (which define a linear source distribution on the subpanel) to the five panel source parameters (that is, the source strengths at the five points on the panel illustrated in figure I.1a). Similarly,  $[SPSPL^D]^{6 \times 9}$  relates the six coefficients  $\mu_0, \dots, \mu_{\eta\eta}$  (which define a quadratic doublet distribution on the subpanel) to the nine panel doublet parameters (whose locations are illustrated in figure I.1b).

The outer spline matrices are defined by equation (5.5.8). That is,  $[B^S]$  defines the five panel source parameters in terms of the neighboring source singularity parameters (generally nine in number), while  $[B^D]$  defines the panel doublet parameters in terms of the neighboring doublet parameters (generally 21 in number).

The subpanel and outer spline matrices are used in the influence coefficient calculations. The subpanel spline matrices are first used in order to compute "panel influence coefficient" (PIC) matrices (see sections 4.4.2 and J.1), and the PIC matrices are multiplied by the outer spline matrices to obtain potential and velocity influence coefficient matrices ( $[\phi IC]$  and  $[VIC]$ ) which give the perturbation potential and velocity at a point, in terms of all singularity parameters, due to all the panels in the configuration (see sections 4.2.3 and 5.9.1).

In section I.1 we discuss the construction of outer spline matrices. While their construction is simple in principle, based on a least square procedure, in practice it is quite involved because there are many special cases. In particular, a special "edge spline" is used near network edges, which, in conjunction with the doublet matching boundary conditions discussed in Appendix F, results in precise matching of doublet strength along network edges. In section I.2 we describe the construction of subpanel spline matrices.

In section I.3 we discuss full panel and half panel spline matrices. These matrices define source and doublet distributions specified by single polynomials over the whole panel or half the panel, respectively, also in terms of the panel singularity parameters. The distributions are rough approximations to the 8 subpanel distributions defined by the subpanel splines. They are used in "intermediate field" influence coefficient calculation.

Next, in section I.4, we discuss "far field moments", matrices describing integrals of the singularity strength over a panel in terms of the panel singularity parameters. The matrices are used in far field influence coefficient calculation. Finally, in section I.5, we discuss the theory of the least squares procedure.

We now briefly discuss the reasoning behind the subpanel and outer spline construction techniques. First (cf. section C.3), we require the spline to be stable: the disturbance in the singularity distribution caused by a perturbation of a boundary condition should die off quickly.

Second, the source spline should be linearly accurate and the doublet spline quadratically accurate. That is, if the source parameters are defined by a linear function, the source distribution defined by the spline matrices should be exactly that linear function. An analogous property should hold for the doublet splines. The justification for using a linear source and quadratic doublet distribution is given in section B.5.

Third, the spline must be local in nature. That is, the singularity distribution on a panel must depend on a reasonably small number of singularity parameters. This is due to the storage problems which would occur otherwise. That is, too much core and disk storage would otherwise be required for each panel.

Fourth, the doublet strength should be continuous (see section B.4). It would be preferable to have continuously differentiable doublet strength, continuous source strength and smooth geometry as well, since these conditions would permit a further integration by parts of the influence coefficient integrals, reducing their singularity. Unfortunately, these goals are not achievable without an unacceptable increase in the cost of evaluation of influence coefficient integrals. Moreover, while it is a fairly straightforward matter to achieve a continuous source distribution, it has been found that without smooth geometry, continuous source splines induce significant errors in the total source strength on a network, seriously degrading the accuracy of the aerodynamic influence coefficient matrix.

Finally, the entries of the PIC matrices, which are defined as sums of integrals, should be computable in closed form. That is, numerical integration should not be required for the evaluation of the integrals. The reason for this requirement is one of simplicity. The integrands in (5.6.9-10) are far too singular to be integrated numerically as they stand. It might be possible to partition the integral into a regular part, integrable numerically, and singular part, integrable in closed form, but such a method has not yet been developed.



It is the avoidance of numerical integration, in combination with the maintenance of geometric continuity, that causes much of the complexity of the spline construction. Geometric continuity between panels can be maintained either by breaking up a panel into flat subpanels, or by defining a single curved panel. The integrals over the curved panel are not computable in closed form in supersonic flow, however.

Once one has decided to use flat subpanels, a minimum of five planar regions (those of figure 5.2) is mandated to achieve geometric continuity while avoiding any kink in the surface near a panel center control point. The use of eight subpanels has been chosen because it offers a convenient method of defining a continuous doublet distribution, while not requiring polynomials of degree greater than two. An explicit polynomial distribution has been chosen rather than a parametric distribution because the integration in parametric coordinates can not be performed in closed form.

## I.1 Outer Splines

There are two basic methods that are used for the construction of outer splines, corresponding to the cases in which the resulting singularity distribution is required to be continuous, or is not. In PAN AIR, a continuous outer spline is constructed for the doublet distribution while both types of outer spline are constructed for the source distribution. The discontinuous source spline is used in the computation of influence coefficients and the evaluation of boundary conditions while the continuous source spline is used just in the post processing modules. (It was originally intended that the continuous source spline be used for all purposes. However its inability to conserve total source strength led to the introduction of discontinuous source splines in the solution portion of the code. Because the post-processing modules had built into them the assumption that source strength is single valued, the continuous source splines were retained for these essentially less demanding functions.)

The construction of continuous outer splines is a two step process. In the first step, row vectors  $SP^S$  and  $SP^D$  (called "spline vectors") are formulated for grid points as illustrated in Figure I.1c for some typical cases. These row vectors define the source or doublet strength at each enriched grid point in the network as a linear combination of surrounding singularity parameter values. In the second step, matrices  $[B^S]$  and  $[B^D]$  are constructed for each panel, giving the source or doublet strength at the appropriate grid points on the panel (panel singularity values) as linear combinations of values of singularity parameters in the neighborhood of the panel.

Thus the matrices  $[B^S]$  have five rows while the  $[B^D]$  have nine rows, since the source strength is defined at five points on a panel (the panel source parameter locations) by row vectors  $SP^S$ , while the doublet strength is defined at nine points by row vectors  $SP^D$  (see Figure I.1). The number of columns in a matrix  $B$  is variable: it equals the total number of distinct singularity parameters on which the panel source or doublet parameters depend. The matrices  $B$  are assembled from the required row vectors  $SP$  in a fairly straightforward manner described in the maintenance manual (see the preface of SUBROUTINE VECUNM of the DQG module). Briefly, first row vectors  $SP$  are computed for every grid point in the configuration (except that row vectors  $SP^S$  are not needed for panel source parameter locations) and stored on disk. Then, when the spline quantities for a single panel are being computed, the five (or nine) row vectors for each of the panel source (or doublet) singularity parameter are fetched from the disk. These row vectors are then amalgamated into a single matrix  $B^S$  (or  $B^D$ ) by VECUNM.

In this section the discussion of continuous outer spline computation will simply describe the computation of individual row vectors  $SP^S$  or  $SP^D$ . The basic principle is simple. For source splines, the source strength at a grid point is fit in a linearly accurate manner to as few surrounding source parameters as possible while for doublet splines we do the same in a quadratically accurate manner. But while the basic principle is simple, implementation is complex because of a myriad of special cases which do not fit the general rules.

The construction of a discontinuous source outer spline matrix is also performed in two steps. First, a linear function of the form  $\sigma_0 + \sigma_\xi \xi + \sigma_\eta \eta$  is obtained by performing a least squares fitting procedure that formally uses the values of the global source parameters in the neighborhood of the panel. (Here, the variables  $\xi$  and  $\eta$  are local coordinates on the mean panel.) Second, this linear function is evaluated at the five panel source parameter locations, each evaluation generating a row of the source spline matrix,  $B^S$ .

### I.1.1 Source Splines for Analysis Networks

#### I.1.1.1 Source Spline Vectors for Continuous Splines

Computing the row vector describing the source strength at the center of a panel in an analysis network is particularly simple, since a source singularity parameter is located there. Thus the source strength is just the singularity parameter value; that is,

$$\sigma_g = \lambda_k^S = [1] \lambda_k^S \quad (I.1.1a)$$

$$\text{or } [SP^S] = [1] \quad (I.1.1b)$$

the row vector of length 1 with unit value.

#### I.1.1.2 Neighboring Singularity Parameters

Next, to find the source strength at a panel corner, we perform a "bilinear fit" (a process to be described below) to the four surrounding source parameter values. In Figure I.2, we show the variety of cases which may occur in the course of determining the four neighboring source parameter locations. In the "standard" case (A), the four source parameters are the obvious adjacent ones. In cases (B) and (C), the network edge precludes the existence of some of the obvious choices, and neighboring parameters must be obtained by reaching toward the interior of the network. The logic used for points B or C, however, when extended to D, results in a large number of neighboring source parameters. To keep storage to a minimum, we choose (in a fairly arbitrary manner) from this set of points, those points which are as far as possible in index from the uncollapsed edges of the network.

#### I.1.1.3 Computation of a Local Coordinate System

Next we compute the source strength at a panel corner in terms of the four surrounding singularity parameter values, once we have in fact located these four parameters. The first step is to form a local coordinate system whose ( $\xi$ ,  $\eta$ ) plane is the one in which the source strength is to vary linearly.

The four singularity parameter locations determine (generally non-orthogonal) basis vectors  $\vec{v}_\xi$  and  $\vec{v}_\eta$ , connecting pairs of panel edge midpoints, for this coordinate system as follows. Let  $P_0$  be the grid point at which we wish to find the source strength. Then for any point  $P$  on the network, we want to be able to determine coordinates  $\xi(P)$ ,  $\eta(P)$ ,  $\zeta(P)$ , such that

$$(\vec{P} - \vec{P}_0) = \xi(P) \vec{v}_\xi + \eta(P) \vec{v}_\eta + \zeta(P) \vec{v}_\zeta \quad (I.1.2)$$

The  $(\xi, \eta, \zeta)$  coordinates used here (in section I.1) are not related to the  $X'$  coordinate system (also denoted  $(\xi, \eta, \zeta)$  at times) used in Appendix E and section I.2. Here,  $\vec{v}_\zeta$  is a vector perpendicular to the plane spanned by  $\vec{v}_\xi$  and  $\vec{v}_\eta$ . Such a vector is, of course, a multiple of  $\vec{v}_\xi \times \vec{v}_\eta$ , but a simple dimensional argument shows that if  $\vec{v}_\zeta$  is to be independent of the scale of coordinates (that is, if  $\vec{v}_\zeta$  is to be doubled when every point coordinate in the network is doubled), we must have

$$\vec{v}_\zeta = \frac{\vec{v}_\xi \times \vec{v}_\eta}{|\vec{v}_\xi \times \vec{v}_\eta|^{1/2}} \quad (I.1.3)$$

Now, to find the functions which define  $\xi$ ,  $\eta$ , and  $\zeta$ , let us first take the cross product of (I.1.2) with  $\vec{v}_\xi$  on the left, and then the dot product with  $\vec{v}_\zeta$ . Next, we take the cross product with  $\vec{v}_\eta$  on the right, and then take the dot product with  $\vec{v}_\zeta$ . Since

$$\begin{aligned} \vec{v}_\xi \times \vec{v}_\xi &= 0 = \vec{v}_\eta \times \vec{v}_\eta \\ \vec{v}_\xi \cdot \vec{v}_\zeta &= 0 = \vec{v}_\eta \cdot \vec{v}_\zeta \\ (\vec{v}_\xi \times \vec{v}_\zeta) \cdot \vec{v}_\zeta &= 0 = (\vec{v}_\zeta \times \vec{v}_\eta) \cdot \vec{v}_\zeta \end{aligned} \quad (I.1.4)$$

we obtain

$$\begin{aligned} \vec{v}_\xi \times (\vec{P} - \vec{P}_0) &= \eta(P) (\vec{v}_\xi \times \vec{v}_\eta) \\ (\vec{P} - \vec{P}_0) \times \vec{v}_\eta &= \xi(P) (\vec{v}_\xi \times \vec{v}_\eta) \\ (\vec{P} - \vec{P}_0) \cdot \vec{v}_\zeta &= \zeta(P) (\vec{v}_\zeta \cdot \vec{v}_\zeta) \end{aligned} \quad (I.1.5)$$

Dotting the first two equations with  $\vec{v}_\zeta$ , we have

$$\vec{v}_\xi \times (\vec{P} - \vec{P}_0) \cdot \vec{v}_\zeta = \eta(P) (\vec{v}_\xi \times \vec{v}_\eta) \cdot \vec{v}_\zeta = \eta(P) |\vec{v}_\xi \times \vec{v}_\eta|^{3/2} \quad (I.1.6)$$

$$\text{Thus, } \xi(P) = \frac{(\vec{P} - \vec{P}_0) \times \vec{v}_\eta \cdot \vec{v}_\zeta}{|\vec{v}_\xi \times \vec{v}_\eta|^{3/2}} \quad \zeta(P) = \frac{(\vec{P} - \vec{P}_0) \cdot \vec{v}_\zeta}{|\vec{v}_\xi \times \vec{v}_\eta|} \quad (I.1.7)$$

#### I.1.1.4 The Bilinear Fit at Panel Corner Points

Now, let  $P_1, \dots, P_4$  be the four source parameter locations for any of the cases illustrated in figure I.2, and let  $\lambda_i^S = \sigma(P_i)$  denote these source singularity parameters. Then these four values of source strength define a "bilinear" function in  $\xi$  and  $\eta$ , that is, a function

$$\sigma(\xi, \eta) = \sigma_0 + \sigma_1 \xi + \sigma_2 \eta + \sigma_3 \xi \eta \quad (I.1.8)$$

(where the symbol  $\sigma_0$  as used in section I.1 has a different meaning than in section 5 or the remainder of Appendix I), which takes on exactly these four values. The function  $\sigma(\xi, \eta)$  is defined by the fitting condition

$$\begin{aligned} \begin{Bmatrix} \lambda_1^S \\ \lambda_2^S \\ \lambda_3^S \\ \lambda_4^S \end{Bmatrix} &= \begin{bmatrix} 1 & \xi(P_1) & \eta(P_1) & \xi(P_1)\eta(P_1) \\ \dots & \dots & \dots & \dots \\ 1 & \xi(P_4) & \eta(P_4) & \xi(P_4)\eta(P_4) \end{bmatrix} \begin{Bmatrix} \sigma_0 \\ \sigma_1 \\ \sigma_2 \\ \sigma_3 \end{Bmatrix} \\ &= [BL] \begin{Bmatrix} \sigma_0 \\ \sigma_1 \\ \sigma_2 \\ \sigma_3 \end{Bmatrix} \end{aligned} \quad (I.1.9)$$

and thus

$$\begin{Bmatrix} \sigma_0 \\ \sigma_1 \\ \sigma_2 \\ \sigma_3 \end{Bmatrix} = [BL]^{-1} \begin{Bmatrix} \lambda_1^S \\ \lambda_2^S \\ \lambda_3^S \\ \lambda_4^S \end{Bmatrix} \quad (I.1.10)$$

The points  $P_1, \dots, P_4$  are not coplanar in general, and thus computing  $\sigma(\xi, \eta)$  by (I.1.10) in terms of surrounding source parameters, ignores the  $\zeta$ -component of the parameter locations; in other words, we project the parameter locations to the plane defined by  $\hat{v}_\xi$  and  $\hat{v}_\eta$ . This is justifiable

in view of the fact that a reasonable number of panels should be used in defining a geometric surface, and thus the distortions due to curvature can be neglected locally.

Now, by (I.1.7),  $\xi(P_0) = \eta(P_0) = 0$ , and thus by (I.1.8),

$$\sigma(P_0) = \sigma_0 \tag{I.1.11}$$

Thus by (I.1.10),

$$\sigma(P_0) = \sigma_0 = \begin{bmatrix} 1 & 0 & 0 & 0 \end{bmatrix} [BL]^{-1} \begin{Bmatrix} \lambda_1^S \\ \vdots \\ \lambda_4^S \end{Bmatrix} \tag{I.1.12}$$

Setting

$$[SP^S] = \begin{bmatrix} 1 & 0 & 0 & 0 \end{bmatrix} [BL]^{-1} \tag{I.1.13}$$

we see that

$$\sigma(P_0) = [SP^S] \begin{Bmatrix} \lambda_1^S \\ \vdots \\ \lambda_4^S \end{Bmatrix} \tag{I.1.14}$$

Note that  $[SP^S]$  is just the first row of  $[BL]^{-1}$ . Now, by (I.1.14),  $SP^S$  is just the row vector we seek; namely, it gives the value of source strength at the point  $P_0$  as a linear combination of four neighboring singularity parameters. A spline vector may similarly be constructed for every panel corner point in the network, whereupon matrices  $BS$  may be computed for each panel as discussed at the beginning of section I.1.

This concludes the discussion of continuous source spline construction for source analysis networks. Two special cases, networks with only one row or column, and networks with only one panel, are discussed in the maintenance document (see section 4-I.4 and SUBROUTINE ONDFIT of the DQG module).

#### I.1.1.5 Discontinuous Source Analysis Splines

The construction of a panel's discontinuous source analysis spline, required for computation of influence coefficients, is achieved by solving for coefficients  $\sigma_0, \sigma_\xi, \sigma_\eta$  of the weighted linear least squares problem

$$\min_{\sigma_0, \sigma_{\xi}, \sigma_n} G$$

where the quadratic form  $G$  is defined by

$$G = \sum_{i=1}^n [w_i (\sigma_0 + \sigma_{\xi} \xi_i + \sigma_n \eta_i - \lambda_i^S)]^2$$

Here,  $w_i$  denotes a weight and  $\lambda_i^S$  is a global source parameter at some point  $\vec{p}_i$  in the neighborhood of the panel. The coordinates  $(\xi_i, \eta_i)$  are obtained by performing a length preserving projection of  $\vec{p}_i$  onto the panel's mean plane followed by a transformation of this projected point into the mean plane coordinate system. Passing over for the present the selection of  $w_i$  and  $\lambda_i^S$ , we observe that the minimization problem we have posed has a solution of

the form

$$\begin{Bmatrix} \sigma_0 \\ \sigma_{\xi} \\ \sigma_n \end{Bmatrix} = \begin{bmatrix} & & \\ & & \\ & & \end{bmatrix} A^+ \begin{Bmatrix} \lambda_1^S \\ \lambda_2^S \\ \vdots \\ \lambda_n^S \end{Bmatrix}$$

Here, we have used the conventional notation  $A^+$  to denote a matrix pseudo-inverse. Now, letting  $(\hat{\xi}_k, \hat{\eta}_k)$ ,  $k = 1, \dots, 5$  denote mean plane coordinates of the projection\* of the five panel source parameter locations onto the mean plane, we may evaluate the five panel source parameters by

$$\sigma_k = \sigma_0 + \sigma_{\xi} \hat{\xi}_k + \sigma_n \hat{\eta}_k$$

This evaluation process induces an expression for  $\sigma_k$  in terms of  $\lambda_i^S$ , providing a definition for  $[BS]$ , the source outer spline,

$$\begin{Bmatrix} \sigma_1 \\ \sigma_2 \\ \vdots \\ \sigma_5 \end{Bmatrix} = \begin{bmatrix} 1 & \hat{\xi}_1 & \hat{\eta}_1 \\ 1 & \hat{\xi}_2 & \hat{\eta}_2 \\ \vdots & \vdots & \vdots \\ 1 & \hat{\xi}_5 & \hat{\eta}_5 \end{bmatrix} \begin{bmatrix} A^+ \end{bmatrix} \begin{Bmatrix} \lambda_1^S \\ \lambda_2^S \\ \vdots \\ \lambda_n^S \end{Bmatrix}$$

$$= [BS]_{\lambda}$$

\* This projection is performed in scaled coordinates.

We now return to the problem of selection of weights and global source parameters to be used in the fitting process. In Figure I.23 we illustrate the variety of cases which may arise when identifying the neighboring source parameters to be used in spline construction. For any given panel, the parameters  $\lambda_i^S$  are selected as indicated. The weights  $w_i$  are chosen as follows:

$$w_i = \begin{cases} 1 & \text{if } \lambda_i^S \text{ does not lie on the panel for which } B^S \text{ is} \\ & \text{being computed} \\ 10000 & \text{if } \lambda_i^S \text{ lies on the panel} \end{cases}$$

The choice of a very large weight for the panel's own source parameter is crucial in that it is this condition that causes total source strength for the panel to be correct to sufficient accuracy.

The foregoing procedure will fail to provide enough data points if the network in which the panel lies has only one row or column of panels. When this happens, points  $\hat{p}_i$  are selected as indicated in Figure I.24. The value of  $\lambda_i^S$  used for points  $\hat{p}_i$  that are not global source parameter points is just the value of source strength at the panel center.

#### I.1.2 Doublet Spline Vectors for Analysis Networks, Doublet Forward Weighted Splines

Doublet spline vectors  $SP^D$  are more complex to compute for a variety of reasons. First, the requirement of quadratic accuracy forces the doublet strength at a grid point to depend on a greater number of singularity parameters than the source strength. Second, to insure doublet continuity across network edges on non-smooth abutments (along which boundary conditions specifying the matching of doublet strength are imposed), we require that the doublet strength at any point on a network edge depend only on the singularity parameters located on the network edge. The example of a thin wing with a curved planform illustrates the need for this requirement (cf. Figure I.3). The doublet strength is zero at the singularity parameter locations on the free network edge. If the doublet strength at a panel corner point on the edge depended on singularity parameters in the interior, it could not be zero, independent of conditions in the network interior, as we wish it to be. But by insisting that it only depend on edge parameters, we insure that it is zero.

A third cause of increased complexity in determining doublet spline row vectors is the introduction of "smooth abutments." These are abutments consisting of portions of two distinct network edges, along which splines rather than boundary conditions are used to enforce continuity of doublet strength.

For grid points which do not lie on a network edge, obtaining the row vector  $SP^D$  which describes the doublet strength at each grid point in terms of surrounding singularity parameters is a two step process. First, the set of surrounding singularity parameters is determined. Second, the doublet strength at the grid point is determined in a quadratically accurate manner in terms of the neighboring singularity parameters.



Doublet forward weighted (DFW) spline vectors are calculated in the same manner as the doublet analysis spline vectors. The only difference being weighting factors used in the least squares fit. A description of the different weighting scheme is given in section I.1.2.4.

### I.1.2.1 The Quadratic Least Squares Fit for Panel Corners or Panel Edge Midpoints

This quadratically accurate procedure is somewhat more complex than the bilinear fit employed for source splines. While there is generally a bilinear function which exactly fits values at four points (unless three of the four lie on a line, which is unlikely if they are panel centers), a quadratic function is less well behaved. There is a unique quadratic through six points, unless these points all lie on two lines. With very regular paneling, however, it is quite likely that six center points chosen as neighbors of a grid point will, in fact, lie on two lines. Thus, the procedure we choose for the quadratic fit is a "least squares" procedure.

That is, we choose an excessive number of neighboring singularity parameters, and find the quadratic function which takes on the values of the closest singularity parameters exactly, while taking on the the values of the remaining singularity parameters in a "least squares" sense. The row vector  $SP^D$  for the grid point is determined by the value the fitting function takes on at the grid point, expressed as a linear combination of the neighboring singularity parameter values.

We now describe this least squares procedure more precisely. Let  $(\lambda_i^D, i = 1, \dots, k)$  be the singularity parameters (in the neighborhood of the selected grid point) to which we fit the quadratic function exactly. Let  $(\lambda_i^D, i = k + 1, \dots, k+m)$  be the remaining neighboring singularity parameters. Let  $\lambda_i^D$  be located at  $(\xi_i, \eta_i, \zeta_i)$ , where the computation of these coordinates will be discussed shortly. Once again, however, this is not the local  $(\xi, \eta, \zeta)$  coordinate system denoted  $X'$  in Appendix E.

Let A be the matrix

$$A = \begin{bmatrix} 1 & \xi_1 & \eta_1 & 1/2 \xi_1^2 & \xi_1 & \eta_1 & 1/2 \eta_1^2 \\ \dots & \dots & \dots & \dots & \dots & \dots & \dots \\ 1 & \xi_k & \eta_k & 1/2 \xi_k^2 & \xi_k & \eta_k & 1/2 \eta_k^2 \end{bmatrix} \quad (I.1.15)$$

This is the matrix for which any function

$$f(\xi, \eta) = f_1 + f_2 \xi + f_3 \eta + 1/2 f_4 \xi^2 + f_5 \xi \eta + 1/2 f_6 \eta^2 \quad (I.1.16)$$

taking on the values

$$f(\epsilon_i, \eta_i) = \lambda_i^D \quad i = 1, \dots, k \quad (I.1.17)$$

satisfies

$$[A]^{k \times 6} \begin{Bmatrix} f_1 \\ f_2 \\ \vdots \\ f_6 \end{Bmatrix} = \begin{Bmatrix} \lambda_1^D \\ \lambda_2^D \\ \vdots \\ \lambda_k^D \end{Bmatrix} \quad (I.1.18)$$

Now, whenever  $k < 6$ , as it will be in the current applications, equation (I.1.18) does not fully specify the coefficients of  $f$ . The coefficients are completely specified by requiring the minimization of

$$I = \sum_{i=k+1}^{k+m} w_i^2 [f(\epsilon_i, \eta_i) - \lambda_i^D]^2 \quad (I.1.19)$$

where  $w_i$  is a "weight", to be discussed shortly, which depends on the relative locations of the singularity parameter and the grid point.

If we write

$$[A_1]^{m \times 6} = \begin{bmatrix} 1 & \epsilon_{k+1} & \eta_{k+1} & 1/2 \epsilon_{k+1}^2 & \epsilon_{k+1} \eta_{k+1} & 1/2 \eta_{k+1}^2 \\ \vdots & \vdots & \vdots & \vdots & \vdots & \vdots \\ 1 & \epsilon_{k+m} & \eta_{k+m} & 1/2 \epsilon_{k+m}^2 & \epsilon_{k+m} \eta_{k+m} & 1/2 \eta_{k+m}^2 \end{bmatrix} \quad (I.1.20)$$

equation (I.1.19) becomes

$$I = \sum_{i=k+1}^{k+m} w_i^2 \left( \sum_{s=1}^6 (A'_{i-k,s}) f_s - \lambda_i^D \right)^2 \quad (I.1.21)$$

The method by which we minimize (I.1.21), subject to the exact conditions (I.1.18), is called a "constrained least squares" procedure, and is discussed in section I.5. The result of performing this procedure is a  $(6 \times (k+m))$  matrix LSQ such that

$$\begin{Bmatrix} f_1 \\ \vdots \\ f_6 \end{Bmatrix} = [\text{LSQ}] \begin{Bmatrix} \lambda_1^D \\ \cdot \\ \cdot \\ \cdot \\ \lambda_{k+m}^D \end{Bmatrix} \quad (\text{I.1.22})$$

Now, we will construct our  $(\xi, \eta, \zeta)$  coordinate system such that at the grid point  $P_0$  we have

$$\begin{aligned} \xi(P_0) &= 0 \\ \eta(P_0) &= 0 \end{aligned} \quad (\text{I.1.23})$$

Thus,

$$f(P_0) = f_1 = [\text{LSQ}_{1,\cdot}] \begin{Bmatrix} \lambda_1^D \\ \vdots \\ \lambda_{k+m}^D \end{Bmatrix} \quad (\text{I.1.24})$$

But we required the row vector  $SP^D$  to define the value at  $P_0$  of the quadratic function  $f$  which satisfied (I.1.18) while minimizing (I.1.21), and thus

$$[SP^D] = [\text{LSQ}_{1,\cdot}] \quad (\text{I.1.25})$$

that is,  $SP^D$  is the first row vector of the matrix LSQ defined by the constrained least squares procedure.

In describing the construction of  $SP^D$  for a grid point in a network interior, we have deferred the discussion of three items. These are the determination of the set of neighboring singularity parameters, their  $(\xi, \eta, \zeta)$  coordinates, and the corresponding weights  $w_i$ . We will discuss them in order as follows.

### I.1.2.2 Neighboring Points for Least Squares Fit

Figure I.4a illustrates the location of neighboring singularity parameters for grid points which do not lie near a network edge. Note that, since a singularity parameter is located at each panel center, the spline vector  $SP^D$  for a panel center point is (like the spline vector  $SP^S$ ) a vector of length 1 with a unit entry.

Now, if the grid point (panel corner or edge midpoint) lies near (but not on) a network edge, the set of neighbors must include singularity parameters on the network edge. Actually, we fit a quadratic function to neighboring grid points, where these grid points need only be singularity parameter locations when they are in the interior of the network. The value of doublet

strength at those grid points which lie on the network edge depends in turn on a small number of singularity parameters located on the network edge. This is a procedure which is defined in detail in the maintenance document (see section 4-I).

Figure I.4.b illustrates the neighboring points we use for the quadratic fit to obtain a spline vector for a grid point which lies near (but not on) a network edge which does not belong to a smooth abutment. Recall that only one singularity parameter is located on a collapsed edge of a network.

Figure I.4c illustrates the set of neighboring points when the grid point in question lies near a smooth abutment. In this case, we see that the set of "neighboring points" may lie in two distinct networks. This is because the singularity parameters on the network edges on the smooth abutment (though not at the corner points at the ends of the abutment) have been removed for reasons of economy. The neighboring points in the same network as the point  $P_0$  are chosen in the usual manner (see Figure I.4a) while those in the adjacent network are chosen as illustrated. The precise method by which the latter points are picked is described in the maintenance document (section 4-I.2.1.2).

### I.1.2.3 Construction of a Local Coordinate System

Next we discuss the construction of a  $(\xi, \eta, \zeta)$  coordinate system. This system is similar but not identical to that of section I.1.1.3, and totally distinct from the  $X'$  coordinate system  $X'$  of Appendix E or section I.2.2.5. First, we construct basis vectors  $\hat{v}_\xi$  and  $\hat{v}_\eta$  as illustrated in Figure I.5. That is,  $\hat{v}_\xi$  and  $\hat{v}_\eta$  span pairs of enriched grid points adjacent to the base point  $P_0$ . Next, we define  $\hat{v}$  by (I.1.3). Then, analogously to (I.1.17), we define

$$\begin{aligned} \bar{\xi}(P) &= \frac{(\vec{P} - \vec{P}_0) \times \hat{v}_\eta \cdot \hat{v}_\zeta}{|\hat{v}_\xi \times \hat{v}_\eta|^{3/2}} & \bar{\eta}(P) &= \frac{\hat{v}_\xi \times (\vec{P} - \vec{P}_0) \cdot \hat{v}_\zeta}{|\hat{v}_\xi \times \hat{v}_\eta|^{3/2}} & \bar{\zeta}(P) &= \frac{(\vec{P} - \vec{P}_0) \cdot \hat{v}_\zeta}{|\hat{v}_\xi \times \hat{v}_\eta|} \end{aligned} \quad (I.1.26)$$

The bars indicate that these are preliminary coordinate values which will be adjusted to account for surface curvature. Consider a cylindrical surface, as illustrated in Figure I.6. If we use the coordinates  $\xi$  and  $\eta$  above, we are essentially projecting the surface down to the tangent plane at the point  $P_0$ . When the surface is highly curved, this makes the points A and D appear to be closer to  $P_0$  than they really are, since we are dealing with their projected images A' and D'. The points B' and C' are also closer to the grid point than B and C, but not in the same proportion.

We rectify this by scaling the  $\xi$  and  $\eta$  coordinates of a point according to its height above the tangent plane. We define a scaling factor

$$A(P) = \frac{\left[ \bar{\xi}(P)^2 + \bar{\eta}(P)^2 + \bar{\zeta}(P)^2 \right]}{\bar{\xi}(P)^2 + \bar{\eta}(P)^2} \quad (I.1.27)$$

Then we define

$$\begin{aligned} \xi(P) &= A(P) \vec{\xi}(P) \\ \eta(P) &= A(P) \vec{\eta}(P) \end{aligned} \quad (I.1.28)$$

This coordinate scaling assures that the contribution of distant points is more accurately measured. Note that the denominator of  $A(P)$  is non-zero provided  $P \neq P_0$ .

#### I.1.2.4 Weights for the Least Squares Fit

Next we consider the weights  $w_i$  for the least squares procedure. In order to provide stability, we would like to fit more closely to nearby singularity parameters than further ones. This is done in part by fitting the quadratic function exactly to the nearest parameters, as illustrated by Figure I.4.

A second consideration in determining weights is the desire to give heavier weights in supersonic flow to points which are upstream of the grid point than to those which are downstream. This weighting has been found experimentally to reduce instabilities which arise at high Mach numbers. In recognition of these requirements, we set  $w_i = w(P)$  where

$$w(P) = \frac{1 + kM_\infty(1 - \hat{c}_0 \cdot (\vec{P} - \vec{P}_0) / |\vec{P} - \vec{P}_0|)}{(1 + 2kM_\infty)} \quad (I.1.29)$$

The constant  $k$  is set to zero in subsonic flow in view of the lack of a preferred upstream direction. That is, the compressibility direction  $c_0$  may be replaced by  $-\hat{c}_0$  without changing the solution to the equation. In supersonic flow,  $k$  has been chosen by experiment, and has order of magnitude 1.

Since the dot product of unit vectors lies between  $-1$  and  $1$ , the numerator of (I.1.29) lies between  $1$  and  $(1 + 2kM_\infty)$ . Thus the ratio of weight (neglecting the effect of distance) at a directly upstream point to that at a directly downstream point is  $1 + 2kM_\infty$ . For  $M_\infty = 3$ , and  $k = 1$  (the provisional choice for  $k$ ), this ratio is  $7$ .

The weights for the doublet forward weighted splines are obtained from equation I.1.29 by setting  $k = 1$  and  $M_\infty = 2$ . Thus, the simple expedient of changing the weights in a least squares fit transforms a doublet analysis spline into a doublet design spline (DFW).

#### I.1.2.5 Edge Splines for Non-Smooth Abutments

Finally we consider grid points (panel corner points or edge midpoints) lying on a network edge. A network edge is divided into distinct portions belonging to different abutments. A doublet parameter is located at the grid points which form the endpoints of the portion of the edge belonging to the abutment (if such an endpoint is not a network corner point, the doublet parameter is an "extra" singularity parameter (see figure 5.13)). Doublet

parameters are also located at the panel edge midpoints unless the abutment is a smooth one, in which case the parameters are removed (doublet parameters located at abutment endpoints are retained for simplicity).

We discuss first the case of a non-smooth abutment. In that case, the value of doublet strength at a grid point depends only on singularity parameters located on the network edge.

Consider the abutment illustrated in Figure I.7a, with one network edge panelled more finely than the other and with a panel corner on the more finely paneled network located wherever the more coarsely paneled network edge has a panel corner. The goal is to find a splining method such that the imposition of doublet matching boundary conditions of some or all of the control points on the edge results in the exact matching of doublet strength on the whole edge.

Experimentation with least-squares-type splines shows that they cannot satisfy the above considerations. Let us consider, on the other hand, a differentiable spline. Let the edge be divided into  $n$  intervals, as illustrated in Figure I.7b. It is reasonable to ask how many differentiable functions exist, defined by a single quadratic on each of the  $n$  intervals. Now, there are  $3n$  linearly independent quadratic functions altogether (since a quadratic function on an interval has 3 coefficients), and requiring continuity at  $P_2, \dots, P_{n-1}$  yields  $(n-1)$  constraints on the set of functions, while requiring continuity of derivative at these points provides  $(n-1)$  additional constraints. Thus, there are  $(n+2)$  linearly independent piecewise quadratic functions with continuous derivatives.

But this is equal to the number of control points on the edge, and so there is a unique differentiable function which takes on a prescribed set of  $(n + 2)$  values at the midpoints of the intervals and the endpoints of the edge.

We can apply this result to the situation illustrated by Figure I.7a. The doublet distribution on the edge 1 will consist of some differentiable function defined by a single quadratic on each interval of edge 1. If we now impose doublet matching boundary conditions at the control points of edge 2, we obtain on edge 2 the unique differentiable doublet distribution defined as a single quadratic on each interval of edge 2, which agrees with the doublet distribution on edge 1 at the specified points. But, since every interval of edge 2 is a subset of a corresponding interval on edge 1, the doublet distribution on edge 1 satisfies the above criterion too. So, since the distribution is unique, the doublet distributions on edge 1 and edge 2 are identical.

Summarizing, we have shown that if edges 1 and 2 form an abutment, and the paneling on edge 2 is a "refinement" of the paneling on edge 1 (that is, every corner point of edge 1 is also a corner point on edge 2, though edge 2 may have additional corner points), then the imposition of doublet matching at the control points of edge 2 results in exact matching of doublet strength along the entire abutment. Generalizing, if several network edges meet in an abutment, and one edge is a refinement of each of the other edges, then the imposition of doublet matching boundary conditions on that edge forces the alternating sum of the doublet strengths to zero:

$$\sum s_j \mu_j = 0 \quad (I.1.30)$$

where  $s_j = \pm 1$ .

Unfortunately, the differentiable edge spline, while leading to doublet continuity under a greater variety of circumstances, does not permit forward weighting in supersonic flow. As a result, the differentiable edge spline is insufficiently stable and cannot be used in Pan Air. This fact was determined fairly late in the development of Pan Air, and thus a discussion of the differentiable edge spline has been included in this document.

The spline which is actually implemented in Pan Air is a one dimension quadratic least squares fit. Consider, for instance, a network edge as illustrated in figure I.7b. The points  $P_1, \dots, P_{n+1}$ , and  $M_i$ ,  $i=1, \dots, n$ , are singularity parameter locations, and the doublet strength there is defined to be equal to the value of the singularity located there. Thus the doublet spline vector  $SP^D$  for each of these points is a unit vector of length one, as it is for panel center points in a doublet analysis network.

Next, the doublet strength at the points  $P_i$ ,  $i=2, \dots, n-1$ , is obtained by a constrained least squares analogous to that described in section I.1.2.1, but in one dimension. That is, the quadratic function  $f(t)$  ( $t$  a variable defining distance along the network edge) is found such that

$$f(M_k) = \mu(M_k) = \lambda_k^D \quad k = i, i+1 \quad (I.1.31a)$$

$$\text{and } f(M_r) = \mu(M_r) = \lambda_r^D \quad r = i-1, i+2 \quad (I.1.31b)$$

in a least squares sense.

Then the row vector  $SP^D$  which defines  $\mu(P_i)$  in terms of the singularity parameters ( $\lambda_k^D$ ,  $k = i-1, \dots, i+2$ ), is such that

$$\mu(P_i) = f(P_i) \quad (I.1.31c)$$

We now discuss the differentiable edge spline which is not implemented in Pan Air. First we must compute the spline matrices which correspond to this differentiable piecewise quadratic distribution. It can be shown numerically that such a function, if it has a non-zero value at one panel center, and is zero at all other panel centers and the endpoints of the edge, is never identically zero. Rather, it behaves as illustrated in Figure I.8; oscillating with an amplitude which diminishes rapidly but never reaches zero. Thus, the spline is stable under doublet specification boundary conditions; however, it is not local, since the doublet strength on an interval depends weakly on the doublet strength at a panel center far away.

In order to avoid storing lengthy spline vectors, we must redefine our doublet parameters to make the spline local. That is, a doublet parameter on a network edge will not have as its value the doublet strength at its location. For this purpose, consider the interval  $[-1, 1]$  on which we define the quadratic function

$$\mu(x) = a + bx + cx^2 \quad (\text{I.1.32a})$$

Now,  $\mu(-1) = a - b + c$

$$\mu(1) = a + b + c \quad (\text{I.1.32b})$$

$$\frac{d\mu}{dx}(-1) = b - 2c$$

$$\frac{d\mu}{dx}(1) = b + 2c \quad (\text{I.1.33})$$

Thus,

$$\mu(-1) + \frac{d\mu}{dx}(-1) = a - c = \mu(1) - \frac{d\mu}{dx}(1) \quad (\text{I.1.34})$$

Generalizing (I.1.34) to the interval  $[P_i, P_{i+1}]$  in Figure I.7b, we have

$$\begin{aligned} \mu(P_i) + 1/2 \mu'(P_i) (P_{i+1} - P_i) \\ = \mu(P_{i+1}) + 1/2 \mu'(P_{i+1}) (P_i - P_{i+1}) \end{aligned} \quad (\text{I.1.35})$$

We thus define

$$\lambda_i^D = \mu(P_i) + 1/2 \widehat{\nabla} \mu(P_i) \cdot (\widehat{P}_{i+1} - \widehat{P}_i) \quad i = 1, \dots, n \quad (\text{I.1.36})$$

$$\lambda_i^D = \mu(P_i), \quad i = 0, n+1 \quad (\text{I.1.37})$$

Now, by (I.1.35)

$$\lambda_{i-1}^D = \mu(P_i) + 1/2 \widehat{\nabla} \mu(P_i) \cdot (\widehat{P}_{i-1} - \widehat{P}_i) \quad i = 2, \dots, n+1 \quad (\text{I.1.38})$$

Combining (I.1.40) and (I.1.42), and noting that  $\widehat{\nabla} \mu$  is continuous, we have



$$\begin{aligned}
& (P_i - P_{i-1}) \lambda_i^D + (P_{i+1} - P_i) \lambda_{i-1}^D = \\
& (P_i - P_{i-1}) \mu(P_i) + 1/2 \frac{d\mu}{dx}(P_i) (P_{i+1} - P_i) (P_i - P_{i-1}) \\
& + (P_{i+1} - P_i) \mu(P_i) + 1/2 \frac{d\mu}{dx}(P_i) (P_i - P_{i-1}) (P_{i+1} - P_i)
\end{aligned} \tag{I.1.39}$$

Thus,

$$\begin{aligned}
\mu(P_i) = & \frac{|\hat{P}_i - \hat{P}_{i-1}|}{|\hat{P}_i - \hat{P}_{i-1}| + |\hat{P}_{i+1} - \hat{P}_i|} \lambda_i^D \\
& + \frac{|\hat{P}_{i+1} - \hat{P}_i|}{|\hat{P}_i - \hat{P}_{i-1}| + |\hat{P}_{i+1} - \hat{P}_i|} \lambda_{i-1}^D
\end{aligned} \tag{I.1.40}$$

This defines the spline vector for  $P_i$  as computed with the differentiable edge spline, which is not implemented in Pan Air.

Now, we wish to evaluate  $\mu(M_i)$ ,  $i=1, \dots, n$ . Again consider a function  $\mu(x)$  on  $[-1, 1]$  defined by (I.1.31).

Then

$$\mu(-1) = a - b + c$$

$$\mu(1) = a + b + c$$

$$\mu(-1) + \frac{du}{dx}(-1) = a - c \tag{I.1.41}$$

So,

$$\mu(0) = a = .$$

$$1/4 \mu(-1) + 1/4 \mu(1) + 1/2 [\mu(-1) + \frac{du}{dx}(-1)] \tag{I.1.42}$$

Applying this to Figure I.7b, we see

$$\begin{aligned}
\mu(M_i) = & 1/4 \mu(P_i) + 1/4 \mu(P_{i+1}) + 1/2 \lambda_i^D \\
& i = 1, \dots, n
\end{aligned} \tag{I.1.43}$$

This defines the spline vector for  $M_i$ .

Equations (I.1.37), (I.1.41), and (I.1.43) together describe  $\mu$  at grid points which lie on a network edge belonging to a non-smooth abutment as linear combinations of neighboring singularity parameters on the edge. We again point out that this procedure is not implemented in Pan Air.

#### I.1.2.6 Edge Splines for Smooth Abutments

We now describe the computation of spline vectors for grid points lying on smooth abutments. Once again, to obtain matching of doublet strength we require that one network be paneled as a refinement of the other, as in the example of Figure I.7a. Then, spline vectors for grid points on the more coarsely paneled edge are computed first, followed by spline vectors for grid points on the more finely paneled edge.

Spline vectors for grid points on the coarser edge are also computed by a constrained least squares procedure, even though again the "neighboring points" lie in two networks. Figure I.9a shows some representative examples which illustrate the procedure for choosing the set of neighboring points. The method is described precisely in the Maintenance Document (see Appendix I of section 4).

Now, continuity of doublet strength along a smooth abutment is insured by requiring the doublet strength at a grid point on the more finely paneled network to be identical (as a linear combination of surrounding singularity parameters) to that at the "corresponding" point on the coarsely paneled network. We determine the corresponding point by "parametrizing" the abutment, that is, assigning to each grid point a real number  $t$ ,  $0 < t < 1$ , which specifies the proportion of the total abutment length that the grid point is distant from the starting point of the abutment. This procedure is discussed in more detail in the maintenance document (see SUBROUTINE PRMEDG of the DQG module).

Figure I.9b illustrates the parametrization of an abutment. Now, some grid point  $P'_i$  on the fine network will have parameter value  $t'_i$ , where

$$t_j < t'_i < t_{j+1} \quad (\text{I.1.44})$$

for some integer  $j$ , that is, the corresponding point on the coarse network is not a grid point. But,  $\mu$  must vary quadratically on the panel edge, so we can obtain  $\mu(P'_i)$  as a linear combination of  $\mu(P_j)$ ,  $\mu(P_{j+1})$ , and  $\mu(P_{j+2})$ .

Now, it follows from (I.1.31-32) that on an interval  $[-1, 1]$ ,

$$\begin{aligned} \mu(x) &= a + bx + cx^2 = \\ &\mu(0) + (1/2\mu(1) + 1/2\mu(-1))x \\ &+ [1/2\mu(1) + 1/2\mu(-1) - \mu(0)]x^2 \end{aligned} \quad (\text{I.1.45})$$

We can apply this to the interval in Figure I.9c by making the transformation

$$x' = \frac{t - t_j}{t_{j+2} - t_j} \quad (\text{I.1.46})$$

$$\begin{aligned} x &= 2x' - 1 \\ &= \frac{2t - t_{j+2} - t_j}{t_{j+2} - t_j} \end{aligned} \quad (\text{I.1.47})$$

Equation (I.1.46) maps the interval in Figure I.9c to  $[0, 1]$ , which in turn is mapped to  $[-1, 1]$  by (I.1.47).

Substituting (I.1.47) in (I.1.45), we obtain

$$\begin{aligned} \mu(t) &= \mu(P_{j+1}) + [1/2 \mu(P_{j+2}) - 1/2 \mu(P_j)] \frac{2t - t_{j+2} - t_j}{t_{j+2} - t_j} \\ &+ [1/2 \mu(P_{j+2}) + 1/2 \mu(P_j) - \mu(P_{j+1})] \left[ \frac{2t - t_{j+2} - t_j}{t_{j+2} - t_j} \right]^2 \end{aligned} \quad (\text{I.1.48})$$

Setting  $t = t'_i$ , we have  $\mu(P_i)$  as a linear combination of  $\mu(P_j)$ ,  $\mu(P_{j+1})$ , and  $\mu(P_{j+2})$ :

$$\begin{aligned} \mu(P'_i) &= (-1/2 + 1/2 \tau^2) \mu(P_j) \\ &+ (1 - \tau^2) \mu(P_{j+1}) + (1/2 + 1/2 \tau^2) \mu(P_{j+2}) \end{aligned} \quad (\text{I.1.49})$$

$$\text{where } \tau = \frac{2 t'_i - t_{j+2} - t_j}{t_{j+2} - t_j} \quad (\text{I.1.50})$$

This concludes our discussion of spline vector construction for doublet analysis networks. We have now discussed the computation of doublet spline vectors for all enriched grid points in a doublet analysis network. In practice, these vectors are all computed and stored on a disk. Then, within a loop over panels, the spline vectors corresponding to the nine panel defining points are retrieved from the disk, and merged into an outer spline matrix  $B^D$  by VECUNM.

### I.1.3 Doublet Spline Vectors for Wake Networks

Singularity parameter locations for doublet wake networks are illustrated in Figure D.3. In addition, if the edge of the wake I networks on which singularity parameters are located forms part of more than one abutment, an extra singularity parameter is located at the abutment endpoints lying in the interior of the edge.

The purpose of a doublet wake 1 network is to model a wake surface on which the doublet strength is constant in the streamwise direction. Thus, spline vectors for grid points are constructed as follows. First, spline vectors are constructed for each grid point on the edge containing singularity parameters, just as though the edge were part of a non-smooth abutment of an analysis network (it should be noted in passing that smooth abutments are only permitted between analysis networks). Then, the spline vector constructed for a particular grid point on the edge is also used for every grid point lying in the column or row of points emanating in an indicially perpendicular direction from the edge. This produces a doublet strength which is constant in one indicial direction, as desired. In general this direction is the direction of increasing row index, though this program default may be overridden by the user. See section 7, record N12, of the User's Manual.

Doublet wake 2 networks are used to define a constant strength doublet sheet, whose strength is the value of the one singularity parameter in the network. Thus, the identical spline vector is constructed for every grid point on the network; namely the row vector of length one with unit entry.

### I.1.4 Source Splines for Design Networks

#### I.1.4.1 Source Design 1

Only one type of source outer spline, a continuous one, is used for source design 1 networks. Singularity locations for source design networks are given by Figure D.1. Since a source parameter is located at every panel corner, the spline vectors for these grid points are just unit vectors of length 1. Spline vectors for panel centers are also straightforward to compute:

$$SP^S = [1/4 \ 1/4 \ 1/4 \ 1/4] \quad (I.1.51)$$

That is, the source strength at a panel center is defined as the average of the source strengths at all the panel corners.

#### I.1.4.2 Source Design 2, Discontinuous Source Splines

For source design 2 networks source parameters are located at those edge midpoints on edges parallel to the matching edge. To reduce the complexities of splines PAN AIR imposes two restrictions on source design 2 networks: They may not have collapsed edges and they may not have just one column or one row of panels.

The discontinuous source spline for a source design 2 network, used for influence coefficient computation and boundary condition evaluation, is computed by means of a three stage process. First, spline vectors are computed for the panel centers and for those panel edge midpoints that are not source parameter locations. (See figure D.1c for an illustration of the source parameter location on a source design 2 network.) Second, the five source values on the panel, (the panel center and four edge midpoint values) are fitted to obtain a source distribution function of the form  $\sigma_0 + \sigma_{\xi} \xi + \sigma_{\eta} \eta$ .

Third, this distribution is evaluated at the five panel source parameter locations.

This process can be summarized by the equation

$$\begin{Bmatrix} \hat{\sigma}_1 \\ \hat{\sigma}_2 \\ \hat{\sigma}_3 \\ \hat{\sigma}_4 \\ \hat{\sigma}_5 \end{Bmatrix} = \begin{bmatrix} 1 & \hat{\xi}_1 & \hat{\eta}_1 \\ 1 & \hat{\xi}_2 & \hat{\eta}_2 \\ 1 & \hat{\xi}_3 & \hat{\eta}_3 \\ 1 & \hat{\xi}_4 & \hat{\eta}_4 \\ 1 & 0 & 0 \end{bmatrix} \begin{bmatrix} A^+ \\ (3 \times 5) \end{bmatrix} \begin{bmatrix} 1 & 0 & 0 & 0 & 0 & 0 \\ * & * & * & * & 0 & 0 \\ 0 & 1 & 0 & 0 & 0 & 0 \\ * & * & 0 & 0 & * & * \\ \frac{1}{2} & \frac{1}{2} & 0 & 0 & 0 & 0 \end{bmatrix} \begin{Bmatrix} \lambda_1 \\ \lambda_2 \\ \lambda_3 \\ \lambda_4 \\ \lambda_5 \\ \lambda_6 \end{Bmatrix}$$

Here, each stage of the process is represented by a matrix.

The first stage of this process requires further explanation. First the source strength at the panel center is taken to be the average of the two global source parameters that lie on the boundary of the panel. Next, the extra panel edge midpoint source strengths are obtained by means of a bilinear fit of neighboring global source parameter data, as illustrated in figure I.25. The bilinear fit performed here is essentially the same as the bilinear fit described in sections I.1.1.3 and I.1.1.4 in connection with continuous source analysis splines.

#### I.1.4.3 Source Design 2, Continuous Source Splines

The continuous source spline for a source design 2 network, used by PAN AIR's post processing modules for pressure, force and moment calculations, is generated by computing spline vectors for the panel center and corners. Taking the source strength at the panel center to be the average of the panel's two global source parameters, we have

$$SP^S = \left[ \frac{1}{2} \quad \frac{1}{2} \right]$$

The panel corner spline vectors are obtained by means of the usual sort of bilinear fit using global source parameter data as indicated by figure I.26.

### I.1.5 Doublet Splines for Design Networks

Figure D.2 shows the location of singularity parameters on a doublet design network. For grid points in the interior of the network, spline vectors are computed by fitting to neighboring points, as illustrated in Figure I.10a. For grid points on the "matching edges" (which have singularity parameters located at the panel edge midpoints), the doublet analysis edge spline of section I.1.2.5 is used.

The only unusual aspect of doublet design splines is the edge spline for non-matching edges. The doublet parameters are located at panel corners along these edges (rather than panel edge midpoints) for stability, since the boundary conditions in the vicinity of non-matching edges tend to be doublet gradient boundary conditions. For nonmatching edges, as for matching edges, a differentiable edge spline and a least squares edge spline are available, though once again the least squares spline is implemented in Pan Air. The least squares spline is similar to that for matching edges, except that now it is at panel edge midpoints that the doublet strength is defined by least squaring to the four surrounding edge doublet parameters, while at panel corners the doublet strength is defined by a unit spline vector.

We now discuss the construction of the differentiable edge spline. Let  $\lambda_i^D$  be the value of the doublet parameter located at a panel corner  $P_i$  as illustrated in Figure I.10b. We define a row vector  $\{\gamma_i\}$ ,  $0 \leq i \leq n$  ( $n$  the number of panel corners on the network edge) of length  $n$  as follows. We define  $\gamma_0$  and  $\gamma_n$  to be row vectors with the entries 1 in the first entry and the  $n$ th entry, respectively, and otherwise zero. For  $1 < i < n - 1$ , we obtain  $\gamma_i$  by performing a one-dimensional least squares fit to the 4 (or 3, if  $i=1$  or  $n-1$ ) neighboring singularity parameters on the edge.

Thus, at each edge midpoint, and at the endpoints of the edge, a row vector  $\gamma_i$  is defined. This is analogous to the situation for the differentiable doublet analysis edge spline. We now obtain  $\mu$  at corner points and edge midpoints by using the doublet analysis edge spline, but in terms of the  $\gamma_i$  rather than the singularity parameters.

For example, we have, analogously to (I.1.40),

$$\mu(P_5) = \frac{|\hat{P}_6 - \hat{P}_5|}{|\hat{P}_6 - \hat{P}_5| + |\hat{P}_5 - \hat{P}_4|} \{\gamma_4\} \{\lambda_i^D\} + \frac{|\hat{P}_5 - \hat{P}_4|}{|\hat{P}_6 - \hat{P}_5| + |\hat{P}_5 - \hat{P}_4|} \{\gamma_5\} \{\lambda_i^D\} \quad (I.1.52)$$

This concludes our discussion of spline vector construction. Details of the construction are contained in the Maintenance Document (section 4-I.2.3). We note that the "RESERVE" spline discussed there is in fact the least squares edge spline implemented in Pan Air.

This page has been left blank intentionally.

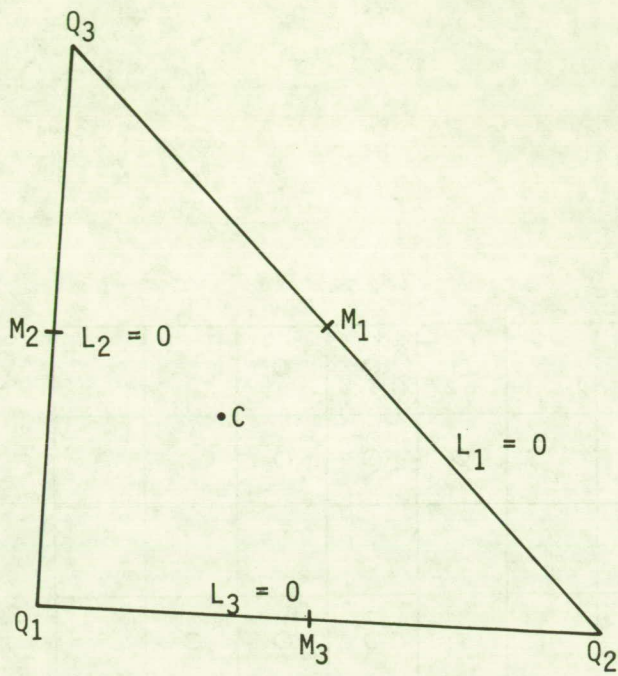


Figure I.21 - Standard half panel

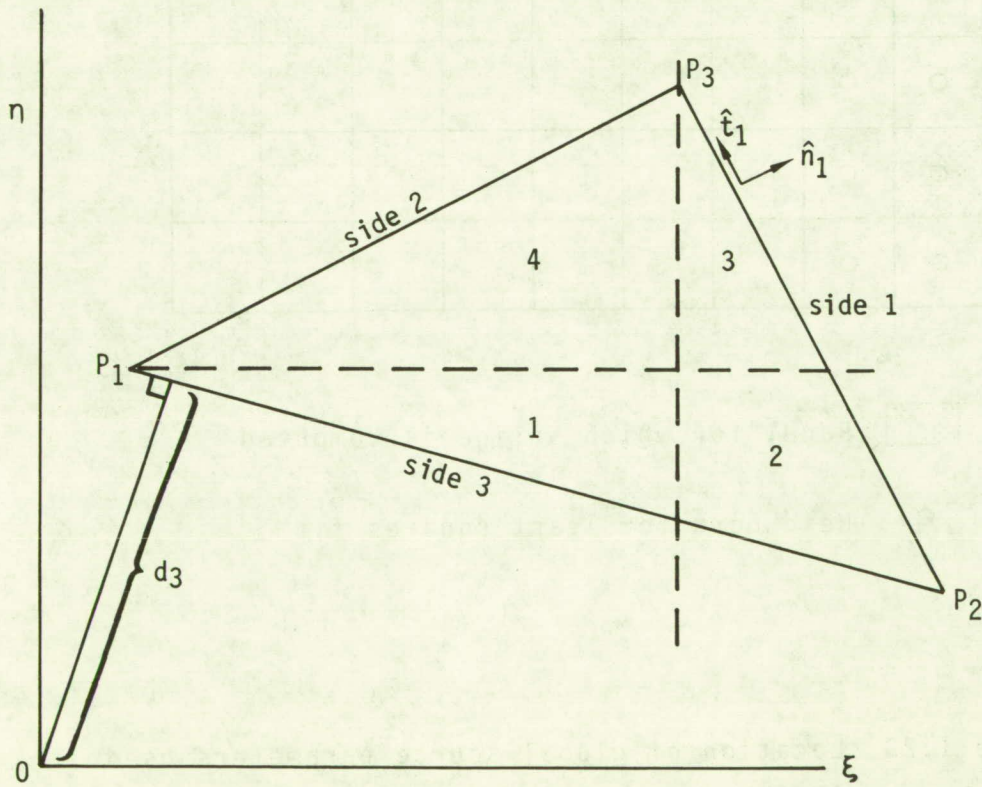
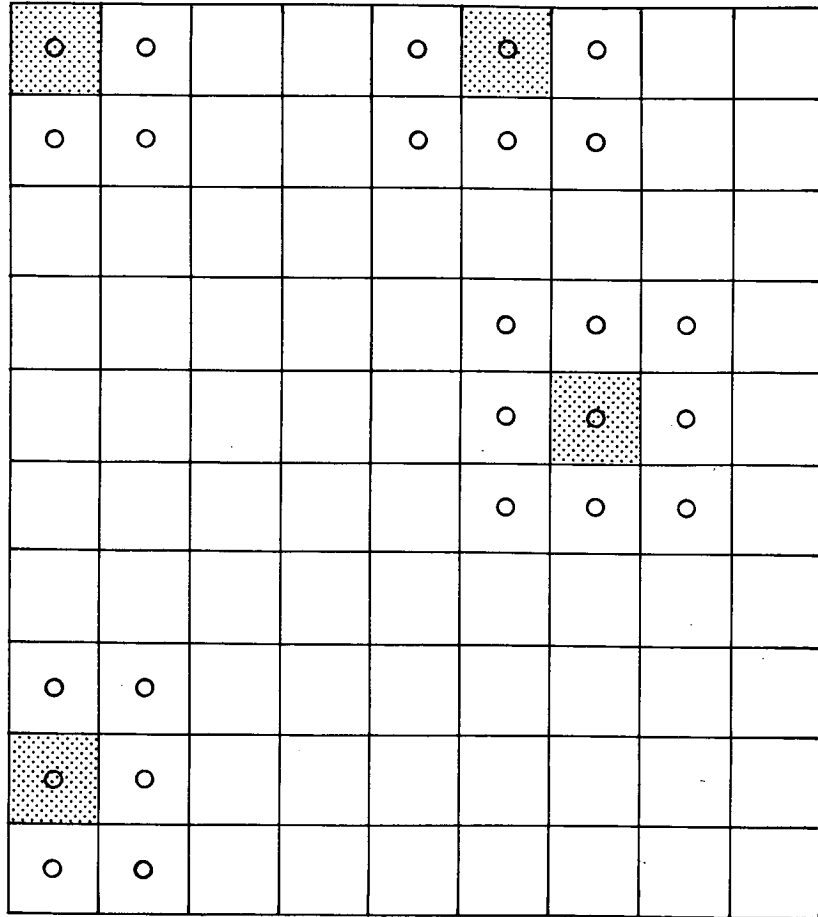


Figure I.22 - Computation of basic far field moments






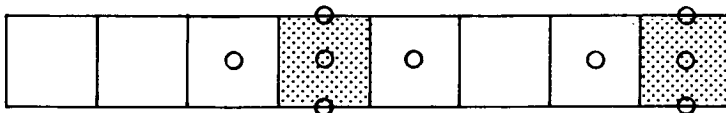
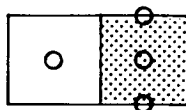
-  Panel for which spline is computed
- Neighbors for least squares fit

Figure I.23 Location of global source parameters used in the construction of the discontinuous source analysis spline.

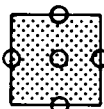
a.



b.



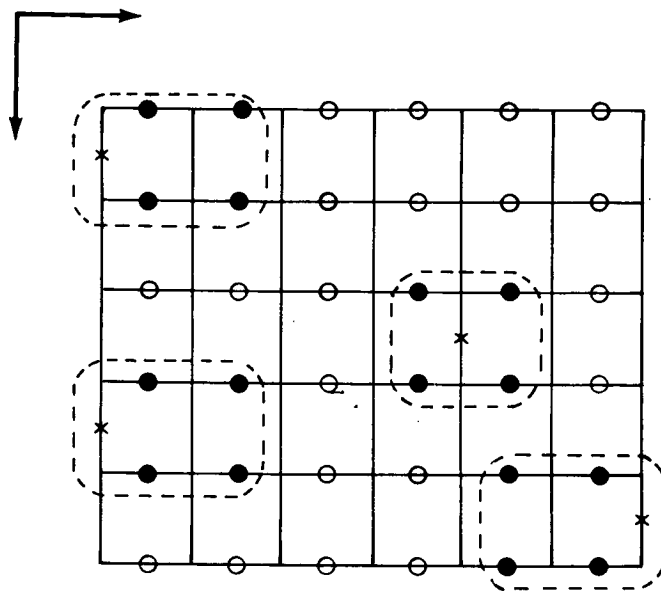
c.



Panel for which spline is computed

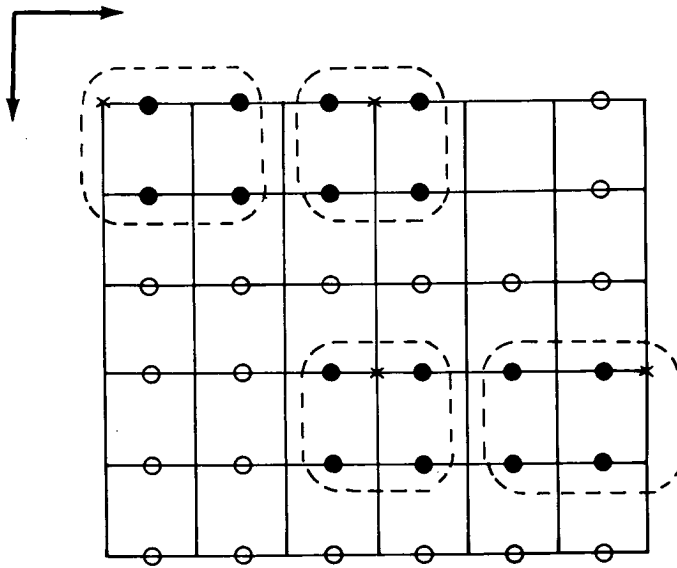
○ Location of points  $\vec{p}_i$

Figure I.24 Location of source parameter points for the special case construction of discontinuous source analysis splines



- × Edge midpoint source strengths to be computed by bilinear fit
- Global source parameters
- Global source parameters used in bilinear fits

Figure I.25 Computation of panel edge midpoint source strengths for discontinuous SD2 source splines



- × Corner points for which spline vectors are to be computed
- Global source parameters
- Global source parameters used in bilinear fits

Figure I.26 Computation of panel corner spline vectors for continuous SD2 source splines

## 0.3 Leading and Side Edge Force

### 0.3.1 Linearized Three-Dimensional Theory

Consider a flat plate at an angle of attack, as illustrated in figure 0.1. It is known that such a configuration experiences zero drag in subsonic two-dimensional potential flow, where drag is the component of force in the freestream or x-direction. Yet the surface normal has an x-component and the surface is impermeable, and thus equation (0.1.1) indicates non-zero drag.

The resolution of this contradiction is found in the existence of a leading edge force resulting from an infinite leading edge velocity (see Ashley and Landahl, Ref. 0.1, section 5.3, or, for more detail, Hancock and Garner, Ref. 5.2, part II). This leading edge force exactly cancels out the drag computed by integrating the pressure over the configuration surface. Since the surface is impermeable, the momentum transfer term gives no contribution to the force on the surface.

A formula for the edge force magnitude per unit distance (on a three dimensional wing) is given in Hancock and Garner (ref. 5.2). This formula, valid for all subsonic edges (there is no edge force on a supersonic edge) gives edge force per unit length by

$$dS/dy_n = (\pi/8) \beta_n \left[ \lim_{x_n \rightarrow 0} (\mu/\sqrt{x_n}) \right]^2 \quad (0.3.1)$$

where,  $S$  is the edge force,  $y_n$  measures distance along the edge,  $x_n$  measures distance perpendicular to the edge and in the plane of the surface,  $\mu$  is the doublet strength on the surface and  $\beta_n$  is given by

$$\beta_n^2 = 1 - M_n^2 \quad (0.3.2)$$

where  $M_n$  is the Mach number in the direction of the edge force. Thus,  $M_n = M_\infty \cos \Lambda$  where  $\Lambda$  is the sweepback angle as shown in figure 0.2. The edge force direction is away from the edge and perpendicular to both the edge and the surface normal, also as shown in figure 0.2.

### 0.3.2 Application in PAN AIR

To apply equation (0.3.1) in PAN AIR, we must first consider the evaluation of the limit. First note that it is known that if  $z_n$  is a polynomial in  $x_n$  and  $y_n$ , then the exact value of  $\mu/\sqrt{x_n}$  can be uniformly approximated by a polynomial. Given this fact, it is tempting to estimate the limit by evaluating  $\mu/\sqrt{x_n}$  at the first and second panels from the edge and extrapolating these values to  $x_n = 0$ . However, because PAN AIR represents  $\mu$  itself as a quadratic polynomial in  $x_n$  and  $y_n$ , the expression  $\mu_{PA}/\sqrt{x_n}$  (we denote the doublet distribution computed by PAN AIR as  $\mu_{PA}$ ) will not converge uniformly to  $\mu/\sqrt{x_n}$  in the neighborhood of the edge. Consequently, if we denote the computed and exact values of  $\mu$  at the center of the first panel by  $\mu_{1,PA}$  and  $\mu_{1,exact}$ , then  $\mu_{1,PA}/\mu_{1,exact}$  will not converge to 1 as the

number of panels is increased. Similarly,  $\mu_{2,PA}/\mu_{2,exact}$  does not converge to 1. These ratios will, however, converge to finite values, the specific values depending upon the solution details, especially the panel spacing and density. For example, different limit ratios are obtained for uniform spacing than for cosine spacing. Also, since a potential flow field near an edge is mathematically similar to two-dimensional flow about a flat plate, the convergence properties for three-dimensional cambered surfaces will be similar to those for three dimensional flat plates. Thus, we assume that the limiting behavior of  $\mu_{1,PA}/\mu_{1,exact}$  for a three-dimensional cambered surface will

closely resemble the behavior of  $\mu_{1,PA}/\mu_{1,exact}$  for a 2-D flat plate as the number of chordwise panels is increased.

In light of these considerations, the following method is proposed as one that (i) will yield reasonably accurate results without an excessive number of panels and (ii) will converge to exact results as the number of panels is increased, provided certain panel spacing rules are followed. Referring to figure 0.3, define  $Y_1, Y_2$  by

$$Y_i = \mu / \sqrt{x_n} \Big|_{x_n, i} \quad i = 1, 2 \quad (0.3.3)$$

where  $x_{n,i}$  denote the values of  $x_n$  at the first and second panel center away from the edge (see figure 0.3 for definition). These two evaluations now immediately provide an extrapolated value of  $\mu / \sqrt{x_n}$  at  $x_n = 0$ :

$$G = (Y_1 x_{n,2} - Y_2 x_{n,1}) / (x_{n,2} - x_{n,1}) \quad (0.3.4)$$

If  $\mu / \sqrt{x_n}$  converged uniformly to its limit value we could approximate

$$\lim_{x_n \rightarrow 0} \mu / \sqrt{x_n} \cong G$$

In fact, using equation (0.3.1) we write

$$dS/dy_n = (\pi/8) \beta_n G^2 f \quad (0.3.5)$$

where the correction factor  $f$  (which is  $O(1)$ ) is determined from program/theory comparisons for a series of two-dimensional flat plate problems. The correction factor  $f$  depends on the number of panels and the panel spacing method. The total leading edge force is computed from the formula

$$S = \int_{y_{n,1}}^{y_{n,2}} (dS/dy_n) dy_n \quad (0.3.6)$$

where the integral is evaluated by the midpoint rule using the formula (0.3.5) to provide values for  $(dS/dy_n)$ .

Correction factors for three types of panel spacing and various panel counts are given in figure 0.4. Correction factors for untabulated values of NPAN, the panel count, are obtained by interpolation, where  $f$  is regarded as a function of  $(1/NPAN)$ . Correction factors have not been computed for any other types of panel spacing, and results obtained by PAN AIR for such types of panel spacing may be neither accurate nor convergent.

The correct use and interpretation of figure 0.4 requires that one know precisely what is meant by "cosine spacing" and "semi-cosine spacing." Let  $t$  be a nondimensional coordinate defined such that the value  $t=0$  coincides with the edge on which the edge force acts and  $t = 1$  coincides with the opposite edge. Then the panel corner points for cosine spacing are located at the  $t$ -stations given by

$$\text{(cosine-spacing) } t_i = (1/2)[1 - \cos((i-1)\pi/NPAN)] \quad i=1, \dots, NPAN+1 \quad (0.3.7)$$

while for semi-cosine spacing these  $x$  stations are given by

$$\text{(semi-cosine spacing) } t_i = 1 - \cos[(i-1)\pi/(2 \cdot NPAN)] \quad i=1, \dots, NPAN+1 \quad (0.3.8)$$

### 0.3.3 Edge Force Verification

A leading edge suction distribution has been computed by PAN AIR using the technique described above for a  $60^\circ$  delta wing in incompressible flow. This distribution is compared in figure 0.5 to the result derived in Medan, (ref. 0.2). Notice that the quantity  $(dS/dy_n)/[(1-n)^{.28154} \alpha^2]$  is plotted against  $n$  where  $n$  represents "spanwise fraction," the fractional transverse distance from the centerline to the outboard tip and  $\alpha$  is angle of attack. This scaling of the leading edge suction distribution is based upon the theoretical results derived in (ref. 0.2). In fact, as  $n$  approaches 1,  $dS/dy_n$  itself tends to zero so that the differences between results shown in figure 0.5 are not significant when scaled and integrated to obtain overall forces. Note also that PAN AIR results appear to converge to the theoretical values except for the panels closest to the tip. In fact, the PAN AIR computed suction force on the tip panel will never converge no matter how densely the wing is panelled. This is another manifestation of nonuniform convergence arising from the fact that PAN AIR constrains the doublet distribution to be a quadratic function of the surface coordinates. Nevertheless, overall forces and moments do converge as panel density increases.

Drag values predicted for a supersonic delta wing are compared in figure 0.6 to the theoretical results presented in figure A,14m of Jones and Cohen (ref. F.1). The PAN AIR results lie very close to the theoretical curve. Since edge suction is a significant contributor to drag, this close comparison provides some verification of the validity of PAN AIR's method of computing edge suction forces.

This page has been left blank intentionally



## 0.5 Added Mass Coefficients

The inertial properties of a submerged body moving in a fluid are affected by the motion of the fluid surrounding the body. These properties, which become quite significant when the mass of the displaced fluid is commensurate with the mass of the body, are concisely summarized by a collection of tensors called "added mass coefficients." In this section we will define the added mass coefficients, describe their computation and derive some of their transformation properties.

### 0.5.1 Formulation of Added Mass Coefficients

Consider an impermeable body B with boundary surface S moving through a fluid. We suppose that the fluid has constant density  $\rho$  and that the fluid motion is itself irrotational. Thus, a velocity potential exists and satisfies Laplace's equation. At the instant of observation, the motion of the fluid is observed from an axis system fixed in the undisturbed fluid and momentarily coincident with a body fixed axis system. The velocity of any point  $\vec{p}$  on the body's surface is given by

$$\vec{u} + \vec{\omega} \times (\vec{p} - \vec{p}_0)$$

where  $\vec{u}$  specifies the body's translational velocity and  $\vec{\omega}$  specifies its rotational velocity about a center of rotation  $\vec{p}_0$ . The harmonic velocity potential for the fluid's instantaneous velocity is now uniquely determined by the impermeable surface boundary condition

$$\partial\phi/\partial n = (\vec{u} + \vec{\omega} \times (\vec{p} - \vec{p}_0)) \cdot \hat{n} \quad \text{on } S \quad (0.5.1)$$

An equivalent form of (0.5.1) using the implied summation notation is

$$\partial\phi/\partial n = u_i n_i + \omega_j (\vec{r} \times \hat{n})_j ; \quad \vec{r} = \vec{p} - \vec{p}_0 \quad (0.5.2)$$

where we introduce the shorthand  $\vec{r}$  for the vector from the center of rotation to a point on the body surface. Evidently,  $\phi$  can be written in the form

$$\phi = u_j \phi_j + \omega_j \psi_j \quad (0.5.3)$$

where  $\phi_j$  and  $\psi_j$  are harmonic velocity potentials satisfying the boundary conditions

$$\begin{aligned} \partial\phi_j/\partial n &= n_j \\ \partial\psi_j/\partial n &= (\vec{r} \times \hat{n})_j \quad \text{on } S \end{aligned} \quad (0.5.4)$$

The potentials introduced in (0.5.3) are associated with motion along an axis in the case of  $\phi_j$ , and with rotation about an axis in the case of  $\psi_j$ .

The expression for added mass coefficients is obtained by computing T, the kinetic energy of the fluid induced by the motion of the body. Summarizing the development given in ref. 0.3, T is given by

$$\begin{aligned}
T &= (\rho/2) \iiint_{R^3-B} (\nabla\phi)^2 dV \\
&= -(\rho/2) \iint_S \phi (\partial\phi/\partial n) dS
\end{aligned} \tag{0.5.5}$$

Substituting (0.5.3) into (0.5.5) yields for T

$$\begin{aligned}
T &= (1/2) u_i M_{ij} u_j + (1/2) \omega_i \sum_{ij} u_j \\
&\quad + (1/2) u_i S_{ij} \omega_j + (1/2) \omega_i I_{ij} \omega_j
\end{aligned} \tag{0.5.6}$$

where we define the various added mass coefficients by the expressions

$$\begin{aligned}
M_{ij} &= -\rho \iint_S \phi_i (\partial\phi_j/\partial n) dS \\
S_{ij} &= -\rho \iint_S \phi_i (\partial\psi_j/\partial n) dS \\
\sum_{ij} &= -\rho \iint_S \psi_i (\partial\phi_j/\partial n) dS \\
I_{ij} &= -\rho \iint_S \psi_i (\partial\psi_j/\partial n) dS
\end{aligned} \tag{0.5.7}$$

The coefficients  $M_{ij}$  are called inertia coefficients while  $I_{ij}$  are called moment of inertia coefficients;  $S_{ij}$  and  $\sum_{ij}$  are called mixed coefficients. Green's second identity implies that M and I are symmetric and further, that

$$S_{ij} = \sum_{ji} \tag{0.5.8}$$

Thus, the full 6x6 added mass coefficient matrix given by

$$A = \begin{bmatrix} M & S \\ \sum & I \end{bmatrix} \tag{0.5.9}$$

is symmetric.

## 0.5.2 Integration Procedures

Because the method by which PAN AIR solves for  $\phi_i$  and  $\psi_i$  ensures internal stagnation ( $\phi_i = \psi_i = 0$  interior to B), the integrals appearing in equation (0.5.7) can be expressed quite simply in terms of the fundamental singularity distributions. Letting  $\mu_i, \tilde{\mu}_i$  denote respectively the doublet distributions associated with  $\phi_i, \psi_i$  and using the boundary conditions (0.5.4), we obtain

$$\begin{aligned}
M_{ij} &= -\rho \iint_S \mu_i n_j \, dS \\
S_{ij} &= -\rho \iint_S \mu_i (\vec{r} \times \hat{n})_j \, dS \\
\Sigma_{ij} &= -\rho \iint_S \tilde{\mu}_i n_j \, dS \\
I_{ij} &= -\rho \iint_S \tilde{\mu}_i (\vec{r} \times \hat{n})_j \, dS
\end{aligned} \tag{0.5.10}$$

Clearly these integrals can be evaluated by techniques similar to those described in section 0.2 by using the moment matrices  $[FFM_1^D]$  and  $[NCPM_2]$ .

It is important to note that the added mass coefficients given by equation (0.5.10) are not precisely the results computed and printed by PAN AIR.

Rather, scaled quantities  $\hat{M}_{ij}$ ,  $\hat{S}_{ij}$ ,  $\hat{\Sigma}_{ij}$  and  $\hat{I}_{ij}$  are printed. These are defined by

$$\begin{aligned}
\hat{M}_{ij} &= M_{ij} / \left( \frac{1}{2} \rho SL \right) \\
\hat{S}_{ij} &= S_{ij} / \left( \frac{1}{2} \rho SL^2 \right) \\
\hat{\Sigma}_{ij} &= \Sigma_{ij} / \left( \frac{1}{2} \rho SL^2 \right) \\
\hat{I}_{ij} &= I_{ij} / \left( \frac{1}{2} \rho SL^3 \right)
\end{aligned} \tag{0.5.11}$$

where  $S$  is a user specified reference area and  $L$  a user specified reference length. Notice that if one takes  $S = L = \rho = 1$ , one finds that  $\hat{M}_{ij} = 2 M_{ij}$ ,  $\hat{S}_{ij} = 2 S_{ij}$ , etc.

### 0.5.3 Orthogonal Transformation

Added mass coefficients computed in a body axis system which has been subjected to an orthogonal transformation  $\Gamma$  can be defined in terms of added mass coefficients in a reference coordinate system. Using primes to denote quantities in the transformed system, the boundary conditions can be written as

$$(\partial \phi'_i / \partial n') = (\Gamma \hat{n})_i \tag{0.5.12}$$

$$(\partial \phi'_i / \partial n') = [\Gamma (\vec{r} \times \hat{n})]_i \quad \text{on } S$$

Equation (0.4.8) was applied to the second part of (0.5.12). For (0.5.12) to be satisfied, it must happen that

$$\begin{aligned}\phi'_i &= \Gamma_{ij} \phi_j \\ \psi'_i &= \Gamma_{ij} \psi_j\end{aligned}\tag{0.5.13}$$

Substituting (0.5.12) and (0.5.13) into a primed form of (0.5.7) will show that

$$M'_{ij} = \Gamma_{ik} M_{kl} \Gamma_{jl}\tag{0.5.14}$$

The other coefficients transform identically.

#### 0.5.4 Translation

Added mass coefficients computed about an arbitrary moment reference point  $\vec{r}_0$  can be defined in terms of coefficients computed about the origin. The technique is similar to that of section 0.5.2. The boundary conditions become

$$\begin{aligned}\partial\phi'_i/\partial n' &= n_i \\ \partial\psi'_i/n' &= (\vec{r} \times \hat{n})_i - (\vec{r}_0 \times \hat{n})_i\end{aligned}\tag{0.5.15}$$

To satisfy these boundary conditions, the potentials in the translated system must take the form

$$\begin{aligned}\phi'_i &= \phi_i \\ \psi'_i &= \psi_i - \epsilon_{ijk} r_{0,j} \phi_k\end{aligned}\tag{0.5.16}$$

where  $\epsilon_{ijk}$  denotes the usual permutation symbol, (cf. eqn. B.3.21 and ff.).

Substitution of (0.5.15) and (0.5.16) into a primed form of (0.5.7) gives

$$\begin{aligned}M'_{ij} &= M_{ij} \\ S'_{ij} &= S_{ij} - \epsilon_{ikl} r_{0,k} M_{lj} \\ \Sigma'_{ij} &= \Sigma_{ij} - \epsilon_{ikl} r_{0,k} M_{lj} \\ I'_{ij} &= I_{ij} - \epsilon_{ilm} r_{0,l} S_{mj} - \epsilon_{jlm} r_{0,l} \Sigma_{im} \\ &\quad + \epsilon_{inp} \epsilon_{jlm} r_{0,n} r_{0,l} M_{pm}\end{aligned}\tag{0.5.17}$$

#### 0.5.5 Symmetric Configuration

If the surface  $S$  consists of a surface  $S'$  and its mirror image  $S''$ , the added mass coefficients on  $S''$  can be defined in terms of those on  $S'$ . Suppose the plane of symmetry passes through  $\vec{r}_s$  and has a unit normal  $\hat{v}$ . A point  $\vec{p}'$  on  $S'$  and its image point  $\vec{p}''$  on  $S''$  are related by

$$p_i'' = R_{ij} p_j' + x_{o,j} \quad (0.5.18)$$

where  $R_{ij} = \delta_{ij} - 2 v_i v_j$

and  $x_{o,j} = r_{s,j} - R_{jk} r_{s,k}$

The point  $\vec{x}_o$  is the image point of the origin and R is the reflection matrix.

With primes and double primes denoting entities related to S' and S'' respectively, the boundary conditions become

$$\begin{aligned} \partial \phi_i'' / \partial n'' &= R_{ij} n_j' \\ \partial \psi_i'' / \partial n'' &= -R_{ij} (\vec{r}' \times \hat{n}')_j + R_{ij} (\vec{x}_o \times \hat{n}')_j \end{aligned} \quad (0.5.19)$$

where  $\vec{r}'$  is the vector from  $\vec{p}_o$ , the center of rotation, to  $\vec{p}'$ .

$$\vec{r}' = \vec{p}' - \vec{p}_o$$

The second part of (0.5.19) required applications of (0.1.12) and (0.5.18). To satisfy (0.5.19), the potentials take the form

$$\phi_i'' = R_{ij} \phi_j' \quad (0.5.20)$$

$$\psi_i'' = -R_{ij} \psi_j' + R_{ij} \epsilon_{jkl} x_{o,k} \phi_l'$$

Applying (0.5.19) and (0.5.20) to a form of (0.5.7) yields

$$\begin{aligned} M_{ij}'' &= R_{ik} M_{kn}' R_{jn} \\ S_{ij}'' &= \epsilon_{jlm} x_{o,l} M_{im}' - R_{ik} S_{kq}' R_{jq} \\ \Sigma_{ij}'' &= -R_{ik} \Sigma_{kl}' R_{jl}' + \epsilon_{ipq} x_{o,p} M_{qj}'' \\ I_{ij}'' &= R_{ik} I_{kq}' R_{jq}' + \epsilon_{ikn} x_{o,k} S_{n,j}'' \end{aligned} \quad (0.5.21)$$

This page has been left blank intentionally

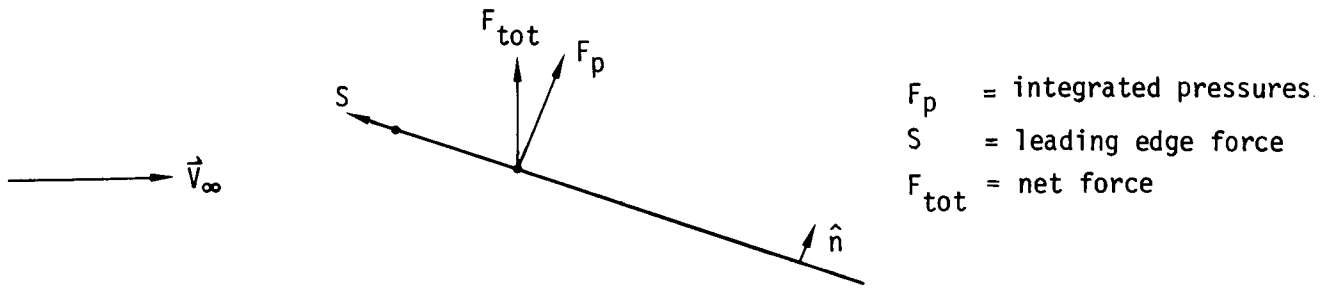


Figure 0.1 - Effect of leading edge force

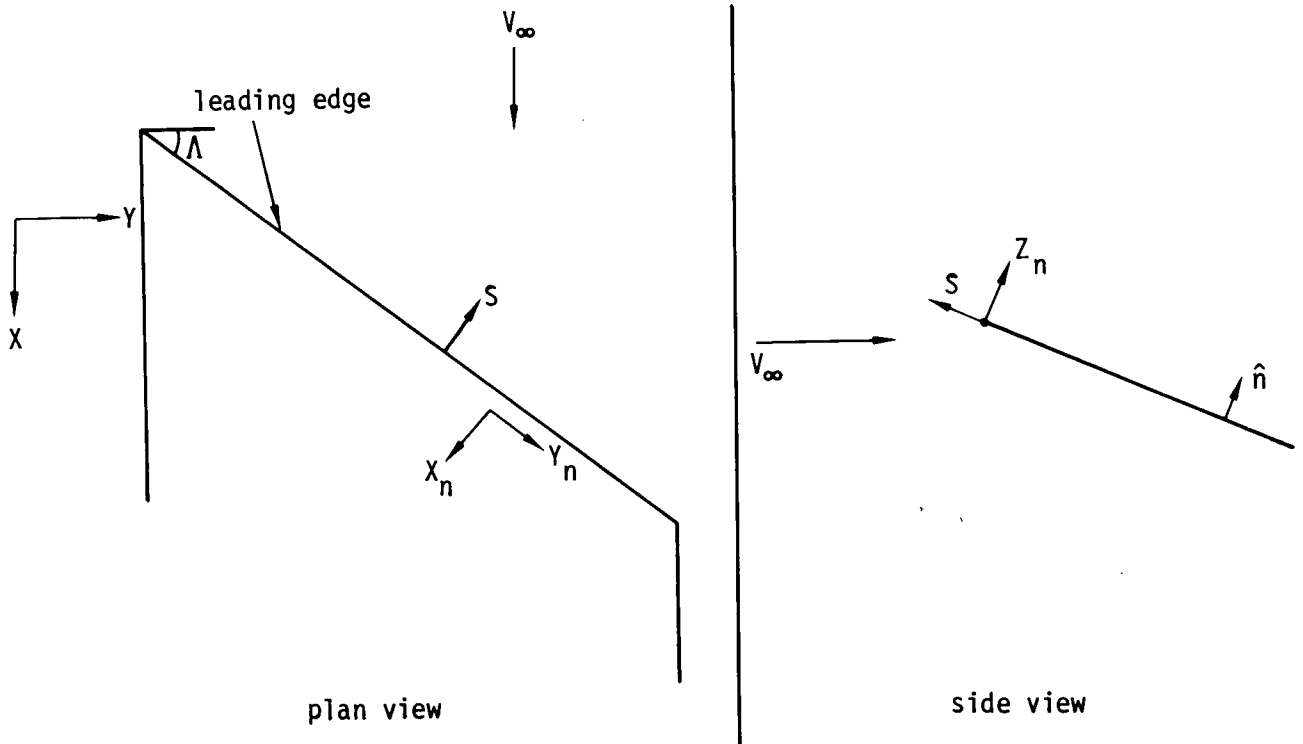


Figure 0.2 - Leading edge force on a three-dimensional thin wing

0.6-1 (11/30/81)

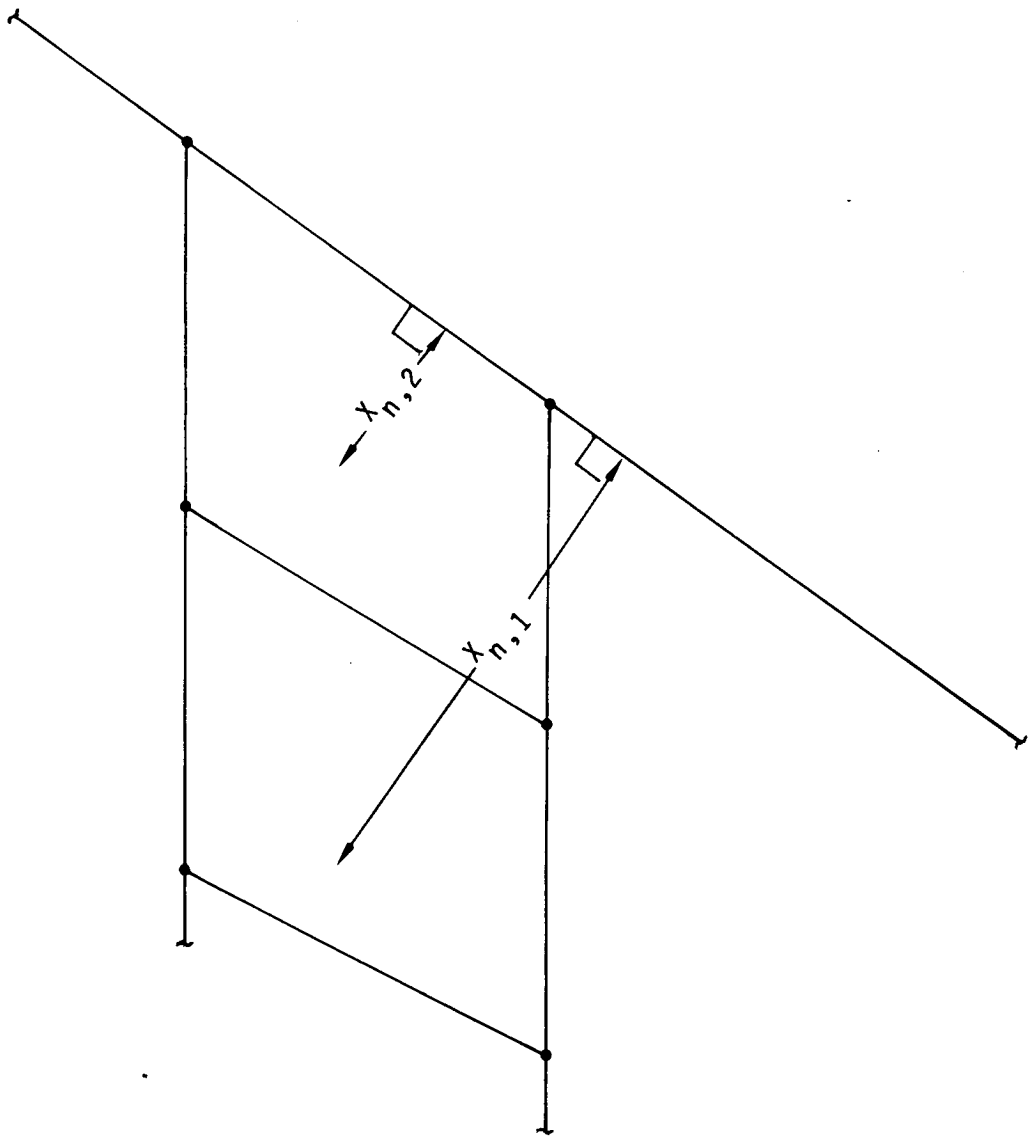


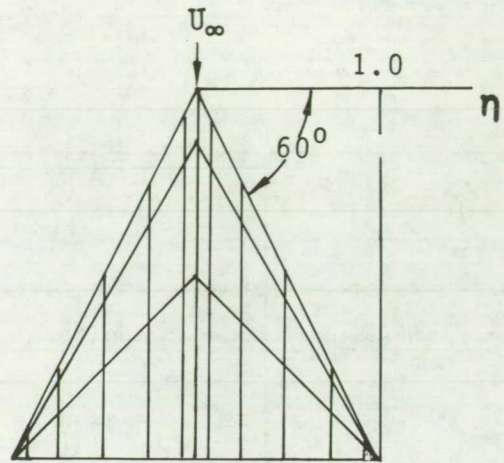
Figure 0.3 - Definition of  $X_{n,1}$  and  $X_{n,2}$



Correction Factors f (Derived Using PAN AIR Version 1.0)			
NPAN	Uniform	Cosine	Semi-Cosine
2	1.1579008	1.1579008	1.4059546
3	1.3289155	1.4039062	1.4977210
4	1.3462617	1.4766240	1.5680541
5	1.3513135	1.5336144	1.5985113
7	1.3544339	1.5852960	1.6212810
10	1.3557162	1.6149452	1.6323902
14	1.3562257	1.6294277	1.6359293
20	1.3564644	1.6373295	1.6407743
40	1.3566063	1.6431274	1.6435113
60	1.3566336	N.A.	1.6442279
80	1.3566417	N.A.	1.6444954

NPAN = Number of panel rows or number of panel columns,  
depending on which edge the edge forces are  
calculated for.

Figure 0.4 - Edge force correction factors



$$\frac{(dS/dy_\eta)}{\alpha^2(1-\eta) \cdot 28154}$$

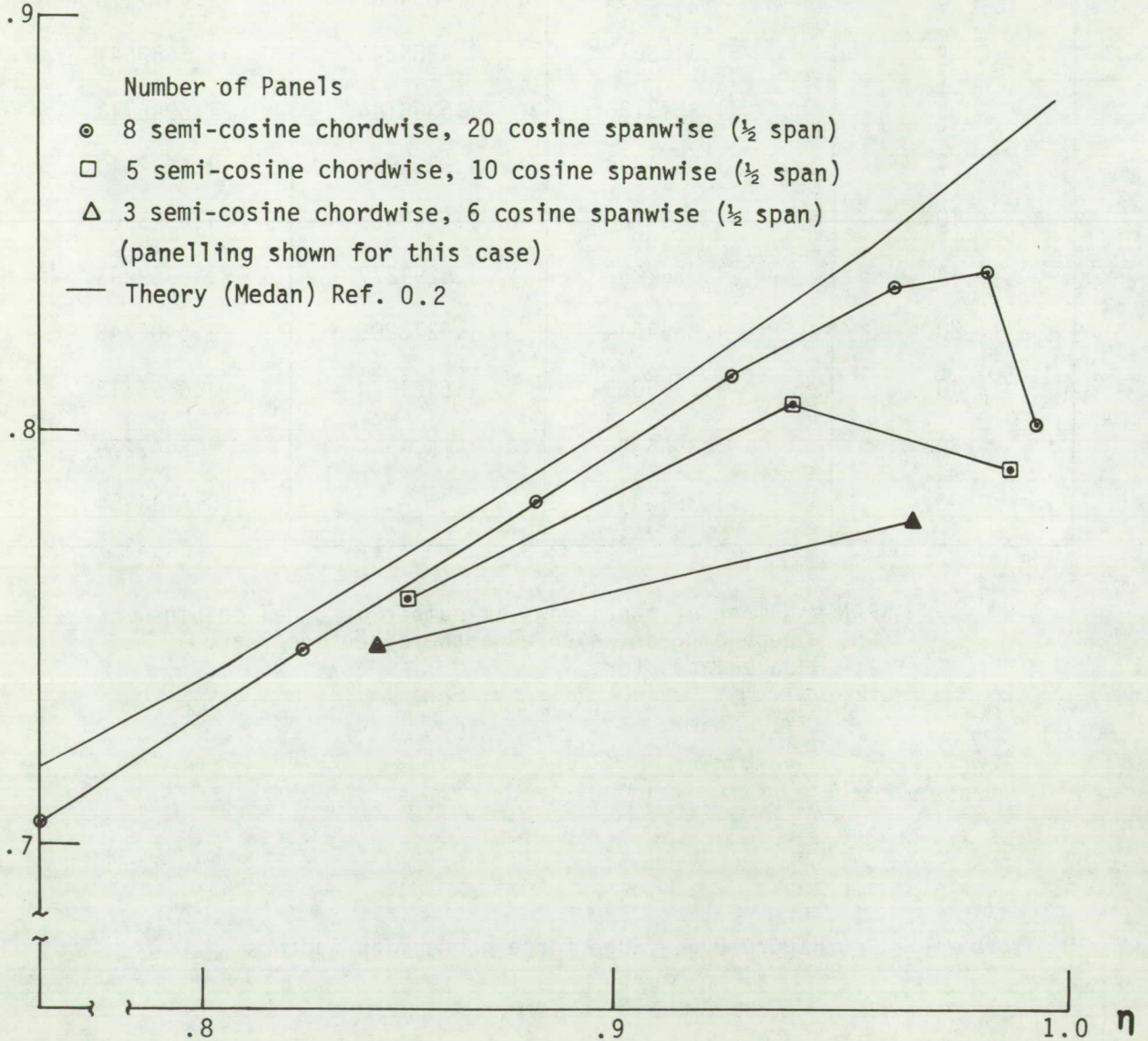


Figure 0.5 - Comparison of leading edge suction predicted by PAN AIR with theoretical results.

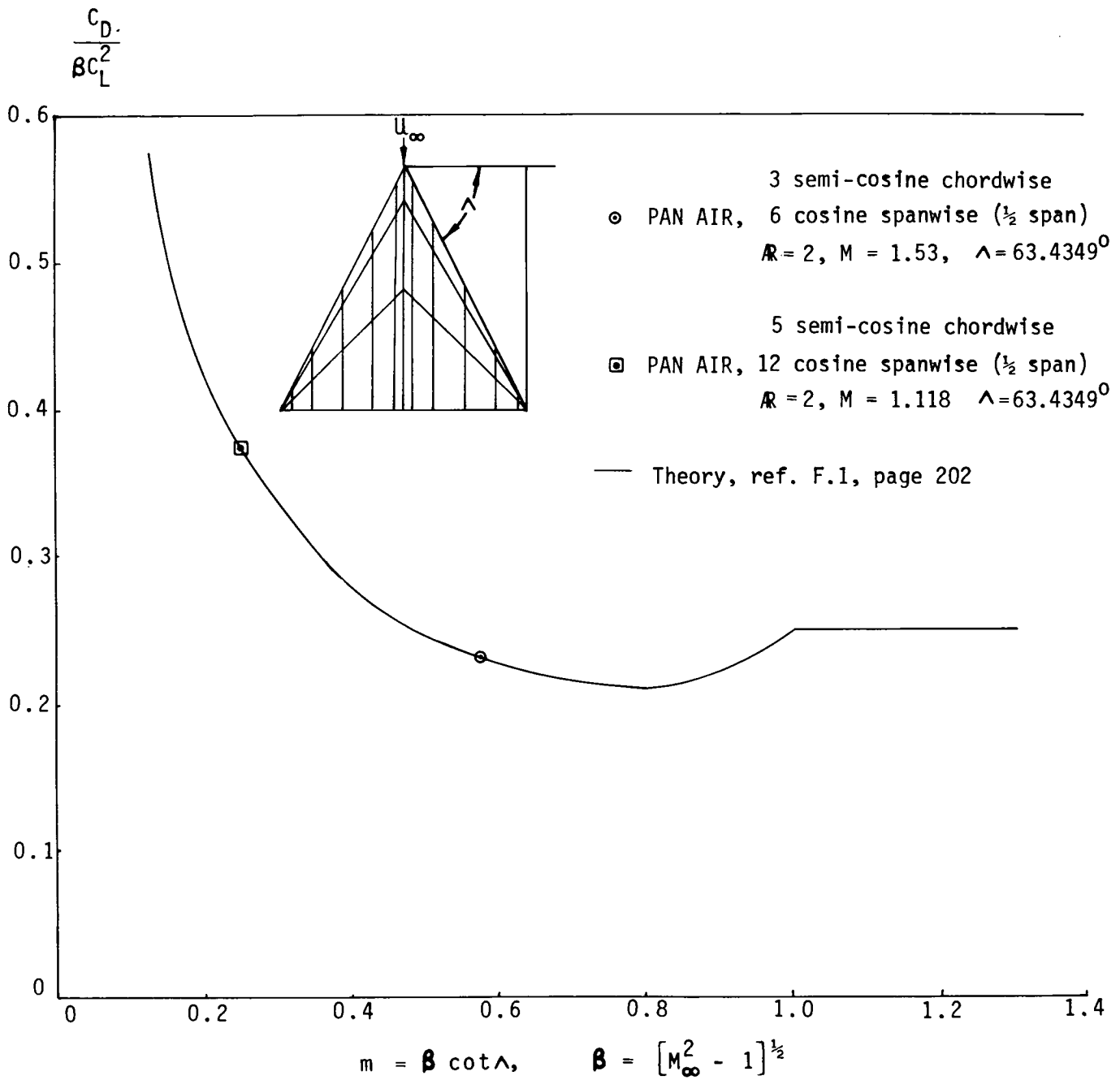


Figure 0.6 - Comparison of drag predicted by PAN AIR with theory for a delta wing in supersonic flow

5.6	Influence Coefficients	5.6-1
5.6.1	Computation of Potential and Velocity	5.6-1
5.6.2	Reformulation of the Doublet Velocity Integral	5.6-4
5.6.3	The Far Field Expansion	5.6-6
5.7	The Aerodynamic Influence Coefficient Matrix	5.7-1
5.7.1	Non-Standard Boundary Conditions	5.7-2
5.7.2	Symmetry	5.7-3
5.7.3	Known Singularity Parameters	5.7-6
5.7.4	Multiple Right Hand Side	5.7-8
5.7.5	Updatability	5.7-9
5.8	Solution of the System of Equations	5.8-1
5.9	Post-Solution Features	5.9-1
5.9.1	Computation of Potential and Velocity	5.9-1
5.9.2	Pressure Computation	5.9-2
5.9.3	Velocity Corrections	5.9-2
5.9.4	Force and Moment Computation	5.9-4
6.0	A Guide to the Appendices	6.0-1
7.0	References	7.0-1
8.0	List of Symbols	8.0-1
9.0	Engineering Glossary	9.0-1
Appendices		
A.0	Fundamental Fluid Mechanics	A.0-1
A.1	The Small Perturbation Assumptions	A.1-1
B.0	The Prandtl-Glauert Equation	B.0-1
B.1	Existence and Uniqueness	B.1-1
B.2	Wakes and Modeling	B.2-1
B.3	Removal of Line Vortex Terms	B.3-1
B.4	Linear Sources and Quadratic Doublets	B.4-1
C.0	The Design Problem	C.0-1
C.1	Linearized Design	C.1-1
C.2	Sequential Design	C.2-1
C.3	Iterative Design	C.3-1
C.4	Stability	C.4-1
D.0	Geometry of Networks and Panels	D.0-1
D.1	Networks	D.1-1
D.1.1	Network Types	D.1-1
D.1.2	Wake Networks and the Kutta Condition	D.1-1
D.1.3	Indexing	D.1-2
D.1.4	Collapsing of Network Edges	D.1-3
D.1.5	Additional Network Processing	D.1-3
D.2	Basic Panel Geometry	D.2-1
D.3	Error Checks	D.3-1
E.0	Matrices and Coordinates	E.0-1
E.1	Vectors and Dual Vectors	E.1-1
E.2	Metric Matrices, Dual Matrices, and Inner Products	E.2-1
E.3	Coordinate Transformations	E.3-1

## Contents

	Page
List of Figures	xi
Preface to Version 1.1.	xvii
1.0 Introduction	1.0-1
2.0 Fundamental Fluid Mechanics	2.0-1
2.1 The Navier-Stokes Equations	2.1-1
2.2 Euler's Equation	2.2-1
2.3 The Unsteady Potential Equation	2.3-1
2.4 The Steady Non-Linear Potential Equation	2.4-1
2.5 The Prandtl-Glauert Equation	2.5-1
3.0 Panel Method Theory	3.0-1
3.1 Coordinate Scaling	3.1-1
3.2 Green's Theorems	3.2-1
3.3 Discretization	3.3-1
4.0 An Overview of PAN AIR	4.1-1
4.1 Historical Development of Panel Methods	4.1-1
4.2 Summary of PAN AIR Technology	4.2-1
4.2.1 Basis Function Computation	4.2-2
4.2.1.1 Subpanel Splines	4.2-2
4.2.1.2 Outer Splines	4.2-3
4.2.2 Panel Influence Coefficients	4.2-4
4.2.2.1 Near Field PIC's	4.2-5
4.2.2.2 Far Field PIC's	4.2-6
4.2.3 Potential and Velocity Influence Coefficient Assembly	4.2-6
4.2.4 Aerodynamic Influence Coefficient Matrix Construction	4.2-7
5.0 Elaboration on the Technology in PAN AIR	5.1-1
5.1 Networks and Panels	5.1-1
5.2 Coordinate Transformations	5.2-1
5.3 Network Edge Matching	5.3-1
5.4 Control Points and Boundary Conditions	5.4-1
5.4.1 Control Point Location	5.4-1
5.4.2 Boundary Conditions	5.4-1
5.4.2.1 Impermeability Boundary Conditions	5.4-2
5.4.2.2 Thin Surfaces	5.4-4
5.4.2.3 Thick Configurations	5.4-5
5.4.2.4 Superinclined Surfaces	5.4-7
5.4.2.5 The General Boundary Condition	5.4-8
5.5 Singularity Splines	5.5-1
5.5.1 The Matrices $B^S$ and $B^D$	5.5-2
5.5.2 The Definition of SPSPL	5.5-3
5.5.3 Construction of B Matrices for Continuous Singularity Distributions	5.5-4
5.5.4 Construction of the Discontinuous Source Outer Spline Matrix	5.5-5a
5.5.5 Construction of SPSPL	5.5-6

PAGE STATUS LOG (Version 1.1)

Current Version Page Number	Action	Previous Version Page Number
iii (11/30/81) to xviii (11/30/81)	Replace	iii to xvi
4.1-1 (11/30/81) to 4.1-2	Replace	4.1-1 to 4.1-2
4.3-1 (11/30/81) to 4.3-2	Replace	4.3-1 to 4.3-2
5.5-1 (11/30/81) to 5.5-6 (11/30/81) (includes 5.5-5a to 5.5-5b)	Replace	5.1-1 to 5.5-6
5.9-5 (11/30/81) to 5.9-6	Replace	5.9-5 to 5.9-6
5.10-11 to 5.10-12 (11/30/81)	Replace	5.10-11 to 5.10-12
7.0-1 (11/30/81) to 7.0-4 (11/30/81)	Replace	7.0-1 to 7.0-2
D.1-1 (11/30/81) to D.1-2 (11/30/81)	Replace	D.1-1 to D.1-2
D.3-1 (11/30/81) to D.3-2 (11/30/81)	Replace	D.3-1 to D.3-2
F.3-1 (11/30/81) to F.3-2 (11/30/81)	Replace	F.3-1 to F.3-2
F.4-1 (11/30/81) to F.4-4 (11/30/81)	Replace	F.4-1 to F.4-4
F.5-1 (11/30/81) to F.5-14 (11/30/81)	Replace	F.5-1 to F.5-6
F.6-1 (11/30/81) to F.6-4 (11/30/81)	Replace	F.6-1 to F.6-4
F.7-1 to F.7-2 (11/30/81)	Replace	F.7-1 to F.7-2
F.7-5 to F.7-14 (11/30/81)	Replace	F.7-5 to F.7-10
G.0-1 (11/30/81) to G.0-4 (11/30/81)	Replace	G.0-1 to G.0-6
G.1.1 to G.1-4 (11/30/81)	Replace	G.1-1 to G.1-4
I.0-1 (11/30/81) to I.0-4 (11/30/81)	Replace	I.0-1 to I.0-4
I.1-1 (11/30/81) to I.1-22 (11/30/81)	Replace	I.1-1 to I.1-18
I.6-17 to I.6-22 (11/30/81)	Replace	I.6-17 to I.6-18
0.3-1 (11/30/81) to 0.3-4 (11/30/81)	Replace	0.3-1 to 0.3-4
0.5-1 (11/30/81) to 0.5-4 (11/30/81)	Add	
0.6-1 (11/30/81) to 0.6-6 (11/30/81)	Replace	0.5-1 to 0.5-2

1. Report No. NASA CR-3251	2. Government Accession No.	3. Recipient's Catalog No.	
4. Title and Subtitle PAN AIR - A Computer Program for Predicting Subsonic or Supersonic Linear Potential Flows about Arbitrary Configurations Using a Higher Order Panel Method. Volume I - Theory Document (Version 1.1)		5. Report Date November 30, 1981	6. Performing Organization Code
		8. Performing Organization Report No. D180-24910-3	10. Work Unit No.
7. Author(s) Alfred E. Magnus and Michael A. Epton		11. Contract or Grant No. NAS2-9830	13. Type of Report and Period Covered Contractor Report January 1978-April 1980
9. Performing Organization Name and Address Boeing Military Airplane Company P. O. Box 3707 Seattle, Washington 98124		14. Sponsoring Agency Code	
		12. Sponsoring Agency Name and Address o NASA, Washington D.C. 20546 o AFWAL and ASD, Wright-Patterson AFB, Ohio 45433 o NCSC, Panama City, Florida 32407	
15. Supplementary Notes Technical Monitors: NASA-Ames: Larry L. Erickson, Ralph L. Carmichael, Alan D. Levin NASA-Langley: David S. Miller, James L. Thomas ASD: James R. Snyder AFWAL: Ken Cramer, William A. Sotomayer NCSC: Neill S. Smith			
16. Abstract <p>An outline of the derivation of the differential equation governing linear subsonic and supersonic potential flow is given. The use of Green's Theorem to obtain an integral equation over the boundary surface is discussed. The engineering techniques incorporated in the PAN AIR (Panel Aerodynamics) program (a discretization method which solves the integral equation for arbitrary first order boundary conditions) are then discussed in detail.</p> <p>Items discussed include the construction of the compressibility transformations, splining techniques, imposition of the boundary conditions, influence coefficient computation (including the concept of the finite part of an integral), computation of pressure coefficients, and computation of forces and moments.</p>			
17. Key Words (Suggested by Author(s)) aerodynamics, linear potential flow, panel methods, Prandtl-Glauert equation, splines, influence coefficients, discretization			
19. Security Classif. (of this report) Unclassified	20. Security Classif. (of this page) Unclassified	21. No. of Pages 725	22. Price